國 立 交 通 大 學

機 械 工 程 學 系

碩 士 論 文

# 放置可移動擾動粒子在一水平加熱銅板上對 FC-72 池沸騰熱傳增強研究

# Enhancement of FC-72 Pool Boiling Heat Transfer by Movable Particles on a Horizontal Plate

研 究 生：魏 周 民

指 導 老 師：林 清 發 教授

中 華 民 國 102 年 6 月

# 放置可移動擾動粒子在一水平加熱銅板上對 FC-72 池沸騰熱傳增強研究

# Enhancement of FC-72 Pool Boiling Heat Transfer by Movable Particles on a Horizontal Plate

研 究 生 ： 魏 周 民　　Student：Chou-Min Wei

指導教授 ： 林 清 發　　Advisor：Prof. Tsing-Fa Lin

國立交通大學

機械工程學系

碩士論文

A Thesis

Submitted to Department of Mechanical Engineering

College of Engineering

National Chiao Tung University

In partial Fulfillment of the Requirements

For the Degree of

Master of Science

In

Mechanical Engineering

June 2013

Hsinchu, Taiwan, Republic of China

中華民國 102 年 6 月

# 誌謝

轉眼間，三年的研究生生活終於劃下句點，碰到許多事不順意的、不如意的，中途有一度想要放棄的念頭，但在家人與朋友的關心與勸導下，我留了下來，如今在畢業口試後仍留在深深的記憶中。本論文之所以可以順利完成，首先要感謝的是指導老師 林清發教授，在受教三年的時光當中，深刻感受到老師獨特的學者涵養、治學嚴謹的態度，在實驗的討論與論文的撰寫潤筆中，不辭辛勞的殷切指導，讓學生受益匪淺，在此由衷致謝。

在研究所期間，要特別感謝博士班汪書磊學長在我的求學過程中給予的熱心討論與指導，沒有學長的指導與幫忙下，我今天就沒辦法順利的畢業，也感謝同學葉庭鈞互相砥礪和幫忙，以及帶來歡樂的學弟學妹薛正宏、李貞儀及吳錫寰，感謝一同在研究室生活的大家。

誠摯地感謝成功大學機械系何清政教授、中央大學機械系陳志臣博士及清華大學工科系潘欽教授，由於各位老師在口試中提出各項建議，使本論文更趨完整。

最後，僅以本文獻給我所關心的人和所有關心我的人。

魏周民

2013, 6 於新竹交大

# 放置可移動擾動粒子在一水平加熱銅板上

# 對 FC-72 池沸騰熱傳增強研究

研 究 生：魏 周 民　　指 導 老 師：林 清 發 教授

國立交通大學機械工程學系

## 摘要

本論文針對放置可移動擾動粒子於加熱銅板上對 FC-72 池沸騰熱傳增強實驗研究。可移動顆粒放置於加熱銅板表面上並且由一個四方型的壓克力圍牆圍住，來防止可移動顆粒不會因為液體的流動，導致可移動顆粒被沖離了加熱銅板表面。在實驗中探討顆粒種類、顆粒直徑和顆粒的數量。在實驗參數範圍上，熱通量 $q$ 從 0.1 到 6 W/cm$^2$，顆粒直徑有 1.0 和 1.5 mm，顆粒的數量從 100 到 1800(對於直徑為 1.0 mm 的顆粒)和 100 到 800(對於直徑為 1.5 mm 的顆粒)。

實驗數據以壁過熱度對應輸入的熱通量及熱傳係數表示，比較對於光滑加熱銅塊下熱傳增強的表現。放置可移動擾動銅粒子相較於光滑表面對於 FC-72 之池沸騰熱傳係數有 430%的增強效果。而對於放置可移動擾動不銹鋼粒子相較於光滑表面，整體的沸騰熱傳係數有 530%的增強效果。甚至當加熱銅板上覆蓋滿顆粒(最多鋪滿兩層)對於整體的散熱效果有明顯的增強。但在高熱通量時，散熱效果有降低的趨勢，特別對於放置直徑 1.5 ㎜ 的顆粒，散熱效果降低的趨勢很明顯。由數據呈現的圖形可得，熱傳增強的表現會因其不同的參數搭配而有不同的增強效果，理想且良好的熱傳增強表現在於適當的顆粒種類、顆粒直徑和顆粒數量的搭配。

由數據呈現的結果指出，放置可移動擾動粒子於加熱銅板上後對於整體的散熱效果有增強的效果也有降低的效果。在高熱通量時，散熱效果有明顯降低的現象。

# Enhancement of FC-72 Pool Boiling Heat Transfer by Movable Particles on a Horizontal Plate

**Student: Chou-Min Wei** **Advisor: Prof. Tsing-Fa Lin**

National Chiao Tung University

## ABSTRACT

An experiment is carried out here to investigate how the saturated pool boiling heat transfer of liquid FC-72 over a horizontal heated copper plate of 3×3 $cm^2$ in surface area is affected by placing metallic particles above the surface, intending to explore the possible pool boiling heat transfer enhancement by the moving particles. Both copper and stainless steel particles are tested. The particles are freely placed above the heated plate with a rectangular fence surrounding the plate so that the particles can be moved by the force induced by the boiling flow without being blown away. In the experiment, the imposed heat flux is varied from 0.1 to 6 W/cm$^2$ for the diameter of the particles fixed at 1.0 and 1.5 mm. Besides, the total particle number placed on the plate ranges from 100 to 1800 and from 100 to 800 respectively for the small and large particles. The measured data are presented in terms of boiling curves and boiling heat transfer coefficients for the heating surface with the presence and absence of the particles. The experimental parameters include the imposed heat flux level and the size, material and number of the particles.

The data obtained from the present study for the saturated pool boiling indicate that placing the movable particles can significantly increase the pool boiling heat transfer coefficient of FC-72 at low and medium heat fluxes (wall superheats). For the copper particles the enhancement can be up to 430% over that for a bare surface for a

certain combination of the experimental parameters. The best enhancement can be as high as 530% for the stainless steel particles. Even when more than one layer of particles are placed on the plate relatively significant boiling heat transfer enhancement can still be obtained. However, the boiling heat transfer enhancement varies nonmonotonically with the particle diameter, number and material and the heat flux applied, reflecting the complex mutual influences of the movable particles and bubble motion near the heated surface. An optimal boiling heat transfer enhancement could be procured by a suitable choice of the experimental parameters. Besides, the wall superheat for the incipient boiling can be substantially reduced by the moving metallic particles. However, at high heat flux (wall superheat) placing the particles on the plate can greatly reduce the boiling heat transfer especially for the large particles.

The results from the visualization of the boiling flow over the copper plate indicate that placing the movable particles above the plate results in two opposite effects of enhancing and retarding the boiling heat transfer. At high heat flux the retarding effect is strong.

# TABLE OF CONTENTS

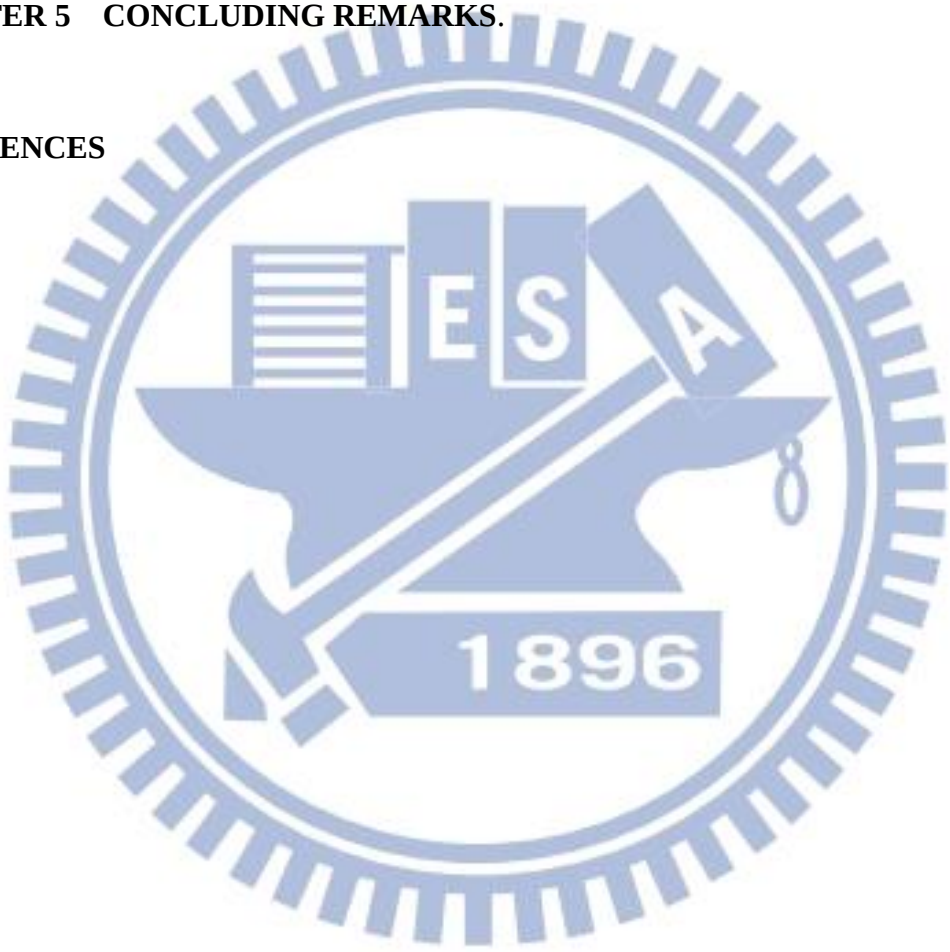

# LIST OF TABLES

# LIST OF FIGURES

**Experimental Apparatus**



**Data Reduction**



**Saturated Pool Boiling Heat Transfer**

# NOMENCLATURE

| | |
|---|---|
| A | area, $mm^2$ |
| $c_p$ | specific heat, J/kg·K |
| $d_p$ | diameters of particles, mm |
| $N_p$ | numbers of particles |
| $N_{pf}$ | maximum particle number forming a single particle layer |
| $h$ | heat transfer coefficient, $W/m^2 \cdot K$ |
| I | measured current from DC power supply, A |
| V | measured voltage from DC power supply, V |
| k | thermal conductivity, W/m·K |
| L | characteristic length, m |
| $Nu_L$ | Nusselt number, $Nu_L = \frac{hL}{k_\ell}$ |
| P | system pressure, kPa |
| $Q$ | heat transfer rate, W |
| $q_n$ | net wall heat flux, $W/cm^2$ |
| Ra | Rayleigh number |
| $T$ | temperature, $^oC$ |
| t | time, sec |
| W | plate width, cm |

Greek Symbols

| | |
|---|---|
| $\nu$ | kinematic viscosity, $m^2/s$ |
| $\rho_{cu}$ | copper density ($\rho_{cu}$=8989.9), $kg/m^3$ |
| $\rho_\ell$ | liquid density, $kg/m^3$ |
| $\rho_p$ | particle density, $kg/m^3$ |
| $\rho_{ss}$ | stainless steel density ($\rho_{ss}$=7984.3), $kg/m^3$ |
| $\mu$ | absolute viscosity, kg/m·s |
| $\beta$ | coefficient of expansion, /K |
| $\sigma$ | surface tension, N/m |
| $\delta$ | the distance between the thermalcouple tips and the upper surface of the copper plate, m |
| $\Delta T_w$ | wall superheat, K |
| $\Delta T_{ONB}$ | incipient boiling superheat, K |

g gravity, $m/s^2$

α Thermal diffusion coefficient, $m^2/s$

$i_{lv}$ Latent heat, kJ/kg

Subscripts

Cu copper

t total

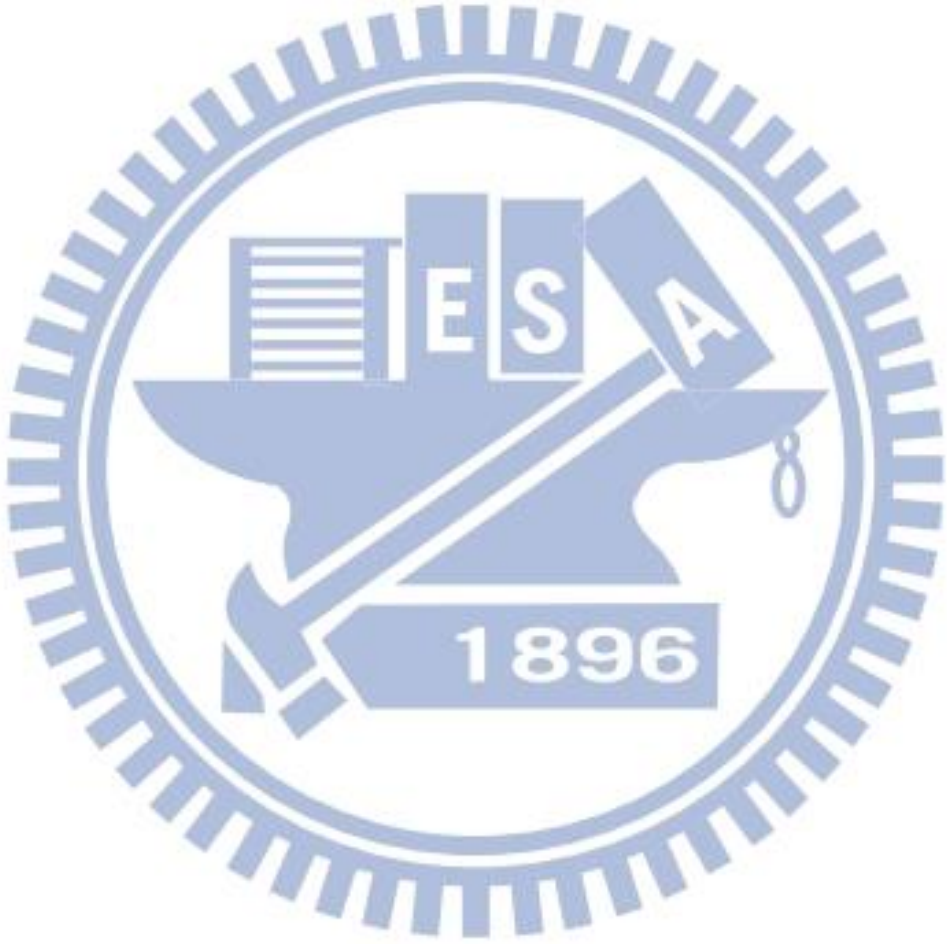

# CHAPTER 1

# INTRODUCTION

## 1.1 Motive of the Present Study

Recent significant technological advances in electronics industry have led to a rapid miniaturization of integrated circuits. Consequently, the power dissipation density in various micro processors increases significantly during their normal operation. How to effectively remove the large amount of dissipating heat from the processors poses a great challenge to heat transfer research community. In order to transfer the large quantity of the dissipating heat from the chips with an ultra high microelectronic component density, highly efficient heat transfer methods are required to control their temperatures at allowable level. Although air cooling has been used commonly today over a long period of time, this method has reached its upper performance limit and is unable to solve the cooling problems encountered in the current electronics industry [1]. Therefore, cooling techniques have to be improved and heat transfer systems with better efficiency have to be used. Cooling based on liquid convection and liquid-vapor phase-change heat transfer have been considered. Among these, boiling heat transfer is regarded as one of the most effective methods in electronics cooling comparing with the methods based on single-phase heat transfer because of the exchange of latent heat involved in the boiling processes. Methods to further improve the boiling heat transfer are therefore of great interest.

Over the past decades a number of passive boiling heat transfer enhancement methods have been proposed by modifying geometrical structure of the heated surface such as adding the micro-structures, pin fins and grooves to the surfaces. Significant pool boiling heat transfer enhancement can be obtained. Besides, coating the surfaces with particles and covering the surfaces with screens have been known to be effective. These enhancement methods are based

on various forms of extended surface fixed firmly onto the surfaces or directly fabricated on the surfaces. Moreover, some active boiling heat transfer enhancement methods such as vibrating and rotating working fluids and/or heated surface by external forces were suggested. These methods are very effective. But they are not welcome because the need to use external force. In the present study, enhancement of FC-72 pool boiling heat transfer by placing a large number of movable small solid particles above a heating plate will be explored. The particles can be moved violently by the vigorous motion of the bubbly flow in the pool boiling on one end. On the other end, the violently moving particles can increase the bubble departing rate from the heated surface and the turbulence level of the boiling flow. These mutual interactions of the particles and bubbly flow can be beneficial in promoting the boiling heat transfer from the heated surface. However, the presence of a large number of the particles can impede the bubble departure from the heated surface and liquid inrush to the surface. This in turn will retard the boiling heat transfer. In the present investigation we intend to delineate the ranges of experimental parameters over which boiling heat transfer can be enhanced by the moving particles.

The working fluid FC-72 is a dielectric fluorocarbon liquid manufactured by the 3M Company and gains popularity in electronics cooling application. It not only has suitable phase-change temperature for thermal control of I.C. components but also owns the quality that does not foul the boiling surface. Importantly, FC-72 has less impact on our environment than alternative liquids like chlorofluorocarbons or organic liquids. Copper has properties of better thermal conductivity than most metals and is often considered to be suitable for heat dissipating elements. Thus the heat transfer enhancement characteristics of pool boiling of the dielectric liquid on a copper plate by placing movable solid particles above the heated surface immersed in FC-72 liquid are explored in the present study. In an earlier study [2] we obtained significant enhancement in pool boiling heat transfer of FC-72 over a small horizontal heated copper plate by placing fine copper strings over the plate with their ends firmly fixed onto the

plate edges when the string length, size and height are suitably chosen.

## 1.2 Literature Review

In what follows the literature relevant to the present study is briefly reviewed. Pool boiling heat transfer is a process of vigorous heat transfer resulting from latent heat exchange associated with liquid-to-vapor phase change in a quiescent liquid. Nukiyama [3] conducted a pioneering pool boiling experiment in 1934 and arranged the experimental heat transfer data as a form of the wall superheat versus the heat flux, which is known as the "boiling curve" today. After that, the pool boiling heat transfer research has received considerable attention.

The state of the art cooling technologies for handling heat dissipation in microelectronic equipments have been developed extensively over the past 30 years. Several products were released including Air-Cooled Modules, High Thermal Conduction Modules, and Liquid-Cooled Modules, as discussed by Bar-Cohen [4].

In an early attempt to improve pool boiling heat transfer by using a micro-configured surface, Miller et al. [5] found that vapor retention could be a function of the scale and geometry of the micro-configurations. They pointed out that the relation between the stability of the potential nucleation sites and the micro-configuration size and geometry required further investigation, so that the size and the site density of the cavities could be optimized for boiling heat transfer enhancement.

Slightly later a few studies have been carried out to examine the influences of the surface fabricated microstructures on the pool boiling heat transfer. These include boiling of FC-72 on micro-porous surfaces with particle coating tested by Chang and You [6] and by Vemuri and Kim[7], adding micro-porous pin-fins and in the meantime coating particles to the surface investigated by Rainey and You [8,9], and fabricating micro-pin-fins and submicron-scale roughness on the surfaces by Honda et al. [10] and Wei et al. [11]. The study of Rainey and You [8, 9] concluded that the microporous coating can significantly enhance the boiling heat

transfer performance over the pin-finned surfaces. In examining the pool boiling on the micro-pin-fin surfaces, Honda et al. [10] and Wei et al. [11] noted that the boiling curves were characterized by that a very small increase in the wall superheat could cause a large increase in the heat flux. And increasing the fin height was found to provide better heat transfer in the nucleate boiling regime and result in a higher critical heat flux. Nucleation site interaction in pool boiling on an artificial surface was investigated by Zhang and Shoji [12] and by Yu et al. [13]. The hydrodynamic interaction can be also influenced by some factors, such as the liquid properties, subcooling, system pressure. The study of Yu et al. [13] concluded that the critical heat flux was dependent on the cavity density. The evaporation/boiling heat transfer regimes in the capillary wicking structures were identified and discussed by Li et al.[14] and Li and Peterson[15]. Anderson and Mudawar [16] reported that microstructures in the forms of fins, studs, grooves and vapor-trapping cavities on the boiling surface significantly shifted the boiling curve toward lower superheats while increasing the incipience excursion. Their results also suggest that the maximum boiling heat flux is a function of surface geometry and orientation but independent of the initial conditions, surface roughness, or the presence of large artificial cavities. Intending to augment boiling heat transfer, O'Connor and You [17] painted silver flakes on the boiling surface. Their experimental data show that the incipience boiling superheats are 70-85% lower and the nucleate boiling superheats are 70-80% lower than the bare surface. Besides, the critical heat flux is increased by 109%. O'Connor et al. [18] then compared two methods of generating surface microstructures, "spraying" and "painting", for pool boiling heat transfer enhancement. They noted that the incipient boiling superheat showed 33-55% reduction for the sprayed alumina and 63-85% reduction for the painted diamond. The enhancement in the critical heat flux can be up to 47% for the sprayed alumina and 103% for the painted diamond microstructures. Chang and You [19] further studied the effects of coating different sizes of the diamond particles on the pool boiling heat transfer performances. They classified the coating thickness into two groups. For coatings thinner than

100 μm, increasing the coating thickness would generate a higher active nucleation density. But for coatings thicker than 100 μm, a further increase in the coating thickness does not always enhance the pool boiling heat transfer. They attributed this result to higher impedance for liquid-vapor exchange channels and higher thermal resistance for the thicker coating. Jung and Kwak [20] investigated the effects of submicron-scale roughness on the subcooled boiling heat transfer over a boiling surface anodized in DMF (dimethylforamide) and HF (hydrofluoric acid). Both surface treatments were found to increase the effective boiling area and served for increasing the nucleation sites and hence showed considerable enhancement in the boiling heat transfer. The critical heat flux also increases linearly. Honda and Wei [21] reviewed recent advances in enhancing boiling heat transfer from electronic components immersed in dielectric liquids through the use of surface microstructures and concluded that most of the surface microstructures were effective in decreasing the wall superheat at the boiling incipience. The nucleate boiling heat transfer also can be improved and the critical heat flux is raised. Rainey and You [22] and Rainey et al. [23] respectively studied the effects of the orientation and pressure on the pool boiling heat transfer from microporous surface. Their data show that nucleate boiling performance increases slightly for the surface inclined from $0^{o}$(horizontal) to $45^{o}$ and then decreases for the inclination angle ranging from $90^{o}$ to $180^{o}$. Moreover, for the plain and microporous surfaces increases in boiling performance and critical heat flux and decrease in the incipience wall superheat were noted as the pressure increased.

Chou et al. [24] arranged several grooved patterns on surfaces intending to enhance boiling heat transfer of distilled water. Their experimental data reveal that the radial grooved pattern has the best enhanced boiling heat transfer performance and the spiral or concentric grooved pattern has poorer boiling heat transfer coefficient. The worst performance is noted for the grid or the spotted grooved pattern. All grooved patterns they investigated have better heat transfer performance than the plain surface and the denser groove is better than the sparser one for the same patterns.

Hasegawa et al. [25] covered a heat pipe with a woven screen to investigate the associated boiling characteristics and burnout phenomena. Their results disclose that the additional screen produces two opposite effects of inhibiting and enhancing the boiling heat transfer. Tsay et al. [26] explored pool boiling heat transfer enhancement by covering the boiling surface with a screen in distilled water. They found that the screen coverage could raise bubble generation frequency and enhance the boiling heat transfer. But the screen can also cover some nucleation sites and hence may retard the boiling heat transfer. They also noted that the boiling heat transfer became poorer at lowering the liquid level. They concluded that covering the heated surface with a screen could augment the pool boiling heat transfer if the mesh size was comparable with the bubble departure diameter. In boiling of methanol and HFE-7100, Liu et al. [27] pointed out that placing a fine mesh layer on the boiling surface enhanced nucleate boiling heat transfer at low wall superheat ($\Delta T_{sat}$<10K) but an opposite trend resulted at a high superheat ($\Delta T_{sat}$>10K). They also reported that the heat transfer in nucleate boiling always became worse with a coarse mesh on the boiling surface when compared with that on a smooth surface. Moreover, Franco et al. [28] used dielectric refrigerant R141b to investigate enhancement in the boiling heat transfer performance by covering the heated surface with wire meshes. The boiling heat transfer coefficient was noted to increase significantly, especially at relatively low heat fluxes. They also found that the wire mesh coverage on the heating surface resulted in slower transition to steady film boiling. In studying the effects of the wall superheat and the mesh layer covering on boiling heat transfer, Kurihara and Myers [29] tested several working fluids including water, acetone, n-hexane, carbon tetrachloride, and carbon disulfide. They found that active nucleation sites on the heating plate increased due to the mesh covering and the boiling heat transfer coefficient was proportional to the one-third power of the bubble column numbers at high numbers.

Shi et al. [30] investigated pool boiling heat transfer in liquid saturated particle bed and fluidized bed of distilled water. The tests were conducted for glass beads, steel ball, find sand

and $Al_2O_3$ particles. They showed that boiling heat transfer could be enhanced greatly by adding the solid particles into the liquid whether in fixed particle bed or in fluidized particle bed. The boiling heat transfer enhancement is closely related to the particle size ($d_p$=0.5, 1.0 and 2.0 mm), initial bed depth ($H_p$=3.0, 6.5, 9.5 and 13.4 mm) and heat flux applied. The best heat transfer enhancement is 120% for the particles diameter $d_p$=1.0 mm and bed height $H_p$=9.5 mm. A similar study was conducted by Matijevic et al. [31] using lead spheres to cover a heating surface. The spheres were packed as closely as possible into a single layer. They noted that boiling heat transfer from the heating surface to water could be enhanced substantially by the metallic spheres (d=3.0, 3.5, 3.6, 4.0 and 4.5 mm), and the smaller spheres resulted in a better enhancement of boiling heat transfer.

Heat transfer enhancement by employing nanofluids has become very popular recently. In nanofluids a very large number of nano particles (diameters smaller than 100 nm) are added into a working fluid which is considered to significantly increase thermal conductivity of the fluid. Wen and Ding [32] reported an enhancement of boiling heat transfer coefficient for about 40% with alumina water based nanofluids. On the other hand, by using the same nanoparticles in the same fluid, Bang and Chang [33] found that the boiling heat transfer coefficient deteriorated for about 20% when the nanoparticles are added.

Some active techniques to enhance boiling heat transfer were also proposed in the literature. Jeong and Kwon [36] found that the CHF augmentation in pool boiling of water due to ultrasonic vibration was closely related to its effects on the process of bubble generation and its departure. They noted that the rate of increase in CHF for downward facing surface ranged from 87~126% as the water subcooling varied from 5 to 40℃. Cipriani et al. [37] imposed electric field on pool boiling of FC-72 over a heated platinum wire (d=0.1 and 0.2 mm)and found that the boiling heat transfer was strongly influenced by the presence of the electric field at a low wire superheat. An increase of the boiling heat transfer coefficient up to 400% was encountered with the maximum applied voltage. But it is almost unaffected by electrical force

at high wire superheat. Through heated surface vibration, Navruzov et al. [38] demonstrated that boiling heat transfer of ethanol could be substantially enhanced at low imposed heat flux. The amplitude of the surface vibration is found to be a governing parameter for heat transfer enhancement at low-frequency vibrations. Besides, the vibration of the heat transfer surface significantly alters the heat transfer process both in subcooled boiling and in free convection. The single-phase heat transfer curves are 70-80% above the basic curve at increasing heat loads.

## 1.3 Objective of Present Study

The above literature review clearly reveals that considerable works have been carried out in the past to investigate the enhancement in the pool boiling heat transfer over a surface by passive methods through fabricating surface microstructures such as roughness and micro-pin-fins and by covering the surface with mesh screens and particle coating. All these microstructures are fixed firmly onto the boiling surface. Besides, some effective active heat transfer augmentation methods such as vibrating or rotating heating surface and/or fluid and applying electric field to vibrate a heating surface have been suggested. In this study, an experimental study is conducted to explore the possible enhancement in the FC-72 pool boiling heat transfer by placing movable metallic particles on the boiling surface. The violent motion of the bubbles in the boiling flow can significantly move the particles. The particles, in turn, can greatly affect the bubble dynamics near the surface. Thus we expect the boiling heat transfer from the surface can be enhanced by the particles. The method proposed here is passive in nature. However, it behaves like an active heat transfer enhancement method.

# CHAPTER 2

# EXPERIMENTAL APPARATUS AND PROCEDURES

A schematic arrangement of the experimental apparatus for the present investigation of the pool boiling heat transfer enhancement by movable metallic particles driven by the boiling flow is similar to that employed in the previous study [2] and is shown in Fig. 2.1. The experimental system includes a main test chamber, a test heater assembly, and other auxiliary parts such as a D.C. power supply, a data acquisition unit and a high-speed photographic unit. The working fluid, FC-72, is a highly wetting dielectric fluorocarbon liquid produced by 3M Industrial Chemical Products Division, which has been considered as a good candidate fluid for liquid immersion cooling applications. It is chemically stable, dielectric, and has a relatively low boiling point ($T_{sat}$=56°C at atmospheric pressure). Some thermophysical properties of FC-72 are given in Table 2.1.

## 2.1 Main Test Chamber

The main test chamber is a hermetic stainless steel pressure vessel of 205 mm in height and 216 mm in diameter. An internal water condenser is installed inside the chamber and connects with a thermostat (LAUDA RK20) to maintain the bulk temperature of the working fluid in the chamber at the preset level. The maximum cooling power of the thermostat is 180W (at 20°C). We further use an external temperature controller (FENWAL MYSPEC Digital Temperature Controller) to control the bulk temperature of FC-72 in the test chamber with an accuracy of ± 0.1°C. Besides, a cartridge heater is located near the bottom of the test chamber to provide additional heating during the degassing process. In order to prevent the heat

loss from the vessel to the ambient, a superlon layer of 10-mm thick is wrapped around the chamber. Moreover, a pressure transducer with an operating range of 0-200 kPa is located at the gate valve to measure the pressure of the work fluid. Meanwhile, the working fluid temperature is measured by two resistance temperature detectors (RTDs) located at the gate valve and at a selected location 5 cm above the bottom surface of the chamber with a calibrated accuracy of $\pm 0.1$°C. An auxiliary tank of 10-liter liquid FC-72 is placed right above the test vessel and it is only used for subcooled pool boiling experiment to prevent regassing of the working fluid after degassing. A pressure transducer and a RTD are placed in the auxiliary tank to measure the internal gas pressure and liquid temperature. In addition, a test heater assembly is mounted to a stainless steel shelf to fix the PEEK substrate. The working fluid is maintained at approximately 80 mm above the heated surface in the experiment.

## 2.2 Test Heater Assembly

A schematic of the test heater assembly is shown in Fig. 2.2. The assembly consists mainly of a film heater and it is adhered to the lower surface of a square copper plate by epoxy Omegabond 200. The plate is 10 mm thick with 30x30 $mm^2$ in surface area. The heater supplies the required power input to the copper plate. The copper plate is flush mounted onto a much larger PEEK (Polyether Ether Ketone) block. Liquid FC-72 boils on the upper surface of the copper plate. More specifically, the copper plate is heated by D.C. current delivered from a D.C. power supply to the film heater. Besides, three calibrated copper-constantan thermocouples (T-type) with a calibrated accuracy of $\pm 0.2$°C are installed at selected locations in the copper plate right below the boiling surface. They are used for the control and determination of the

boiling surface temperature. The detailed locations of the thermocouples installed in the copper plate are shown in Fig. 2.3. Note that the whole copper plate is inserted into a PEEK block which serves as a heat insulator ( $k_T \approx 0.25 \mathrm{W/m \cdot K}$ ), intending to reduce the heat loss from the lateral and bottom surfaces of the plate to the ambient. Besides, the locations of thermocouples in the PEEK block are shown in Fig. 2.4.

## 2.3 Confinement of Particles and Experimental Parameters

Solid particles of the same material and uniform size are placed freely on the upper surface of the copper plate, as schematically shown in Fig. 2.5. In order to insure that the particles would not be blown away by the vigorous motion of the bubbles, we install an acryl fence of 2-cm high and 1-cm thick around the edges of the heating copper plate. In the present study tests will be conducted for copper and stainless steel (type304) particles. The densities of copper and stainless steel are measured before the experiment with $\rho_{cu} = 8990\ kg/m^3$ and $\rho_{ss} = 7984\ kg/m^3$. These two kinds of metallic particles are chosen here because the copper and stainless steel have much higher densities than liquid FC-72. Besides, the chosen particles should not be too small so that they float in the liquid above the plate and do not contact the heating surface. Moreover, they should not be too large and cannot be moved by the boiling flow. Here, the particle diameter is selected to be 1.0 and 1.5 mm. The chosen particle size and number for the cases tested here are summarized in Table 2.2. The measured data expressed in terms of boiling curves and boiling heat transfer coefficients will be compared with that of a bare heating surface.

## 2.4 DC Power Supply

The power generated in the film heater in the test heater assembly is provided

by a programmable D.C. power supply (Gpc 3030D). It offers a maximum D.C. power of 180W for an output voltage of 60V and an output current of 3A. The power input to the copper block is transmitted through a GPIB interface to a personal computer. In order to measure the D.C. current, a precision ammeter (KYORITSU A.C./D.C. DIGITAL CLAMP METER) is arranged in series connection with the electric circuit. Besides, a YOKOGAWA data recorder is used to measure the voltage drop across the test heater assembly. All the voltage, current and power measurement devices are calibrated by a YOKOGAWA WT200 power meter according to the Center of Measurement Standards in Industrial Technology Research Institute of Taiwan.

## 2.5 Data Acquisition

A 20-channel YOKOGAWA data recorder (MX-100) combined with a personal computer is used to acquire and process the data from various transducers. All signals detected from the T-type thermocouples, RTDs, pressure transducer, ammeter, data recorders and power meter are all collected and converted by the internal calibration equations in the computer during the data acquisition.

## 2.6 Optical Measurement Technique

A high-speed camera along with a microscope is installed in front of the observation window to observe the boiling activity in the flow. The photographic apparatus consists mainly of a high speed digital video camera (IDT High-speed CMOS Camera), a micro-lens (Optem Zoom 16), and a three-dimensional positioning mechanism. The high-speed motion analyzer can take photographs up to 143,307 frames/sec. In the present experiment the recording rate is 1000 frames/sec. After the

experimental system reaches a statistical state, we start capturing the images of the particles and bubbles in the boiling flow. Besides, we store and display the images in the personal computer through an image-capturing software.

## 2.7 Experimental Procedures

The boiling surface is polished by fine sand paper (Number 3000, 2000 and 1000) and cleaned by ethyl alcohol before each experimental run. In each test, we place the chosen metallic particles on the heated plate. Besides, we remove non-condensable gases existing in the empty test chamber by running a vacuum pump for about 15 minutes and then fill the FC-72 liquid into the chamber until the liquid level is higher than the heating plate for about 8 cm. Next, the FC-72 liquid in the test chamber is heated to the saturation state which is detected and maintained by a digital temperature controller. Moreover, the FC-72 liquid is boiled vigorously for 1 hour to further remove the dissolved non-condensable gases in it. After the working fluid pressure and temperature stabilize to one atmosphere and at the saturation state, we turn on the test heater. The imposed heat flux on the boiling surface is adjusted by controlling the electric current delivered to the heater from the D.C. power supply. Upon reaching the statistical state, we begin collecting the required heat transfer data and visualizing the boiling activity. Effects of the particle material, size and number density on the possible heat transfer enhancement are investigated in the experiment.

Table 2.1 Thermophysical properties of FC-72.

| **Properties at 25°C** | **FC-72** |
|---|---|
| Appearance | Clear, colorless |
| Average Molecular Weight | 338 |
| Boiling Point (1atm) | 56°C |
| Pour Point (1atm) | -90°C |
| Estimated Critical Temperature | 449K |
| Estimated Critical Pressure | $1.83 \times 10^6$ Pa |
| Vapor Pressure | $3.09 \times 10^4$ Pa |
| Latent Heat of Vaporization $h_{fg}$ (at normal boiling point) | 88 J/g |
| Liquid Density $\rho_\ell$ | 1680 kg/m$^3$ |
| Absolute Viscosity $\mu$ | $6.4\times 10^{-3}$ poises ; $6.4\times 10^{-4}$ kg/m·s |
| Kinematic Viscosity $\nu$ | $3.8 \times 10^{-3}$ stokes ; $3.8 \times 10^{-7}$ m$^2$/ s |
| Liquid Specific Heat $c_p$ | 1100 J/kg·°C |
| Liquid Thermal Conductivity $k$ | 0.057 W/m·°C |
| Coefficient of Expansion $\beta$ | 0.00156 /°C |
| Surface Tension $\sigma$ | 10 dynes/cm ; $10^{-2}$ N/m |

Table 2.2 Cases covered in present study

| Particle | $N_p$ | Particle | $N_p$ |
|---|---|---|---|
| Copper ($d_p$=1.0 mm) | 100 | Stainless steel ($d_p$=1.0 mm) | 200 |
| | 200 | | 400 |
| | 300 | | 600 |
| | 400 | | 800 |
| | 500 | | 1000 |
| | 600 | | 1200 |
| | 700 | | 1400 |
| | 800 | | 1600 |
| | 900 | | 1800 |
| | 1000 | Particle | $N_p$ |
| | 1100 | Stainless steel ($d_p$=1.5 mm) | 200 |
| | 1200 | | 400 |
| | 1400 | | 600 |
| | 1600 | | 700 |
| | 1800 | | 800 |
| Copper ($d_p$=1.5 mm) | 100 | | |
| | 200 | | |
| | 300 | | |
| | 400 | | |
| | 500 | | |
| | 600 | | |
| | 700 | | |

| | |
|---|---|
| | 800 |

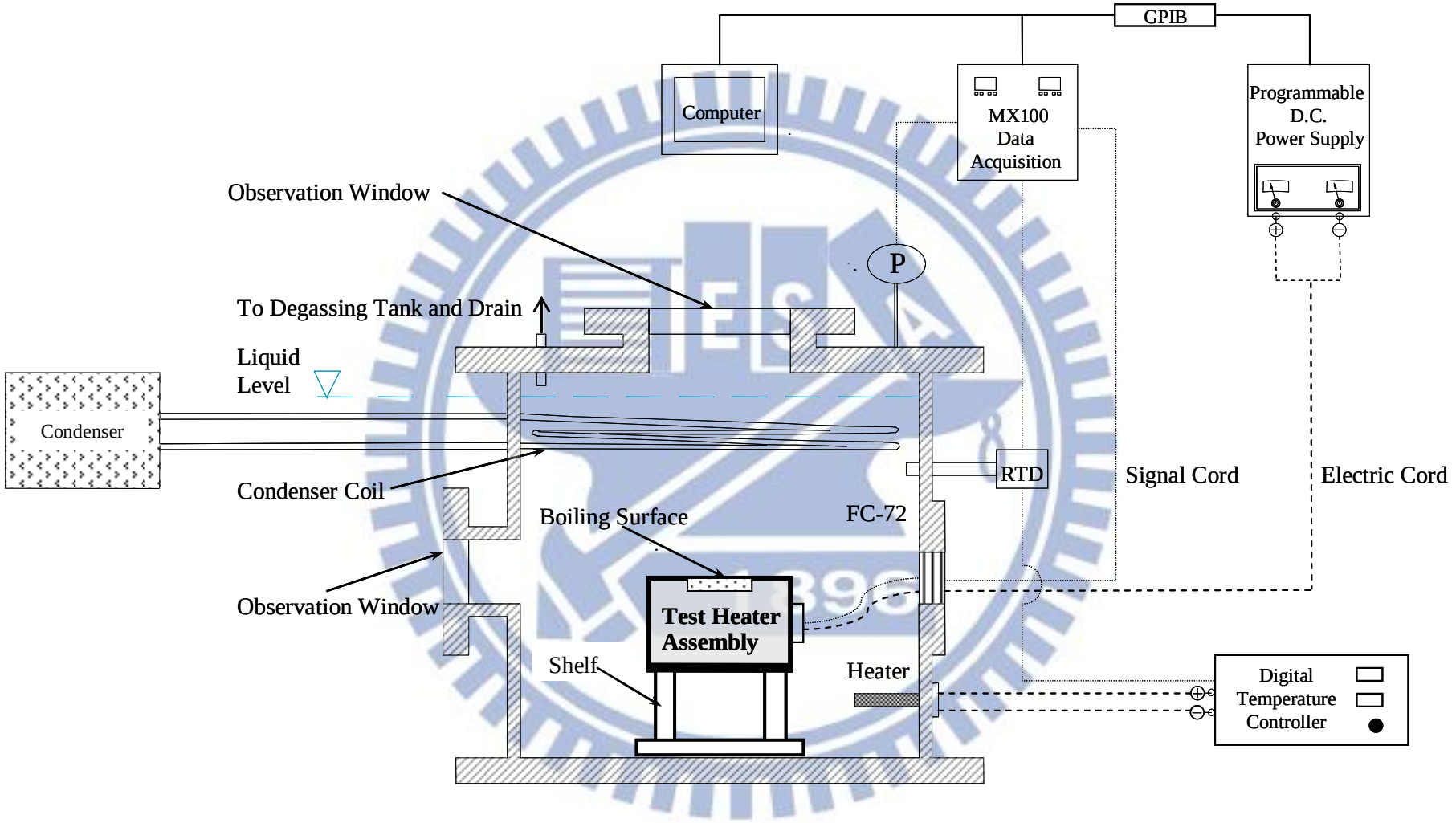


Fig. 2.1 Schematic diagram of the test apparatus.

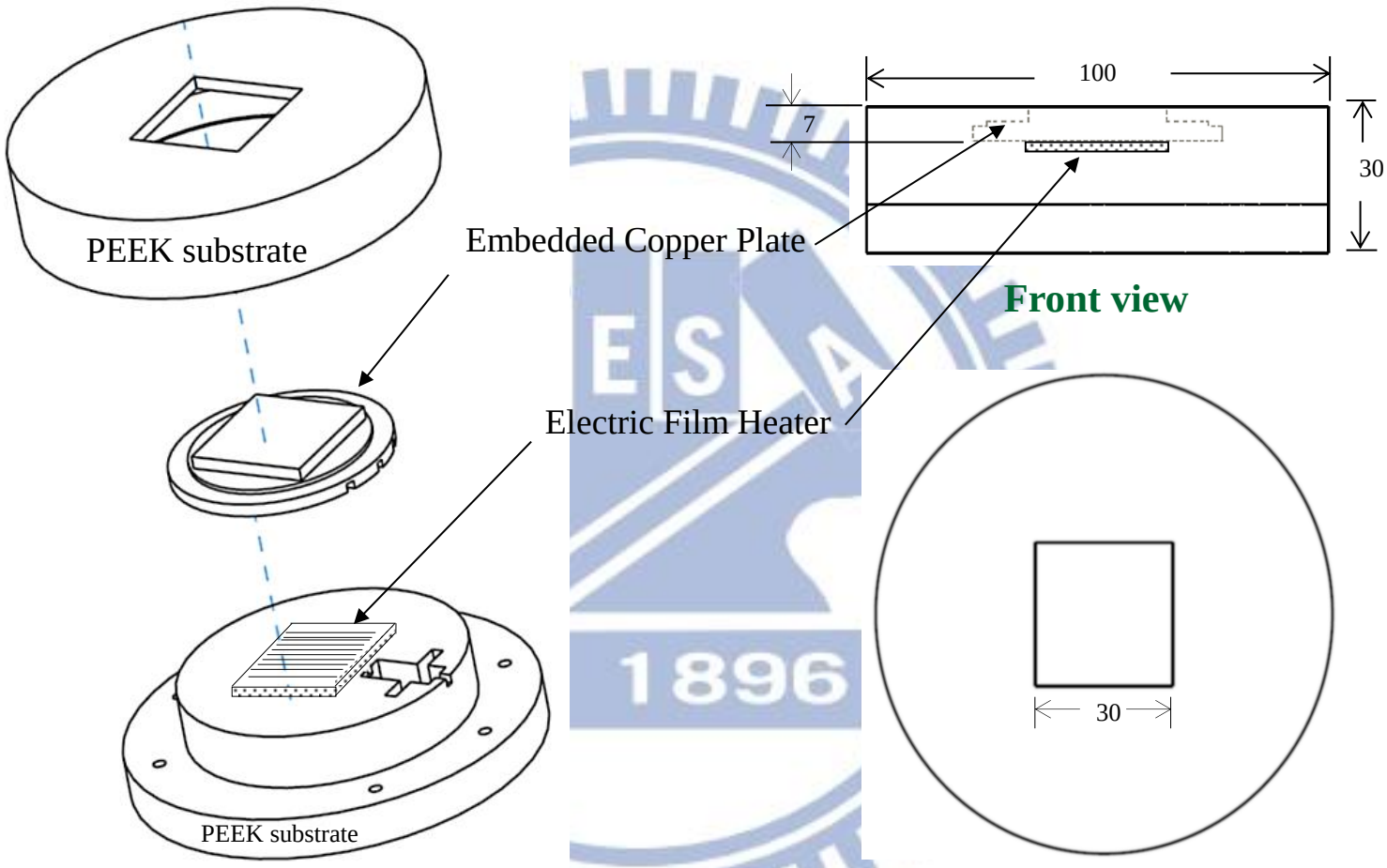


Fig. 2.2 Schematic diagram of the test heater assembly (not to scale).

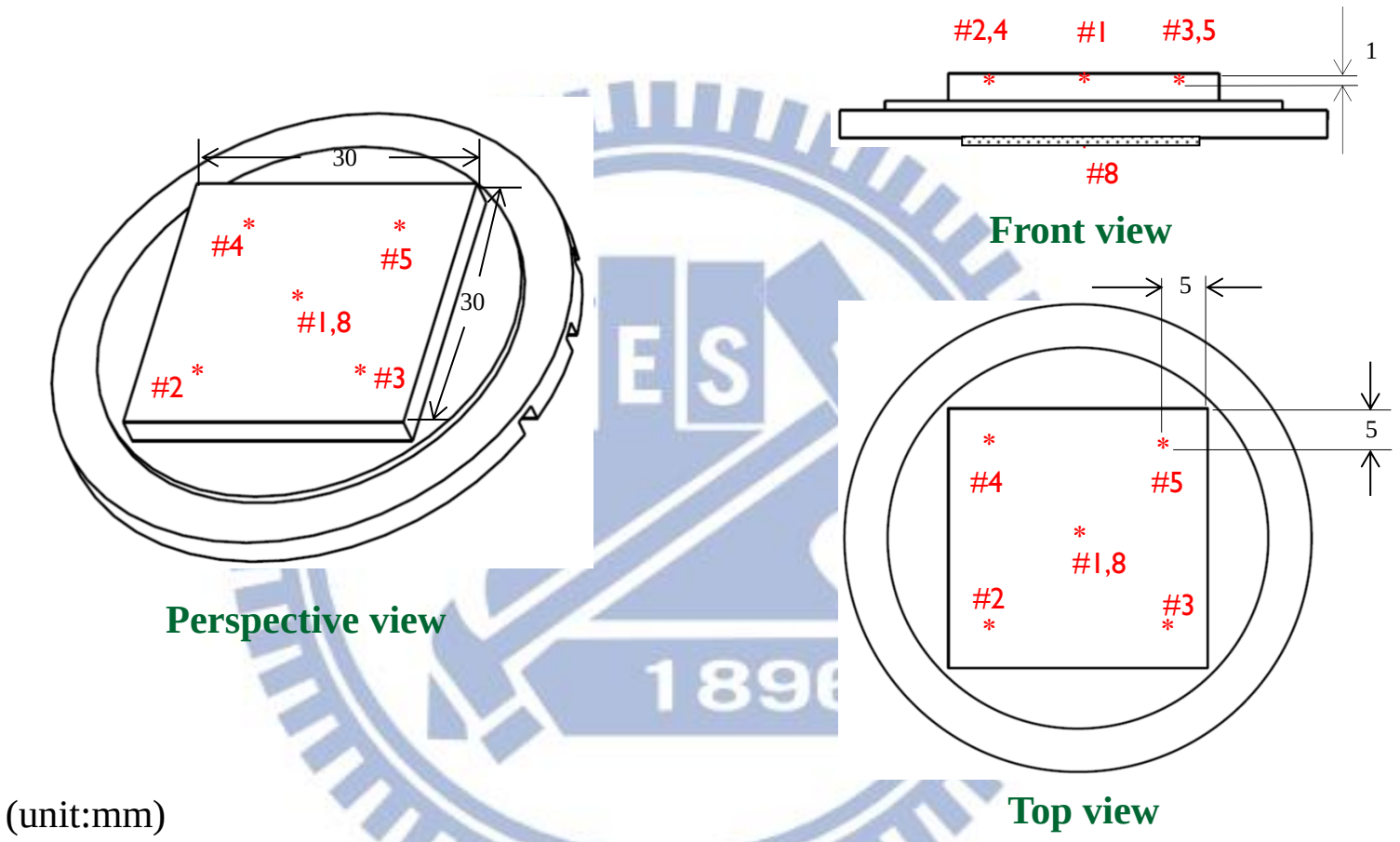


Fig. 2.3 Locations of three thermocouples in the copper plate and one thermocouple below the heater (not to scale).

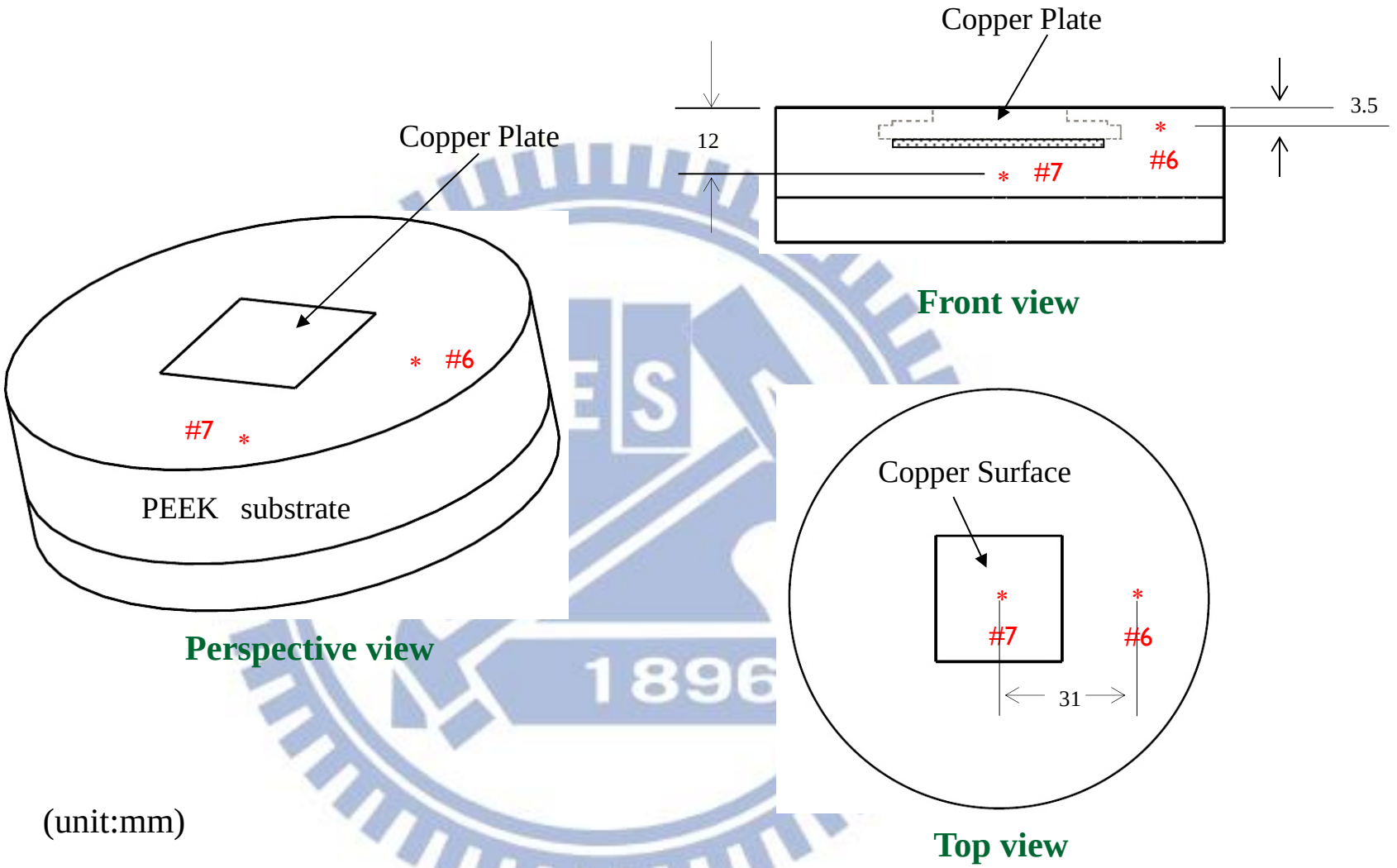


Fig. 2.4 Locations of two thermocouples in the PEEK (not to scale).

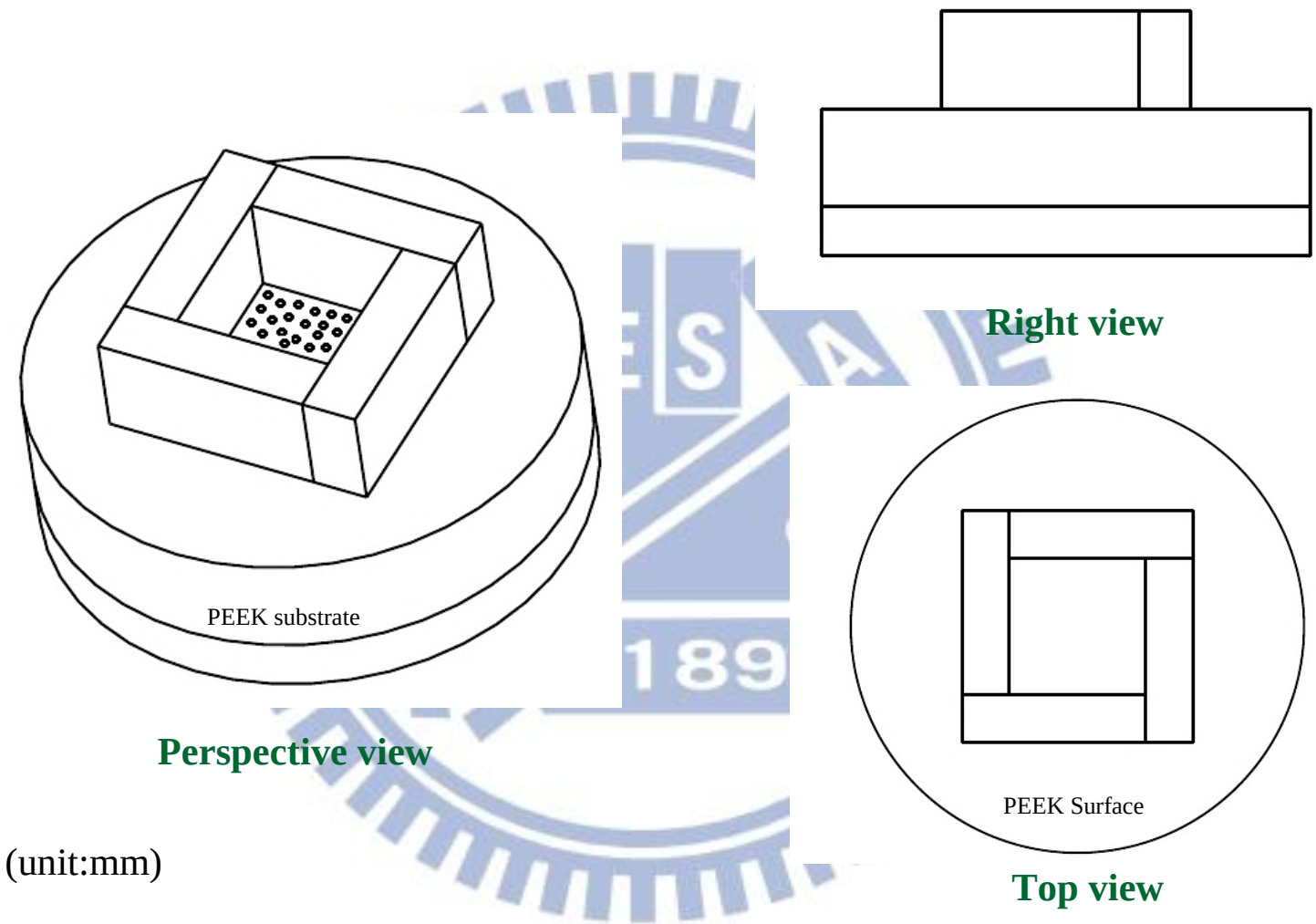


Fig. 2.5 Schematic diagram of placing movable particles on heating surface with acryl rectangular enclosure (not to scale).

# CHAPTER 3

# DATA REDUCTION

## 3.1 Boiling Heat Transfer Coefficient

The space-average natural convection and boiling heat transfer coefficients over the upper surface of the heated square copper plate when the flow is at a statistical state are both defined as

$$h = {}^{q_n}/_{\Delta T_w} \tag{3.1}$$

where $q_n$ is the net heat flux imposed on the upper surface and $\Delta T_{sat}$ is the wall superheat defined as the difference between the average surface temperature and the saturated temperature of FC-72. The average heated surface temperature $T_w$ is estimated from the measured average temperature from the thermocouples installed at different locations near the upper surface of the copper plate according to the steady-state one-dimensional conduction heat transfer. Specifically,

$$T_w = T_{Cu} - \left( q_n \times \frac{\delta}{k_{Cu}} \right) \tag{3.2}$$

where

$T_{Cu}$ = the average measured temperature from the thermocouples (°C)

$k_{Cu}$ = the thermal conductivity of copper (W/m·K)

$\delta$ = the vertical distance between the thermocouple tips and the upper surface of the copper plate (m)

The total power input $Q_t$ to the copper plate can be obtained from the measured voltage drop across the film heater in the test heater assembly and the current passing through it,

$$Q_t = I \cdot V \tag{3.3}$$

where

$Q_t$ = total power input to the upper surface of the copper plate (W)

$I$ = electric current passing through the film heater (Amp.)

$V$ = voltage drop across the film heater (Volts)

The substrate of the test section is made from PEEK, which have a much lower thermal conductivity ($k_T \approx 0.25 \mathrm{W/m \cdot K}$) than the copper ($k \approx 386 \mathrm{W/m \cdot K}$). In evaluating total heat loss from the heater assembly, we focus on heat transfer from the heater and copper plate surface to the PEEK. Figures 2.3 and 2.4 are the schematic diagrams of the thermocouples buried in the copper plate and PEEK. The heat dissipation model used to estimate the heat loss is shown in Fig. 3.1, and the total heat loss can be estimated as follows:

$$Q_{loss} = k_p \cdot \frac{(T_8 - T_7)}{L_1} \cdot A_1 + 4 \cdot k_p \cdot \frac{(T_{Cu} - T_6)}{L_2} \cdot A_2 + \frac{2\pi \cdot k_p \cdot L_3 \cdot (T_{Cu} - T_6)}{\ln(\frac{r_6}{r_{Cu,2}})} + \frac{2\pi \cdot k_p \cdot L_4 \cdot (T_{Cu} - T_6)}{\ln(\frac{r_6}{r_{Cu,3}})} + k_p \cdot \frac{(T_{Cu} - T'_5)}{L_5} \cdot A_5 + k_p \cdot \frac{(T_{Cu} - T'_6)}{L_6} \cdot A_6 \tag{3.4}$$

where

$T_6$, $T_7$, $T_8$: the average measured temperatures at the measured locations inside the PEEK insulator, as schematically shown in Figs. 2.3 & 2.4

$L_1$, $L_2$, $L_3$, $L_4$, $L_5$, $L_6$: shortest distances between locations No.1~No.6 and the film heater or copper plate (m)

$A_1$, $A_2$, $A_3$, $A_4$, $A_5$, $A_6$: bottom and lateral surface areas of the copper plate

$T'_5$, $T'_6$: these two temperatures are calculated by using interpolation method based on $T_6$, as schematically shown in Fig. 3.2

Finally, the net imposed input heat flux to the upper surface of copper plate can be evaluated from the relation

$$q_n = \frac{Q_t - Q_{loss}}{A_{Cu}} \tag{3.5}$$

where $A_{Cu}$ is the area of the upper surface of the copper plate.

## 3.2 Uncertainty Analysis

An uncertainty analysis is carried out here to estimate the uncertainty levels in the experiment. Kline and McClintock [34] proposed a formula for evaluating the uncertainty in the result $F$ as a function of independent variables, $X_1, X_2, X_3 \cdots\cdots\cdots X_n$,

$$F=F\ (X_1, X_2, X_3 \cdots\cdots\cdots X_n) \tag{3.6}$$

The absolute uncertainty of $F$ is expressed as

$$\delta F = \left\{ \left[ \left( \frac{\partial F}{\partial X_1} \right) \delta X_1 \right]^2 + \left[ \left( \frac{\partial F}{\partial X_2} \right) \delta X_2 \right]^2 + \left[ \left( \frac{\partial F}{\partial X_3} \right) \delta X_3 \right]^2 + \cdots + \left[ \left( \frac{\partial F}{\partial X_n} \right) \delta X_n \right]^2 \right\}^{\frac{1}{2}} \tag{3.7}$$

and the relative uncertainty of $F$ is

$$\frac{\delta F}{F} = \left\{ \left[ \left( \frac{\partial \ell nF}{\partial \ell nX_1} \right) \left( \frac{\delta X_1}{X_1} \right) \right]^2 + \left[ \left( \frac{\partial \ell nF}{\partial \ell nX_2} \right) \left( \frac{\delta X_2}{X_2} \right) \right]^2 + \left[ \left( \frac{\partial \ell nF}{\partial \ell nX_3} \right) \left( \frac{\delta X_3}{X_3} \right) \right]^2 + \cdots + \left[ \left( \frac{\partial \ell nF}{\partial \ell nX_n} \right) \left( \frac{\delta X_n}{X_n} \right) \right]^2 \right\}^{\frac{1}{2}} \tag{3.8}$$

If $F = X_1^a X_2^b X_3^c \ldots\ldots$ , then the relative uncertainty is

$$\frac{\delta F}{F} = \left\{ \left[ a \left( \frac{\delta X_1}{X_1} \right) \right]^2 + \left[ b \left( \frac{\delta X_2}{X_2} \right) \right]^2 + \left[ c \left( \frac{\delta X_3}{X_3} \right) \right]^2 + \cdots\cdots \right\}^{\frac{1}{2}} \tag{3.9}$$

where $\frac{\partial F}{\partial X_i}$ and $\partial X_i$ are, respectively, the sensitivity coefficient and uncertainty level associated with the variable $X_i$. The values of the uncertainty intervals $\partial X_i$ are

obtained by a root-mean-square combination of the precision uncertainty of the instruments and the unsteadiness uncertainty, as recommended by Moffat [35]. The choice of the variable $X_i$ to be included in the calculation of the total uncertainty level of the result $F$ depends on the purpose of the analysis.

The uncertainties of the parameters in the present study are calculated as follows:

(1) Uncertainty of temperature difference, $\Delta T_w = T_w - T_{sat}$

$$\frac{\delta(T_w - T_{sat})}{(T_w - T_{sat})} = \left\{ \left[ \left( \frac{\partial \ell n(T_w - T_{sat})}{\partial \ell n T_w} \right) \left( \frac{\delta T_w}{T_w} \right) \right]^2 + \left[ \left( \frac{\partial \ell n(T_w - T_{sat})}{\partial \ell n T_{sat}} \right) \left( \frac{\delta T_{sat}}{T_{sat}} \right) \right]^2 \right\}^{\frac{1}{2}}$$

$$= \left\{ \left[ \left( \frac{T_w}{T_w - T_{sat}} \right) \left( \frac{\delta T_w}{T_w} \right) \right]^2 + \left[ \left( \frac{T_{sat}}{T_w - T_{sat}} \right) \left( \frac{\delta T_{sat}}{T_{sat}} \right) \right]^2 \right\}^{\frac{1}{2}}$$

$$= \left\{ \left[ \frac{\delta T_w}{T_w - T_{sat}} \right]^2 + \left[ \frac{\delta T_{sat}}{T_w - T_{sat}} \right]^2 \right\}^{\frac{1}{2}} \tag{3.10}$$

(2) Uncertainty of total power input, $Q_t$

$$Q_t = I \cdot V \tag{3.3}$$

and

$$\frac{\delta Q_t}{Q_t} = \left[ \left( \frac{\delta I}{I} \right)^2 + \left( \frac{\delta V}{V} \right)^2 \right]^{\frac{1}{2}} \tag{3.11}$$

(3) Uncertainty of net wall heat flux, $q_n$

$$q_n = \frac{Q_t - Q_{loss}}{A_{Cu}} \tag{3.5}$$

and

$$\frac{\delta q_n}{q_n}=\left\{\left[\left(\frac{\partial \ell n q_n}{\partial \ell n A_{Cu}}\right)\left(\frac{\delta A_{Cu}}{A_{Cu}}\right)\right]^2+\left[\left(\frac{\partial \ell n q_n}{\partial \ell n Q_t}\right)\left(\frac{\delta Q_t}{Q_t}\right)\right]^2+\left[\left(\frac{\partial \ell n q_n}{\partial \ell n Q_{loss}}\right)\left(\frac{\delta Q_{loss}}{Q_{loss}}\right)\right]^2\right\}^{\frac{1}{2}}$$

$$=\left\{\left[1\cdot\left(\frac{\delta A_{Cu}}{A_{Cu}}\right)\right]^2+\left[\left(\frac{Q_t}{Q_t-Q_{loss}}\right)\left(\frac{\delta Q_t}{Q_t}\right)\right]^2+\left[\left(\frac{Q_{loss}}{Q_t-Q_{loss}}\right)\left(\frac{\delta Q_{loss}}{Q_{loss}}\right)\right]^2\right\}^{\frac{1}{2}}$$

$$=\left\{\left[\frac{\delta A_{Cu}}{A_{Cu}}\right]^2+\left[\frac{\delta Q_t}{Q_t-Q_{loss}}\right]^2+\left[\frac{\delta Q_{loss}}{Q_t-Q_{loss}}\right]^2\right\}^{\frac{1}{2}} \tag{3.12}$$

Where

$$Q_{loss}=k_p\cdot\frac{(T_8-T_7)}{L_1}\cdot A_1+4\cdot k_p\cdot\frac{(T_{Cu}-T_6)}{L_2}\cdot A_2+\frac{2\pi\cdot k_p\cdot L_3\cdot(T_{Cu}-T_6)}{\ln(\frac{r_6}{r_{Cu,2}})}+\frac{2\pi\cdot k_p\cdot L_4\cdot(T_{Cu}-T_6)}{\ln(\frac{r_6}{r_{Cu,3}})}+k_p\cdot\frac{(T_{Cu}-T'_5)}{L_5}\cdot A_5+k_p\cdot\frac{(T_{Cu}-T'_6)}{L_6}\cdot A_6 \tag{3.4}$$

(4) Uncertainty of space-average heat transfer coefficient, *h*

$$h=q_n/\Delta T_{sat} \tag{3.1}$$

and

$$\frac{\delta h}{h}=\left\{\left[\left(\frac{\partial \ell n h}{\partial \ell n q_n}\right)\left(\frac{\delta q_n}{q_n}\right)\right]^2+\left[\left(\frac{\partial \ell n h}{\partial \ell n(T_w-T_{sat})}\right)\left(\frac{\delta(T_w-T_{sat})}{T_w-T_{sat}}\right)\right]^2\right\}^{\frac{1}{2}}$$

$$=\left\{\left[1\cdot\left(\frac{\delta q_n}{q_n}\right)\right]^2+\left[1\cdot\left(\frac{\delta T_w-T_{sat}}{T_w-T_{sat}}\right)\right]^2\right\}^{\frac{1}{2}}$$

$$=\left\{\left[\frac{\delta q_n}{q_n}\right]^2+\left[\frac{\delta T_w-T_{sat}}{T_w-T_{sat}}\right]^2\right\}^{\frac{1}{2}} \tag{3.13}$$

A summary of the results from the present uncertaintly analysis is given in Table 3.1.

Table 3.1 Summary of the results from the uncertainty analysis.

| **Parameter** | **Uncertainty** |
|---|---|
| Geometry | |
| Length & thickness (%) | ± 0.167% |
| Area (%) | ± 0.334% |
| Particle diameter (%) | ± 10% |
| Particle density(%) | ± 13.4% |
| Parameter measurement | |
| Temperature, $T$ (°C) | ± 0.2 |
| Temperature difference, $\Delta T_{sat}$ (°C) | ± 0.36 |
| System pressure, P (kPa) | ± 0.5 |
| Boiling heat transfer on the copper flat plate | |
| Total power input, $Q_t$ (%) | ± 5.9% |
| Imposed net heat flux, $q_n$ (%) | ± 8.3% |
| Heat transfer coefficient, $h$ (%) | ± 8.5% |

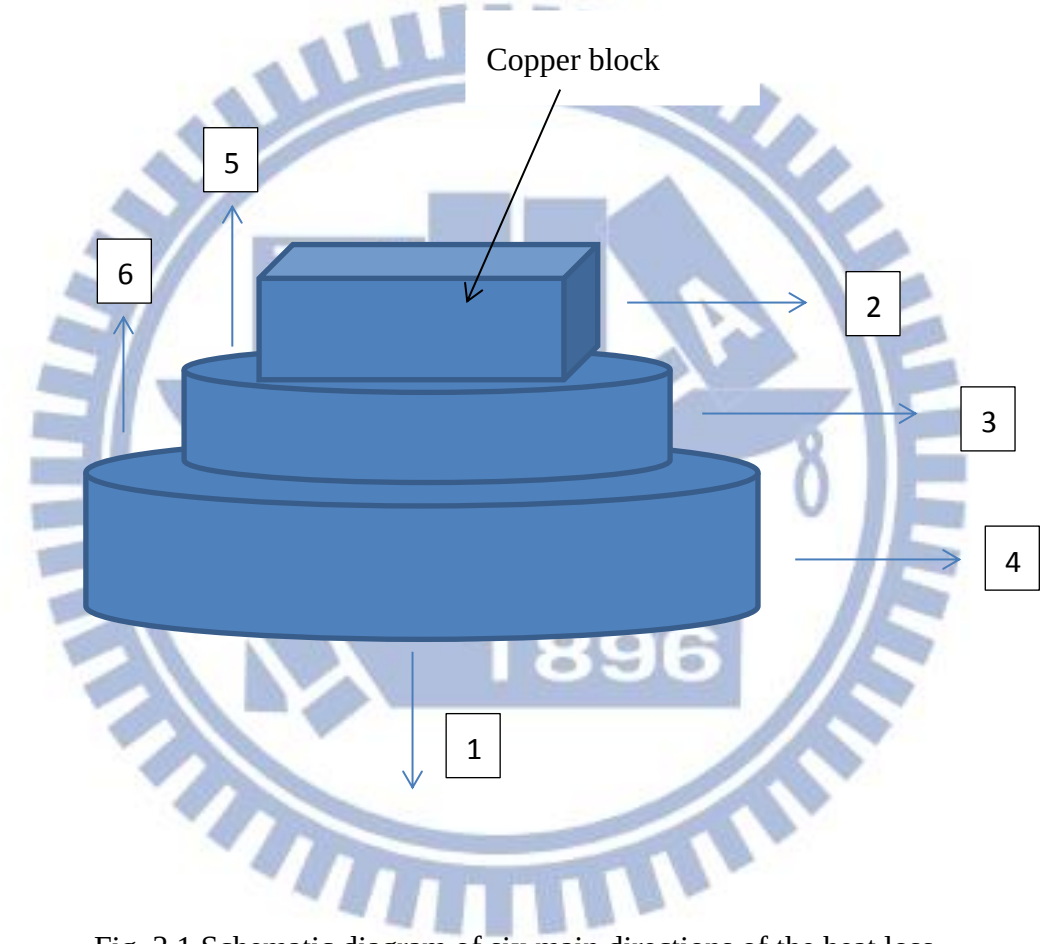


Fig. 3.1 Schematic diagram of six main directions of the heat loss.

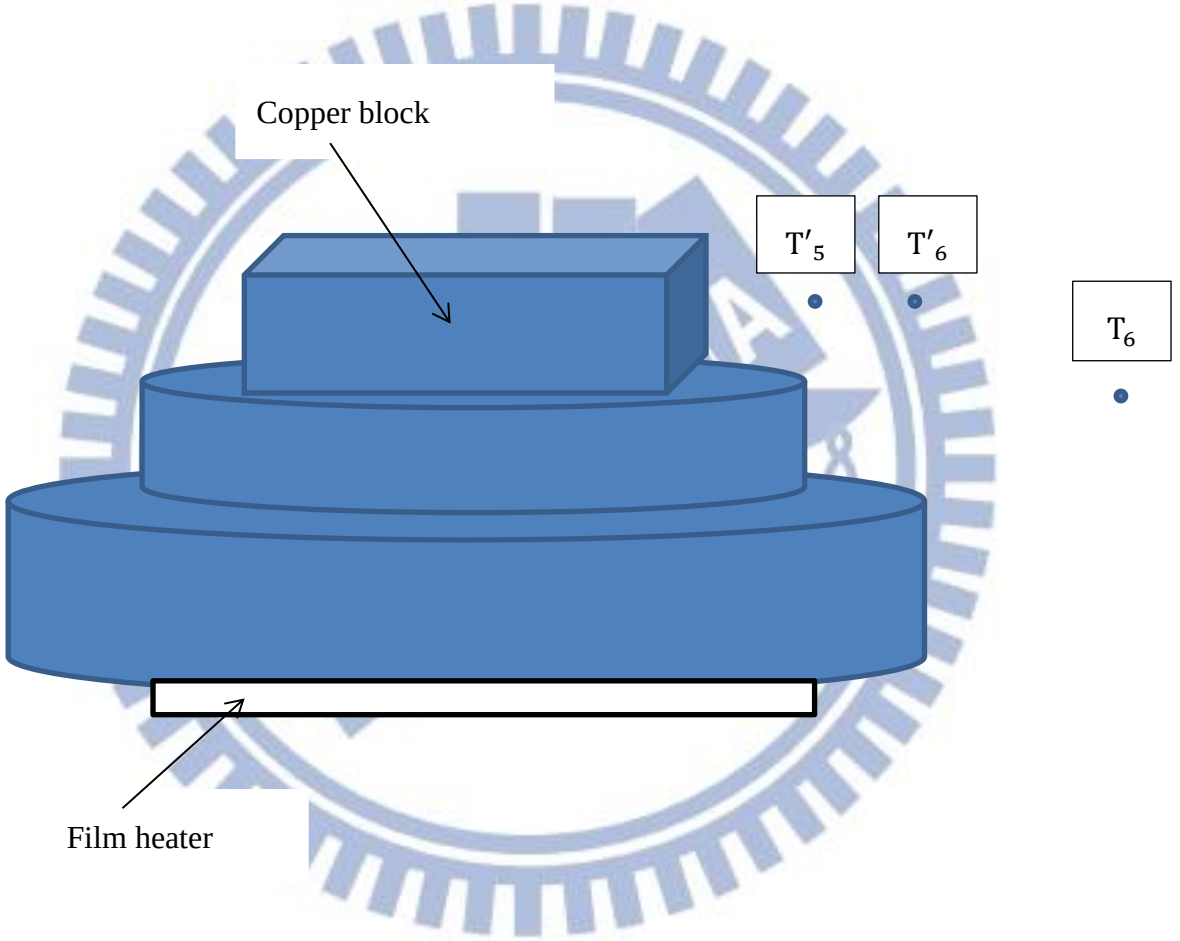


Fig. 3.2 Schematic diagram of T'$_5$ and T'$_6$

# CHAPTER 4

## POSSIBLE POOL BOILING HEAT TRANSFER ENHANCEMENT OF FC-72 OVER HEATED COPPER SURFACE

The experimental results to illustrate possible enhancement of saturated pool boiling heat transfer of FC-72 by placing movable particles on the heating surface obtained in the present study are examined in this chapter. The present experiments are carried out for the copper and stainless steel particles with the diameter of the particles $d_p$ fixed at 1.0 and 1.5 mm, and the total number of particles $N_p$ varied from 100 to 1800 for the particles with the diameter 1.0 mm or from 100 to 800 for the particles with the diameter 1.5 mm. The FC-72 liquid in the test chamber is maintained at saturated liquid state corresponding to the atmospheric pressure. Note that the maximum number of particles forming a single closely packed particle layer over the boiling surface $N_{pf}$ is 900 and 400 respectively for the particles with the diameter of 1.0 mm and 1.5 mm when each particle contact directly with neighboring particles. In the experiment tests are also conducted for the particle number well exceeds $N_{pf}$ and many particles are on top of the other particles. The measured data are presented in terms of the boiling curves and boiling heat transfer coefficients for various diameters and numbers of the copper and stainless steel particles and for a bare heating surface. Effects of the experimental parameters on the possible boiling heat transfer enhancement will be examined in detail. Selected data are presented in the following to illustrate the possible pool boiling heat transfer enhancement by the boiling flow driven metallic particles.

## 4.1 Single-phase Natural Convection Heat Transfer

Before conducting the pool boiling experiment, we first measure steady natural convection heat transfer of FC-72 liquid over the heated copper surface without the presence of any particles which prevails at low imposed heat flux, intending to verify the present experimental setup. The measured data for the natural convection heat transfer coefficient are compared with the empirical correlation of Radziemska and Lewandowski [39] in Fig. 4.1. Their correlation is

$$Nu_L=(2.1e^{-48W}+1.2)Ra_L^{0.2} \tag{4.1}$$

where w is the width of the heating plate (m). The correlation given in Eq.(4.1) is based on the data for a small horizontal plate heated from below for $10^5<Ra_L<10^8$. Note that the characteristic length L used in defining the dimensionless groups in the above equation is chosen to be the ratio of the heated surface area and its perimeter, and the Nusselt and Rayleigh numbers are respectively defined as

$$Nu_L = \frac{h\mathrm{L}}{k_\ell} \tag{4.2}$$

and

$$Ra_L = \frac{g\beta(\Delta T_{sat})\mathrm{L}^3}{\alpha\nu} \tag{4.3}$$

The results in Fig. 4.1 indicate that our natural convection data are in good agreement with that calculated from Eq. (4.1). Thus the experimental system established here is considered to be suitable for the present study.

## 4.2 Saturated Pool Boiling on Bare Copper Surface

To further verify the suitability of the present experimental system, the measured boiling curve for saturated pool boiling of liquid FC-72 on the bare heated copper plate is obtained next. These data are compared with that from Rainey and You [22] in Fig. 4.2 for pool boiling of FC-72 on a square copper plate of $5 \times 5$ cm$^2$ in

surface area. Note that the present data are in good agreement with theirs.

## 4.3 Effect of Surface Aging on Boiling over Bare Copper Plate

It is well known that the change of the boiling surface properties with time, the so called “aging effect”, can be significant in affecting the boiling heat transfer from a surface after the surface has been used over certain period of time. Obviously, the measured boiling heat transfer data for the cases with and without the presence of the particles on the surface can be meaningfully compared only when the surface aging effect is small. Thus tests are carried out here to investigate the aging effect of FC-72 liquid boiling on the present heated surface. The results show that the boiling curves and heat transfer coefficients measured over a time interval of 6 hours do not differ to a noticeable degree, as seen from Fig. 4.3. But a significant aging effect is found for an interval of 24 hours. Thus in the present experiment the boiling heat transfer data for the corresponding cases with and without the presence of particles on the surface are obtained within 6 hours.

## 4.4 Effects of Moving Copper Particles on Boiling Heat Transfer

Possible boiling heat transfer enhancement by particles moving on the heated surface is then examined. Results are presented first for the FC-72 nucleate boiling heat transfer affected by the moving copper particles freely placed on the heated surface by showing the heat transfer data for the bare surface and for the surface with copper particles on it for various $d_p$ and $N_p$ in Figs. 4.4-4.28. The results in Figs. 4.4-4.6 for $d_p$=1.0 mm and $N_p$=100 to 300 indicate that at a small particle number the boiling heat transfer can be slightly enhanced by the copper particles only at low wall superheat near the onset of nucleate boiling. The enhancement gets smaller at

increasing wall superheat. Besides, the moving copper particles does not affect the boiling heat transfer to a significant degree in the single-phase flow at very low wall superheat and in the fully developed nucleate boiling region at high wall superheat. Moreover, a slight reduction in the boiling heat transfer by the copper particles is noted at an even higher wall superheat.

As the total number of the copper particles is increased to 400, 500 and 600, noticeable augmentation in the boiling heat transfer by the copper particles appears at low wall superheat (Figs. 4.7-4.9). Correspondingly, the degradation in the boiling heat transfer at high wall superheat is also noticeable. Note that the degradation is larger at a higher wall superheat. For a further increase in the number of the copper particles to 700-900, the particles on the copper plate are rather crowded. However, enhancement in the boiling heat transfer by the copper particles is even more significant at low $\Delta T_{sat}$ (Figs. 4.10-4.12), implying strong interactions between the particles and boiling flow at this large $N_p$. Apparently, substantial retardation in the boiling heat transfer by the copper particles exists at high $\Delta T_w$. It is of interest to find from the data given in Figs. 4.13-4.18 that even when the total number of the copper particles well exceeds $N_{pf}$ for $N_p \geq 1{,}000$ the boiling heat transfer enhancement by the copper particles is still significant at low $\Delta T_w$. This suggests that the presence of a large number of metallic particles on top of the other particles dose not lower the boiling heat transfer performance at low wall superheat.

To be more quantitative on the boiling heat transfer affected by the small copper particles presented above for $d_p$=1.0 mm, the ratios of the boiling heat transfer coefficients for the cases with the presence of the particles to the bare surface $h_p/h$ are shown in Fig. 4.19 for various $\Delta T_w$ and $N_p$. Note that the enhancement in the boiling heat transfer can exceed 200% for $N_p \geq 800$. The best enhancement for these

cases is 430% for $N_p$=1600 at $\Delta T_w$ ≈13K. Note that the best enhancement usually occurs at very low $\Delta T_w$ near the onset of nucleate boiling. Beyond this low $\Delta T_w$ the boiling heat transfer enhancements are nearly the same for $N_p = 1400 \sim 1800$. On the contrary the reduction in the boiling heat transfer at high $\Delta T_w$ can be as high as 25%. Besides, in the single-phase natural convection flow the change in the heat transfer coefficient by the particles is within $\pm$20% of that for the bare surface.

Aside from the boiling heat transfer, the above results also show that the presence of the copper particles can substantially lower the wall superheat needed for the onset of nucleate boiling for most cases (Table 4.1). This is also beneficial in electronics cooling by employing moving metallic particles on the boiling surface.

Next, the measured heat transfer data for the larger copper particles with $d_p$=1.5 mm are given in Figs. 4.20-4.27 for $N_p$ ranging from 100 to 800. By and large, these results are similar to those for the smaller copper particles presented above. However, some noted differences do exist. Specifically, the larger particles exhibit more pronounced effects on enhancing and retarding boiling heat transfer. Besides, the onset of nucleate boiling is much earlier for the large particles. For instance, at $N_p$=600 a 55% reduction in the incipient boiling wall superheat can be obtained by the moving particles. Checking with the data for $h_p/h$ given in Fig. 4.28 for $d_p$=1.5 mm indicates that boiling heat transfer coefficient can be increased up to more than 440% by placing the larger copper particles on the boiling surface for $N_p$=800 at $\Delta T_w$ ≈12.5 K. At higher $\Delta T_w$ the best boiling heat transfer augmentation can be procured at $N_p = 700$.

## 4.5 Effects of Moving Stainless Steel Particles on Boiling Heat Transfer

Attention is then turned to examining the data for the stainless steel particles, which have a slightly lower density than copper. The measured heat transfer data for the stainless steel particles with $d_p$=1.0 mm shown in Figs. 4.29-4.37 qualitatively resemble that for the copper particles given in Figs. 4.4-4.18. But for the lighter stainless steel particles, the boiling heat transfer augments more drastically with a large number of the particles present in the liquid FC-72 on the heated plate. Relatively substantial boiling heat transfer augmentation has been achieved already at $N_p$=400 for the lighter particles. Besides, the boiling heat transfer enhancement extends to a slightly higher wall superheat. The data in Fig. 4.38 show that the best boiling heat transfer enhancement can be up to 530% for the small stainless steel particles at $\Delta T_w \approx 12.7\,K$. Moreover, the enhancement reduces faster with the wall superheat. Furthermore, the lighter particles cause even earlier onset of nucleate boiling. It is of interest to note from the data for the large stainless steel particles given in Figs. 4.39-4.43 that the resulting boiling heat transfer exhibits opposite trends when compared with the large copper particles shown in Figs. 4.20-4.27. Specifically, the large stainless particles produce worse boiling heat transfer enhancement than the large copper particles. This can be seen by comparing the data for $h_p/h$ given in Figs. 4.38 and 4.44 for the stainless steel particles with Figs. 4.19 and 4.28 for the copper particles.

## 4.6 Proposed Correlations

The data for $h_p/h$ presented in Figs. 4.19, 4.28, 4.38 and 4.44 can be correlated empirically as

$$\frac{h_p}{h} = \left\{a + b\ln\left(\frac{N_p}{N_{pf}}\right)\right\} \cdot \left[\frac{C_{pl}(\Delta T_w - \Delta T_{ONB,b} + 1)}{i_{lv}}\right]^{\left[c + d\left(\frac{N_p}{N_{pf}}\right)^{1.5}\right]} \quad (4.4)$$

$$a = \left[-0.69 + 0.14\left(\frac{\rho_p}{\rho_l}\right)\right] + \left[12.1 - 2.33\left(\frac{\rho_p}{\rho_l}\right)\right]\left(\mathrm{d_p}/\sqrt{\sigma/\mathrm{g}\Delta\rho}\right)$$

$$b = \left[1.683 - 0.325\left(\frac{\rho_p}{\rho_l}\right)\right] + \left[-30.77 + 5.8\left(\frac{\rho_p}{\rho_l}\right)\right]\left(\mathrm{d_p}/\sqrt{\sigma/\mathrm{g}\Delta\rho}\right)$$

$$c = \left[-10.61 + 1.8\left(\frac{\rho_p}{\rho_l}\right)\right] + \left[164.08 - 30.28\left(\frac{\rho_p}{\rho_l}\right)\right]\left(\mathrm{d_p}/\sqrt{\sigma/\mathrm{g}\Delta\rho}\right)$$

$$d = \left[2.88 - 0.55\left(\frac{\rho_p}{\rho_l}\right)\right] + \left[-50.89 + 9\left(\frac{\rho_p}{\rho_l}\right)\right]\left(\mathrm{d_p}/\sqrt{\sigma/\mathrm{g}\Delta\rho}\right)$$

The present data for the boiling heat transfer coefficient for the bare surface can be expressed empirically as

$$\begin{cases} \mathrm{h} = 436.55 + 748.581 \cdot (\Delta T_w - \Delta T_{ONB}) & \text{for} \quad 0 < [\Delta T_w - \Delta T_{ONB}] < 1K \\ \mathrm{h} = 61.58 + 1135.51 \cdot (\Delta T_w - \Delta T_{ONB}) & \text{for} \quad 1K < [\Delta T_w - \Delta T_{ONB}] < 4K \end{cases} \quad (4.5)$$

The mean absolute error (MAE) for the above correlation for $h_p/h$ when compared with the present data is 17.3%. For the correlation given in Eq. (4.5) for h the mean absolute error is 14.2%.

Finally, we illustrate the ranges of the experimental parameters in which the boiling heat transfer can be enhanced by placing the metallic particles on the heated surface in Fig. 4.45. The results manifest that the lower bounds of the imposed heat flux for enhancing boiling heat transfer do not significantly vary with the ratio of the

particle number placed on the plate to the maximum particle number forming a single particle layer on the plate $N_p/N_{pf}$ and with the particle size and material. But the lower bounds for the wall superheat decrease noticeably with $N_p/N_{pf}$ (Fig. 4.45 (b)). The upper bounds of q and $\Delta T_w$ for enhancing boiling heat transfer, however, show nonmonotonic variations with $N_p/N_{pf}$, particle size and material. Specifically, at small and large $N_p/N_{pf}$ the upper bound of q is higher for the small stainless steel particles. While for $N_p/N_{pf} > 1.0$ placing the large stainless steel particles results in a lowest upper bound.

Based on the above data, the ranges of the imposed heat flux and wall superheat in which the boiling heat transfer can be enhanced by the movable particles are correlated as

$$3 \cdot 10^{-5} + 0.04 \cdot 10^{-6}\left[\ln\left(\frac{N_p}{N_{pf}}\right)\right]^2 < \frac{q}{\rho_l \alpha_l i_{lv}/\sqrt{\frac{\sigma}{g\Delta\rho}}} < 3.4 \cdot 10^{-4} - 4.93 \cdot 10^{-5}\left[\ln\left(\frac{N_p}{N_{pf}}\right)\right]^2 \quad (4.6)$$

$$0.15 - 0.03\left(\frac{N_p}{N_{pf}}\right) < \frac{C_{pl}\cdot\Delta T_w}{i_{lv}} < 0.21 - 9.38 \cdot 10^{-3}/\left(\frac{N_p}{N_{pf}}\right) \quad (4.7)$$

The mean absolute errors (MAE) between the above correlations and the present data for q and $\Delta T_w$ are 11.5% and 5.8%, respectively.

## 4.7 Interactions between Particles and Boiling Flow

To delineate the complicate effects of the moving metallic particles on the boiling heat transfer, motions of the particles and bubbles in the boiling flow are visualized. The results from this visualization for selected cases are presented in Figs. 4.46-4.51. More specifically, photos taken from the top view of the boiling flow in a

small region around the geometric center of the heated surface are shown in Fig. 4.46 for the small copper particles with $N_p$=600 at low imposed heat flux of 0.85 $^{w}/_{m^2}$. In these figures, the symbol "t=0" denotes an arbitrary time instant in the statistical state. At high heat flux and large particle number the vigorous motions of the particles and bubbles and their strong interactions are prone to overshadow each other, causing the top view photos to be rather ambiguous. Instead the side view photos of the flow are given in Figs. 4.47-4.51 under this situation for various imposed heat fluxes.

Our flow visualization reveals that when a given heat flux is imposed to the boiling surface the fast growth of bubbles after their incipience on the heated surface can push the surrounding particles to move away from these original sites horizontally over a certain distance. As the particles move on the heated surface, they in turn can push the bubbles along their path to depart from the surface, resulting in earlier bubble departure. Besides, the moving particles can collide with other particles. At higher imposed heat flux more bubbles nucleate from the heated plate and the force resulting from the growth of bubbles can be very strong. Consequently, the particles can be lifted directly up by the growing bubbles too. Later, the heavy metallic particles may drop back to the plate due to gravity and the surrounding bubbles and liquid can be pushed away. Besides, collision between the particles is frequent. These mutual particle-bubble interactions in the boiling flow schematically shown in Fig. 4.52 get more intense at increasing heat flux, causing the three-phase liquid-vapor-particle flow over the heated surface to become highly turbulent and tending to enhance boiling heat transfer from the plate.

At an even higher heat flux a very large number of bubbles nucleate at the heated surface and the metallic particles can impede the bubbles of certain size to grow further and depart from the heated surface. The bubbles are then trapped beneath

the particles, as schematically illustrated in Fig. 4.53. Meanwhile, the particles can reduce the inrush of the bulk liquid to the heated surface especially at large particle number. Therefore the boiling heat transfer is retarded by the particles. These heat transfer retarding effects are more severe at higher heat flux when more particles are placed on the heated plate.

Table 4.1 Wall superheats at onset of nucleate boiling for copper particles

| Particle diameter $d_p$(mm) | $N_p$ | $(\Delta T_w)_{ONB}$ ($^{O}$C) | $(\Delta T_w)_{ONB}$ ($^{O}$C) For bare surface |
|---|---|---|---|
| 1.0 | 100 | 10.7 | 12.5 |
| | 200 | 10.8 | 11.6 |
| | 300 | 10.8 | 10.7 |
| | 400 | 9.8 | 11.7 |
| | 500 | 9.12 | 12.4 |
| | 600 | 9.9 | 10.5 |
| | 700 | 9.06 | 12.1 |
| | 800 | 9.3 | 11.7 |
| | 900 | 9.7 | 12.4 |
| | 1000 | 8.01 | 13.1 |
| | 1100 | 8.5 | 9.6 |
| | 1200 | 6.2 | 11.8 |
| | 1400 | 6.89 | 12.84 |
| | 1600 | 6.29 | 13.14 |
| | 1800 | 6.12 | 12.89 |
| 1.5 | 100 | 10.3 | 11.7 |
| | 200 | 9.5 | 11.9 |
| | 300 | 9.3 | 12.8 |
| | 400 | 5.6 | 12.9 |
| | 500 | 8.5 | 12.4 |
| | 600 | 6 | 13.2 |
| | 700 | 6.61 | 13.32 |
| | 800 | 5.97 | 12.78 |

Table 4.2 Wall superheats at onset of nucleate boiling for stainless steel particles

| Particle diameter $d_p$(mm) | $N_p$ | $(\Delta T_w)_{ONB}$ ($^O$C) | $(\Delta T_w)_{ONB}$ ($^O$C) For bare surface |
|---|---|---|---|
| 1.0 | 200 | 8.3 | 10 |
| | 400 | 7.9 | 12.2 |
| | 600 | 7.8 | 12.8 |
| | 800 | 7.9 | 11.7 |
| | 1000 | 7.77 | 12.2 |
| | 1200 | 7.5 | 12.77 |
| | 1400 | 7.13 | 12.76 |
| | 1600 | 7.06 | 12.57 |
| | 1800 | 6.73 | 12.84 |
| 1.5 | 200 | 10.7 | 11.6 |
| | 400 | 8 | 11.5 |
| | 600 | 7 | 11 |
| | 700 | 7.1 | 12.67 |
| | 800 | 6.07 | 12.24 |

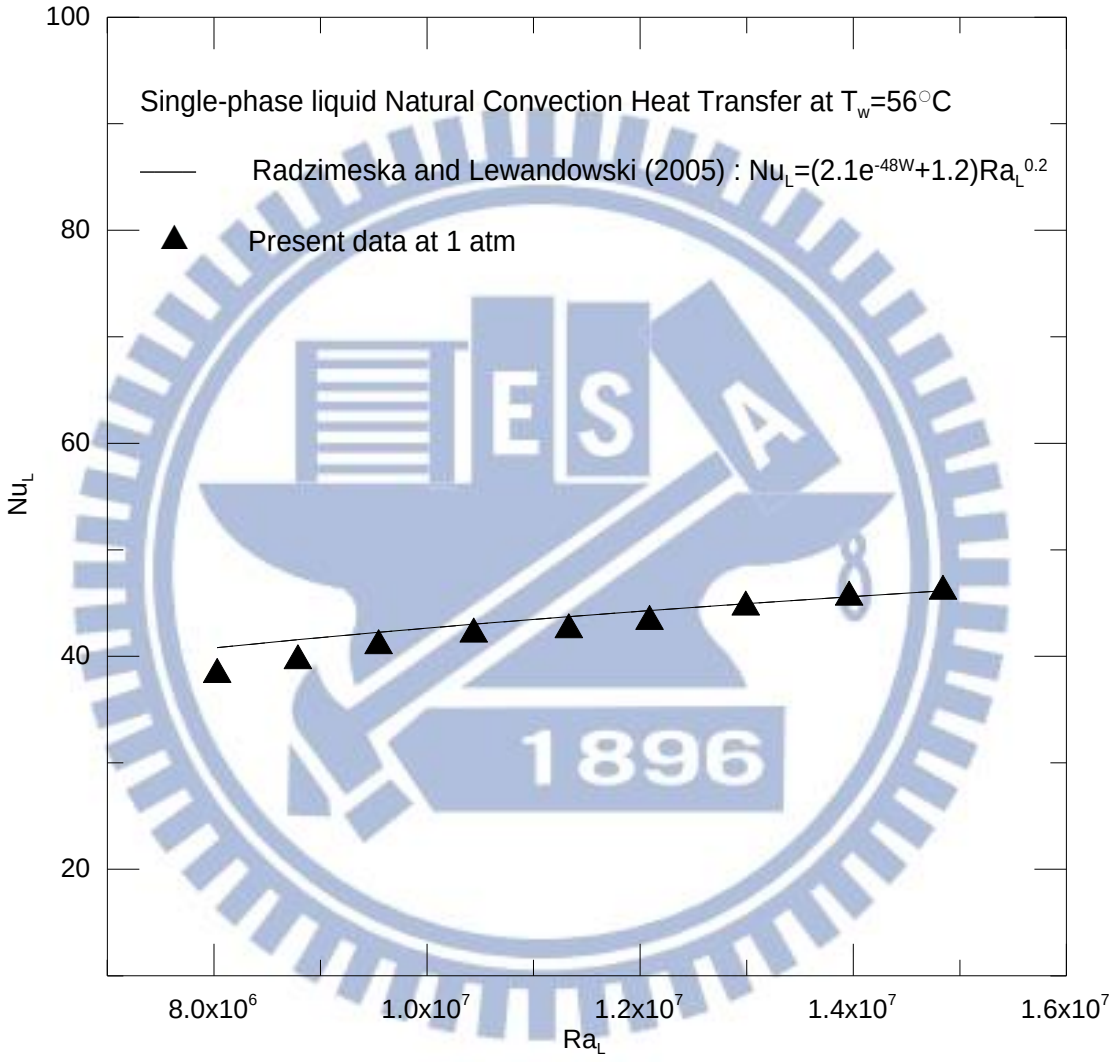


Fig. 4.1 Comparison of the present single-phase natural convection data with the empirical correlation of Radziemska and Lewandowski (2005).

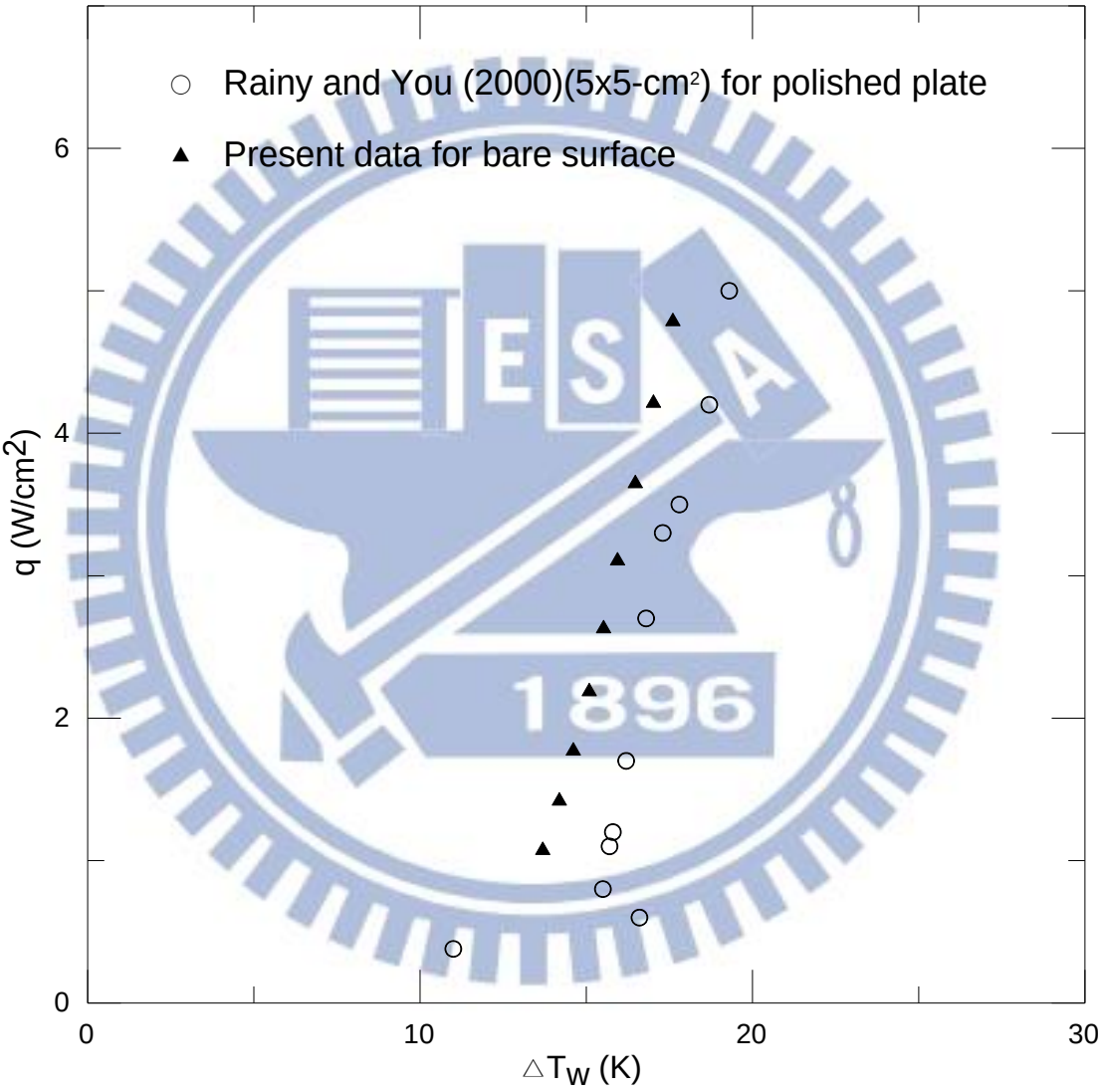


Fig. 4.2 Comparison of the present nucleate boiling heat transfer data for bare surface with Rainy and You (2000).

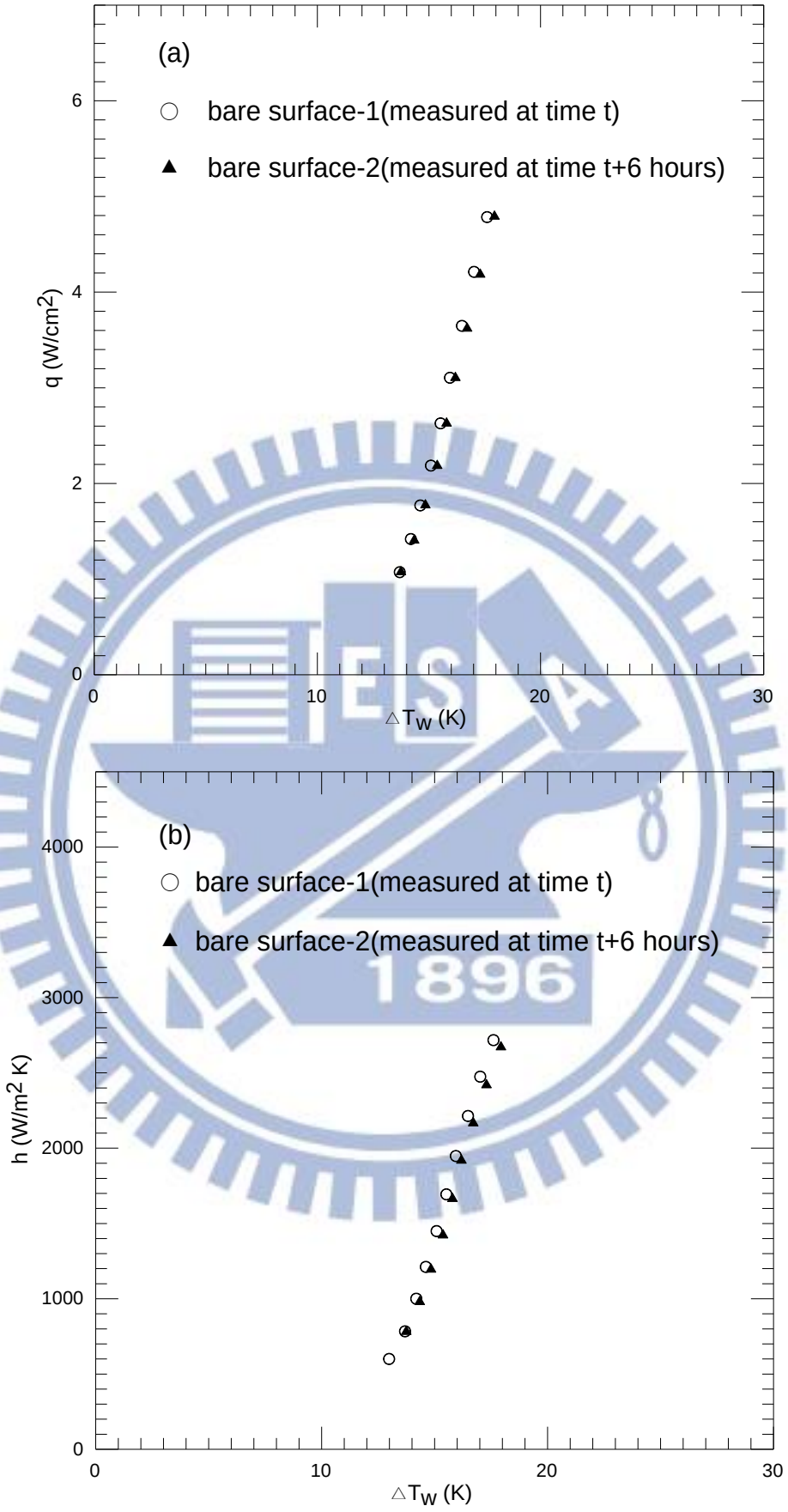


Fig. 4.3 Effects of surface aging on saturated pool boiling curves (a) and boiling heat transfer coefficients (b) for bare surface.

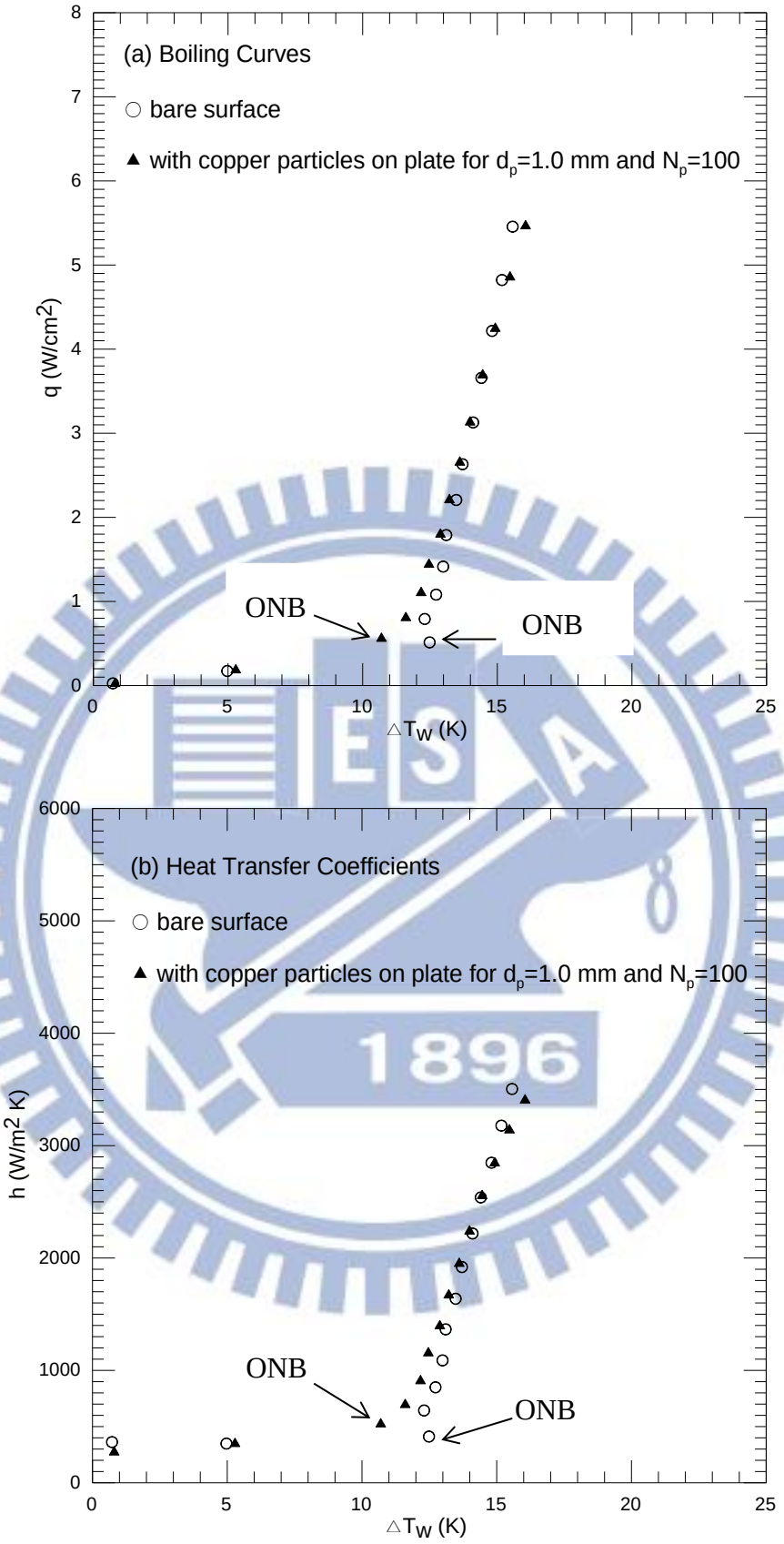


Fig. 4.4 Effects of copper particle diameter and number on saturated pool boiling curves (a) and boiling heat transfer coefficients (b) at $d_p$=1.0 mm and $N_p = 100$ .

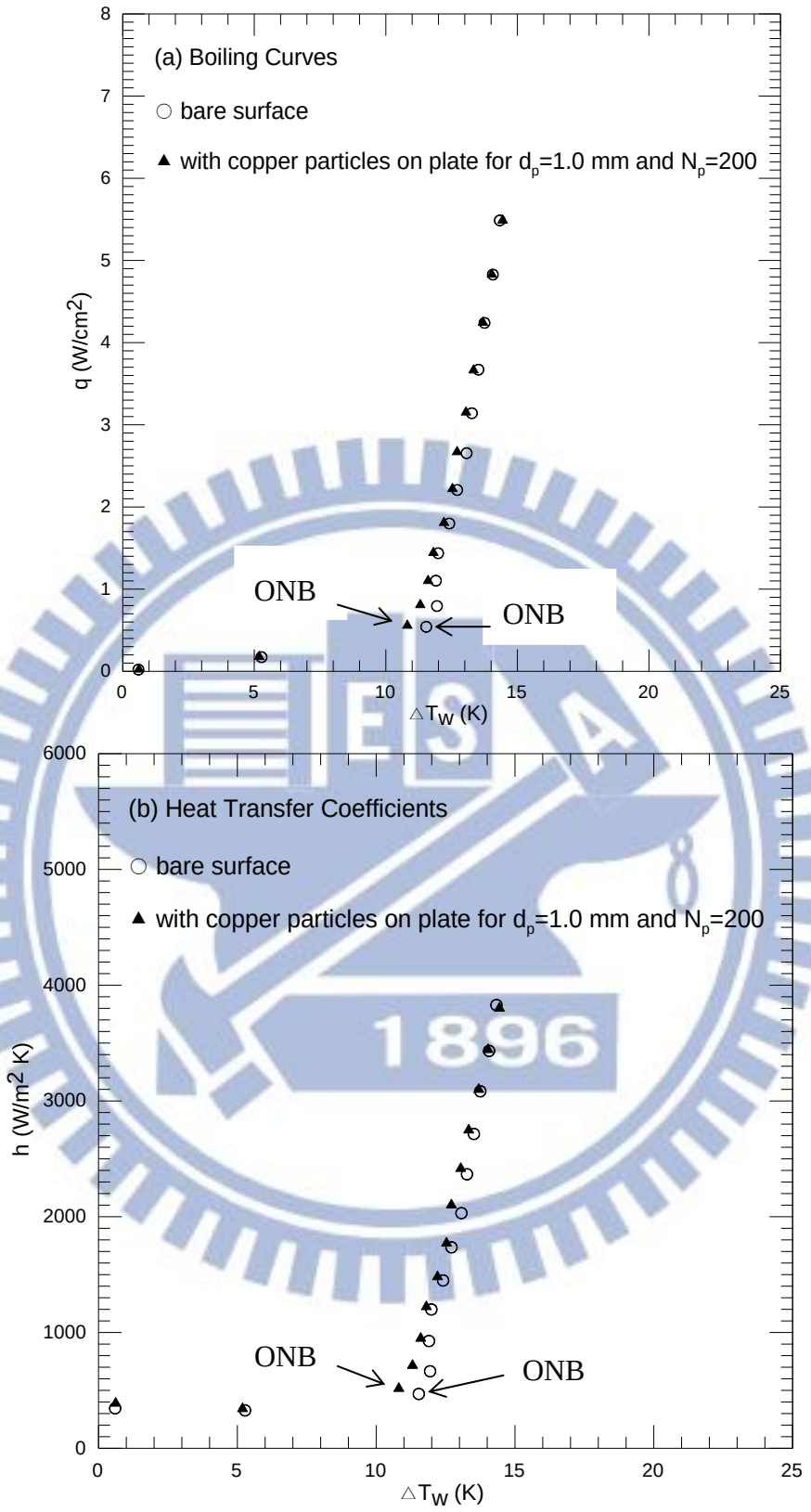


Fig. 4.5 Effects of copper particle diameter and number on saturated pool boiling curves (a) and boiling heat transfer coefficients (b) at $d_p$=1.0 mm and $N_p = 200$ .

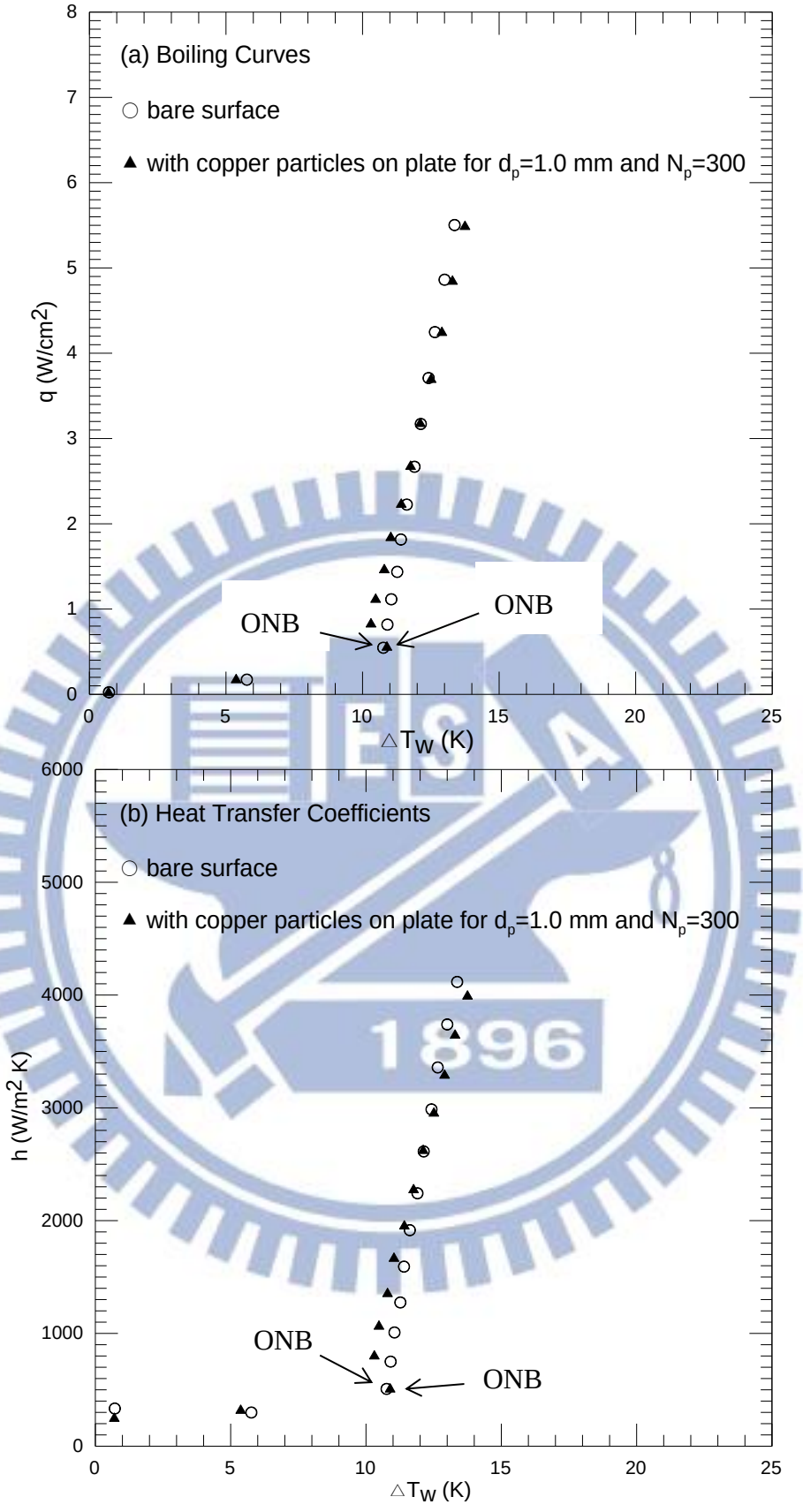


Fig. 4.6 Effects of copper particle diameter and number on saturated pool boiling curves (a) and boiling heat transfer coefficients (b) at $d_p$=1.0 mm and $N_p = 300$ .

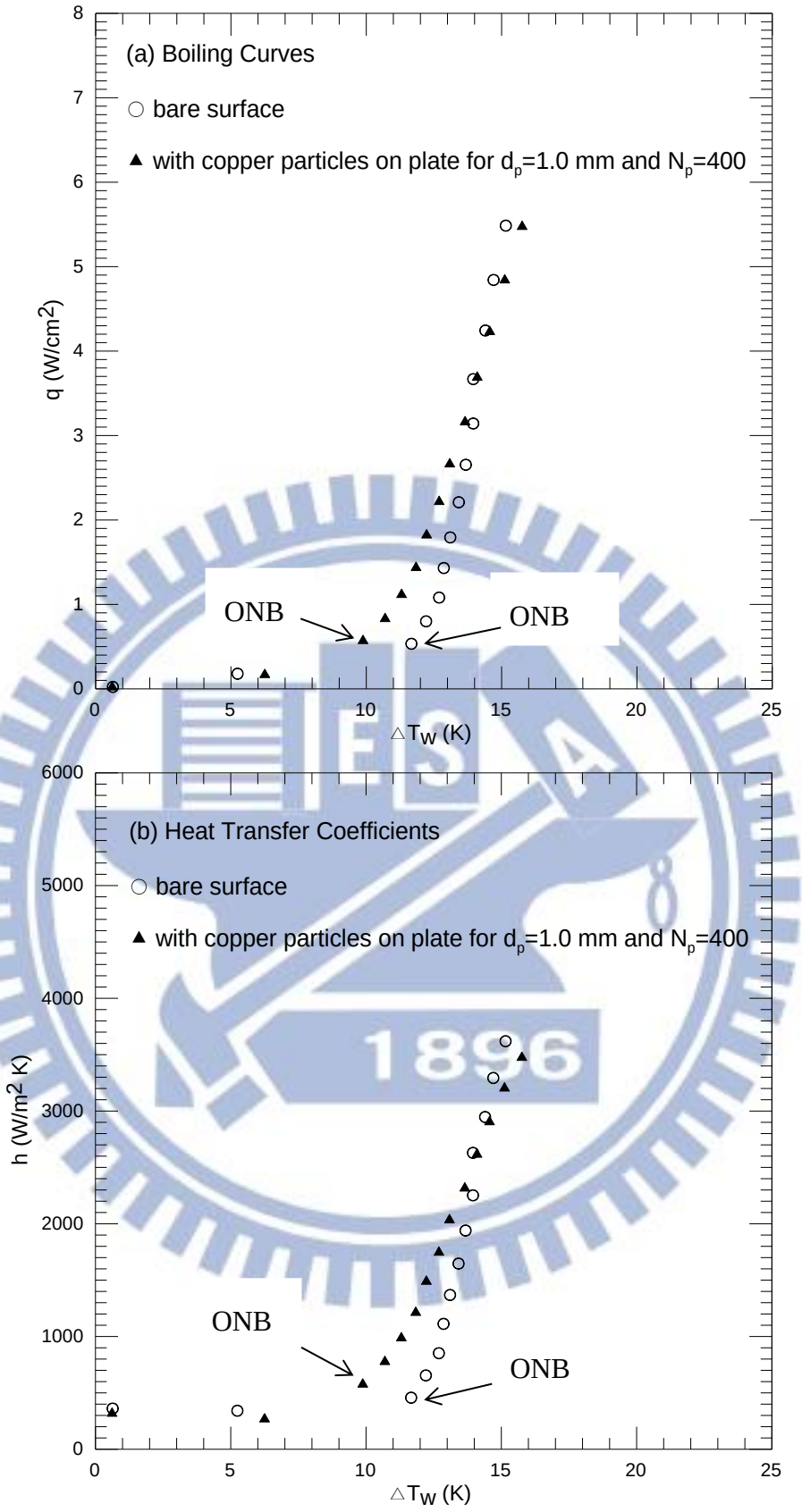


Fig. 4.7 Effects of copper particle diameter and number on saturated pool boiling curves (a) and boiling heat transfer coefficients (b) at $d_p$=1.0 mm and $N_p = 400$ .

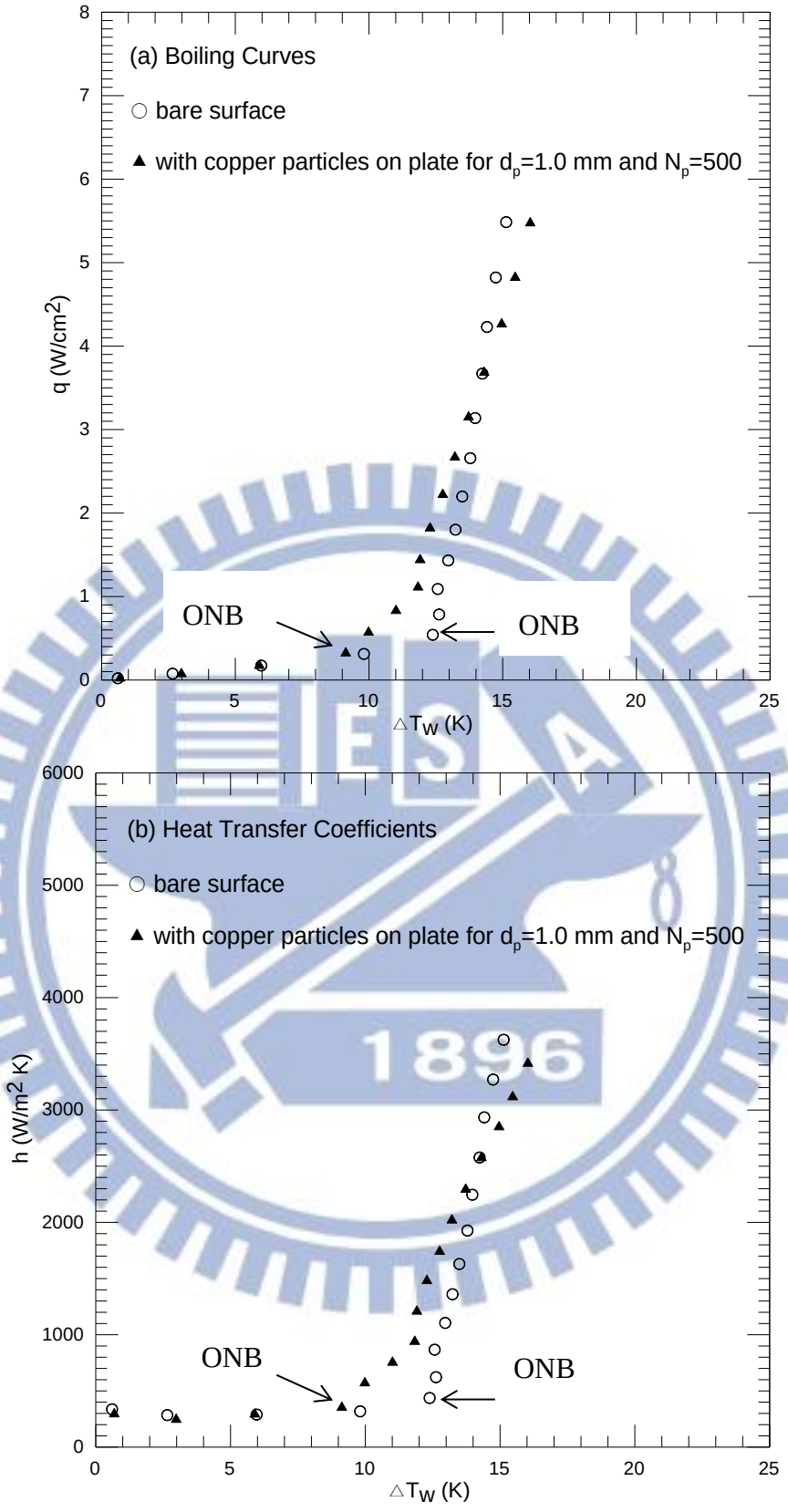


Fig. 4.8 Effects of copper particle diameter and number on saturated pool boiling curves (a) and boiling heat transfer coefficients (b) at $d_p$=1.0 mm and $N_p = 500$ .

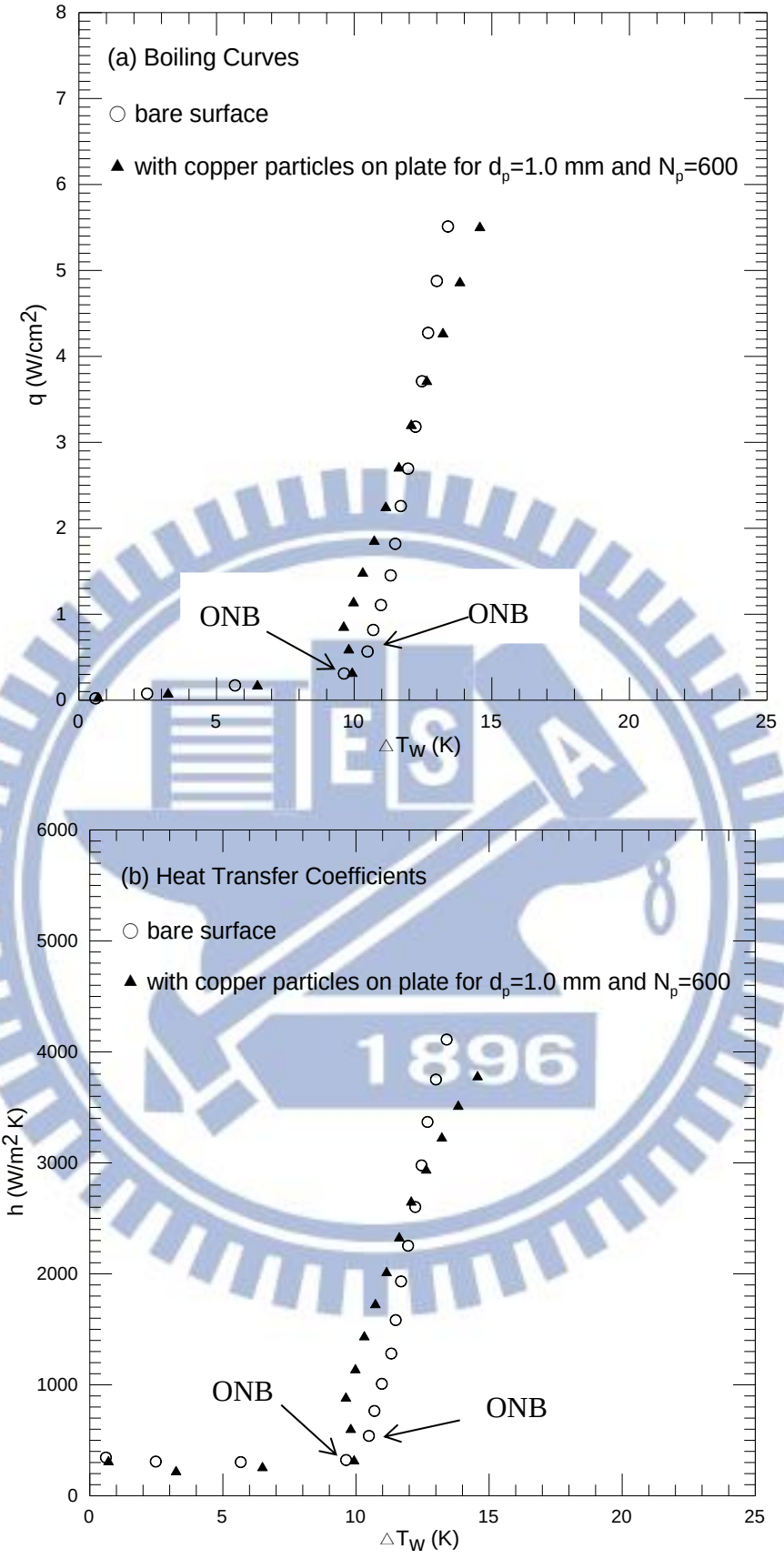


Fig. 4.9 Effects of copper particle diameter and number on saturated pool boiling curves (a) and boiling heat transfer coefficients (b) at $d_p$=1.0 mm and $N_p = 600$.

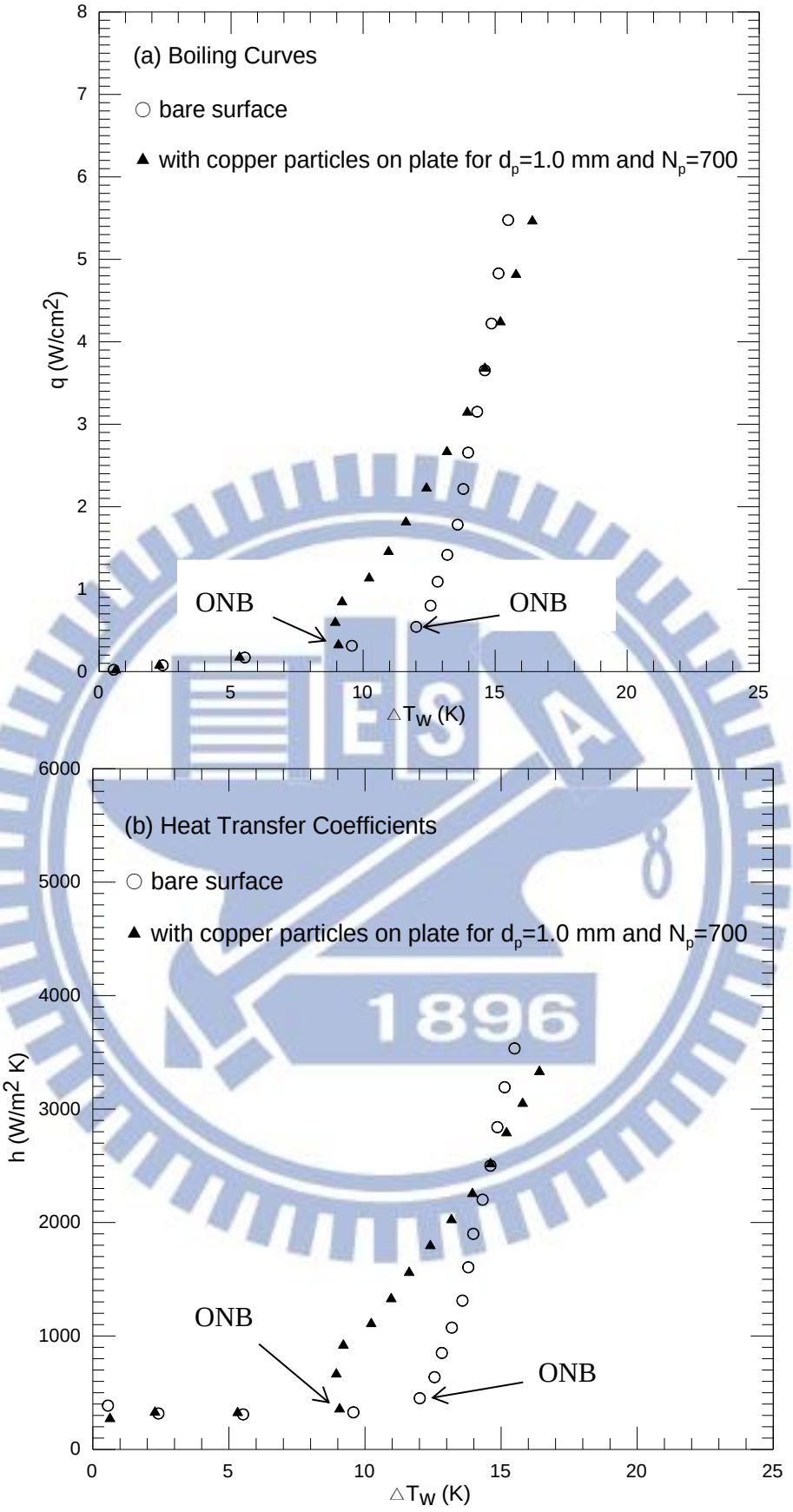


Fig. 4.10 Effects of copper particle diameter and number on saturated pool boiling curves (a) and boiling heat transfer coefficients (b) at $d_p$=1.0 mm and $N_p = 700$ .

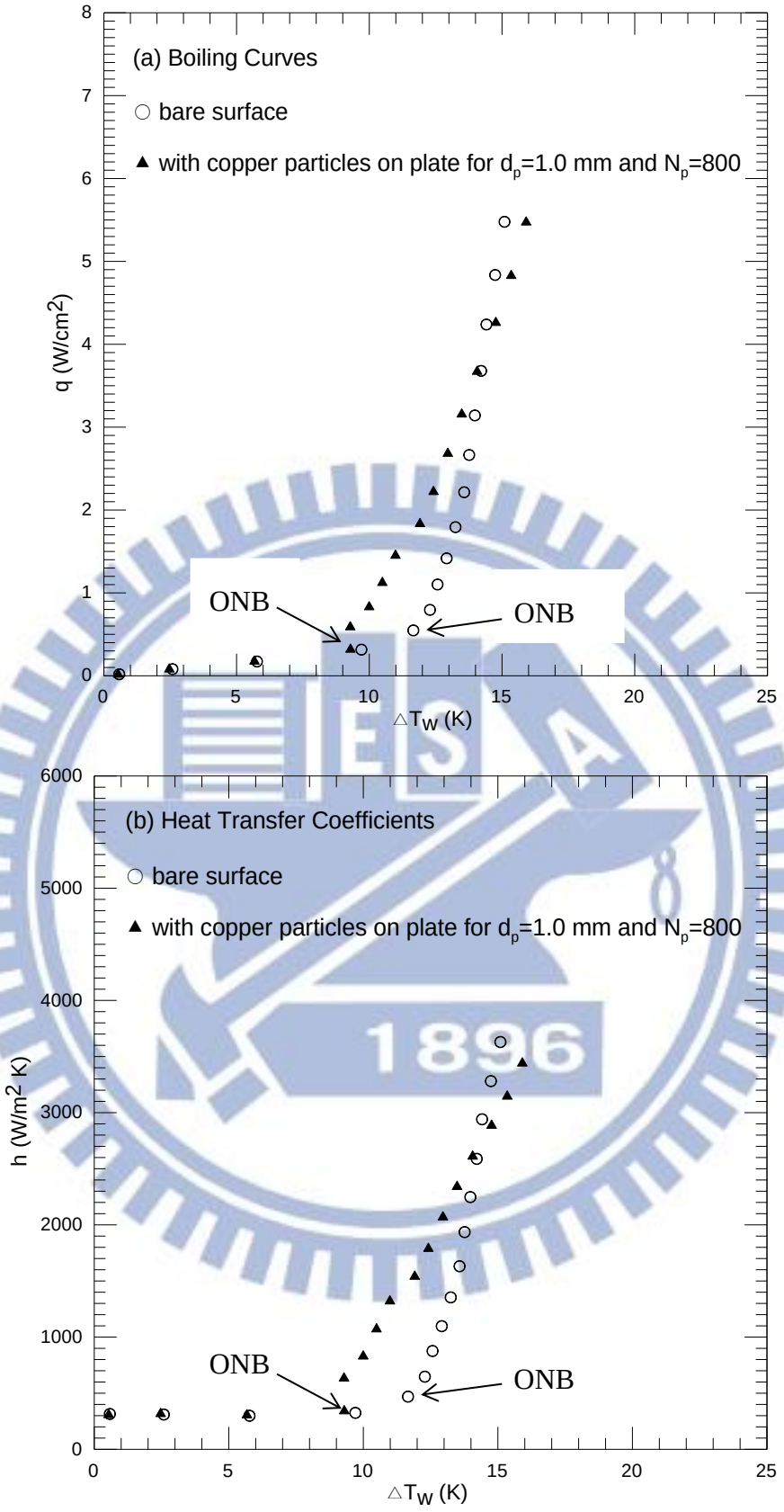


Fig. 4.11 Effects of copper particle diameter and number on saturated pool boiling curves (a) and boiling heat transfer coefficients (b) at $d_p$=1.0 mm and $N_p = 800$ .

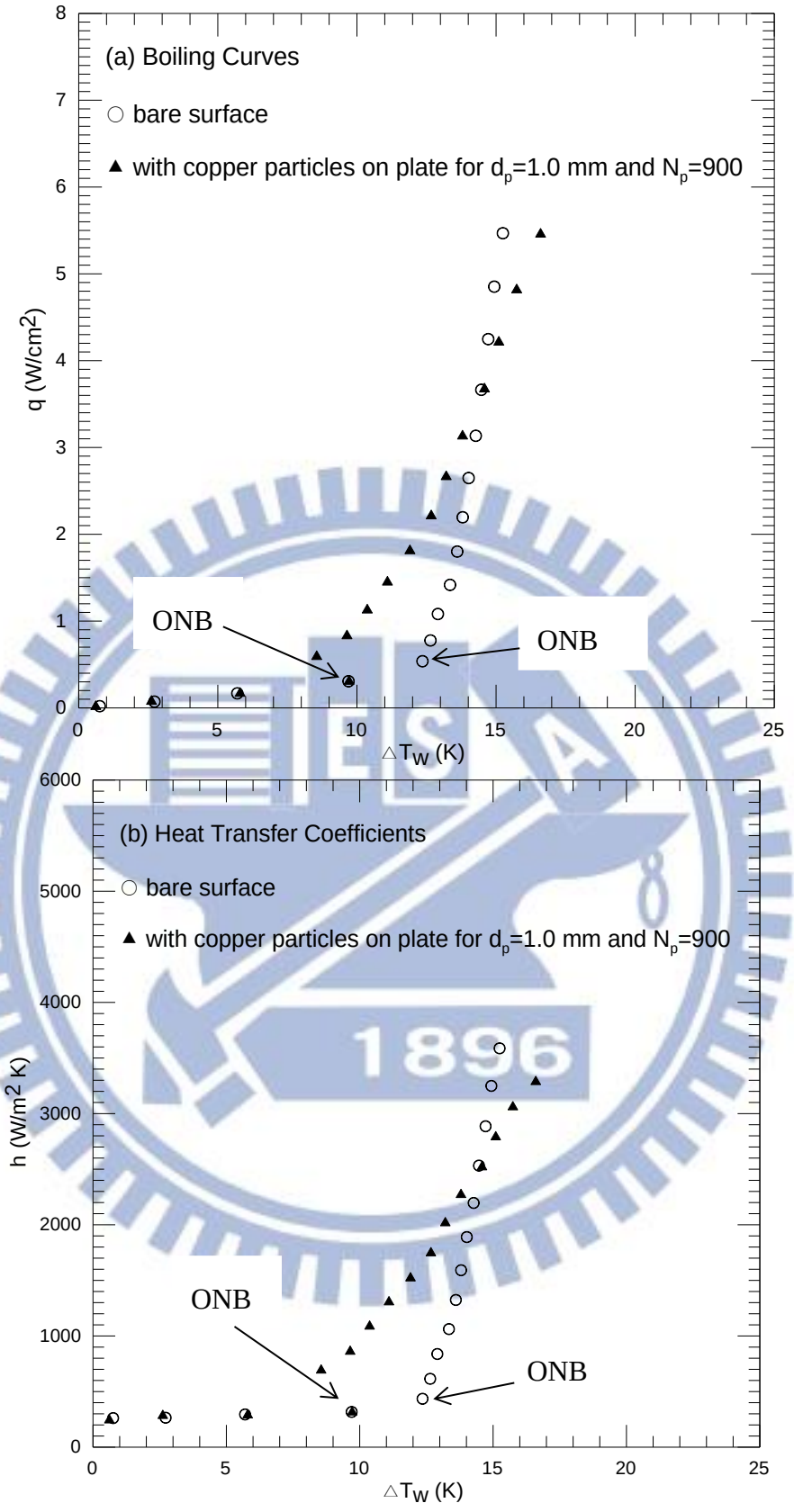


Fig. 4.12 Effects of copper particle diameter and number on saturated pool boiling curves (a) and boiling heat transfer coefficients (b) at $d_p$=1.0 mm and $N_p = 900$ .

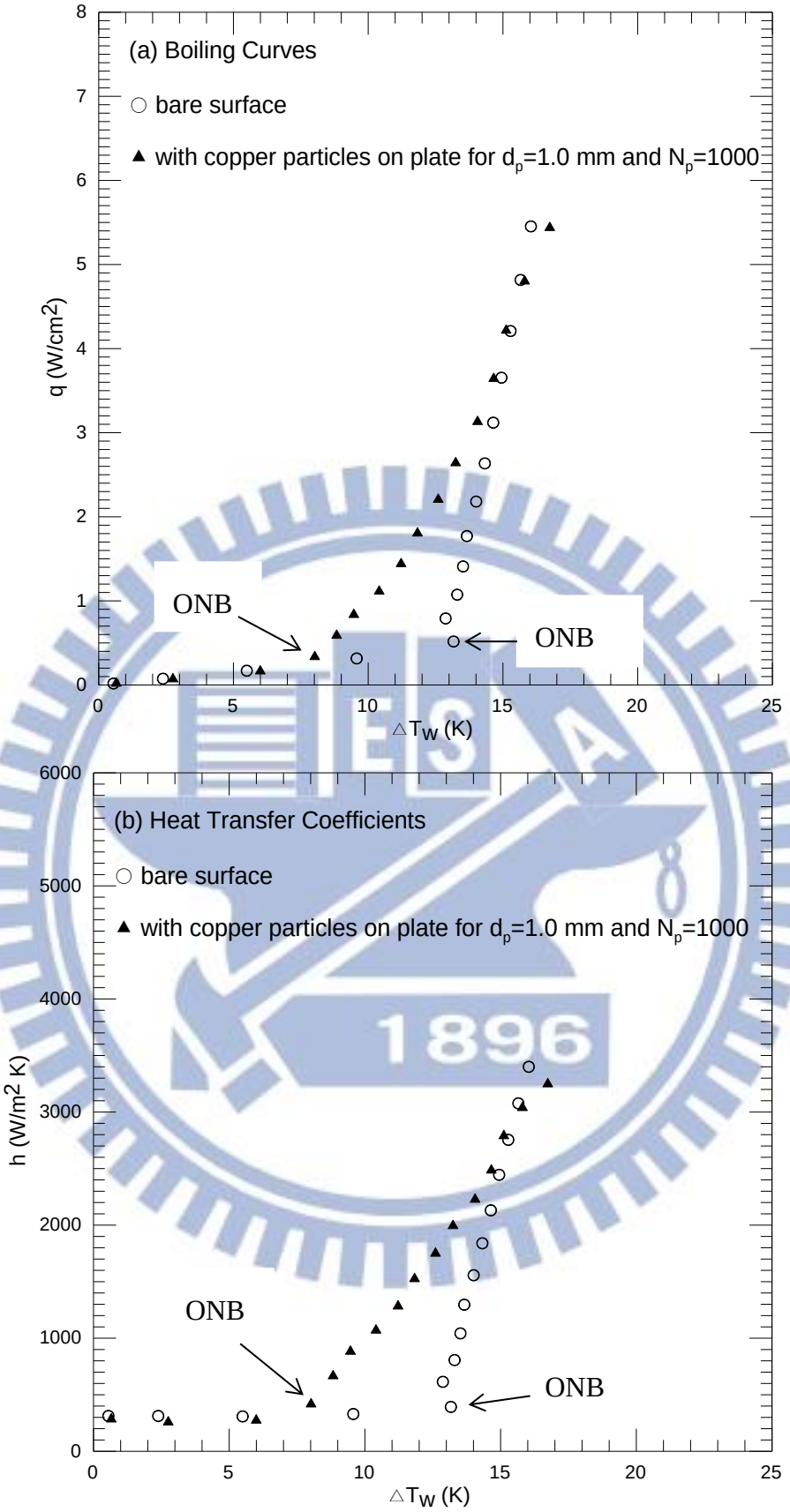


Fig. 4.13 Effects of copper particle diameter and number on saturated pool boiling curves (a) and boiling heat transfer coefficients (b) at $d_p$=1.0 mm and $N_p = 1000$ .

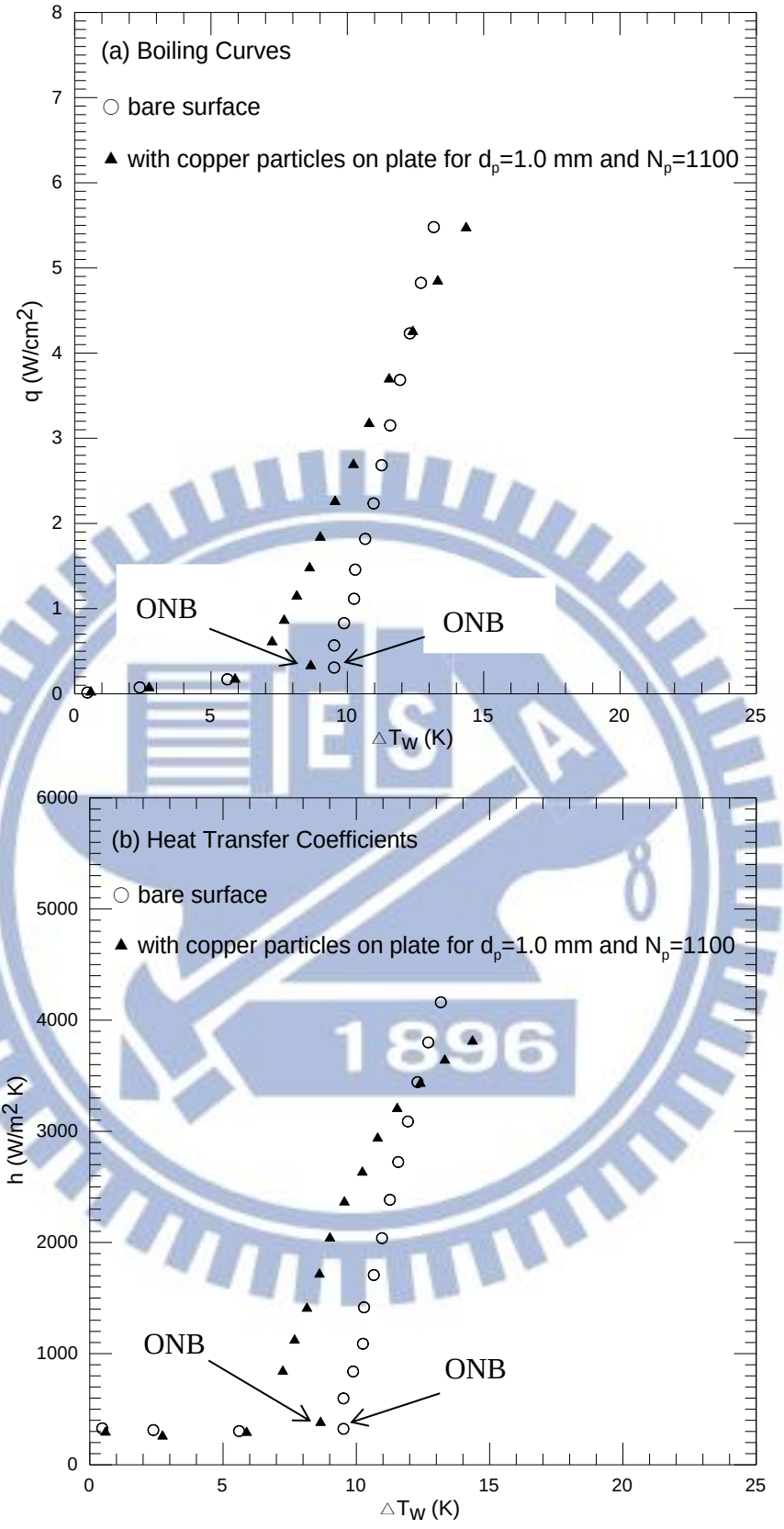


Fig. 4.14 Effects of copper particle diameter and number on saturated pool boiling curves (a) and boiling heat transfer coefficients (b) at $d_p$=1.0 mm and $N_p = 1100$ .

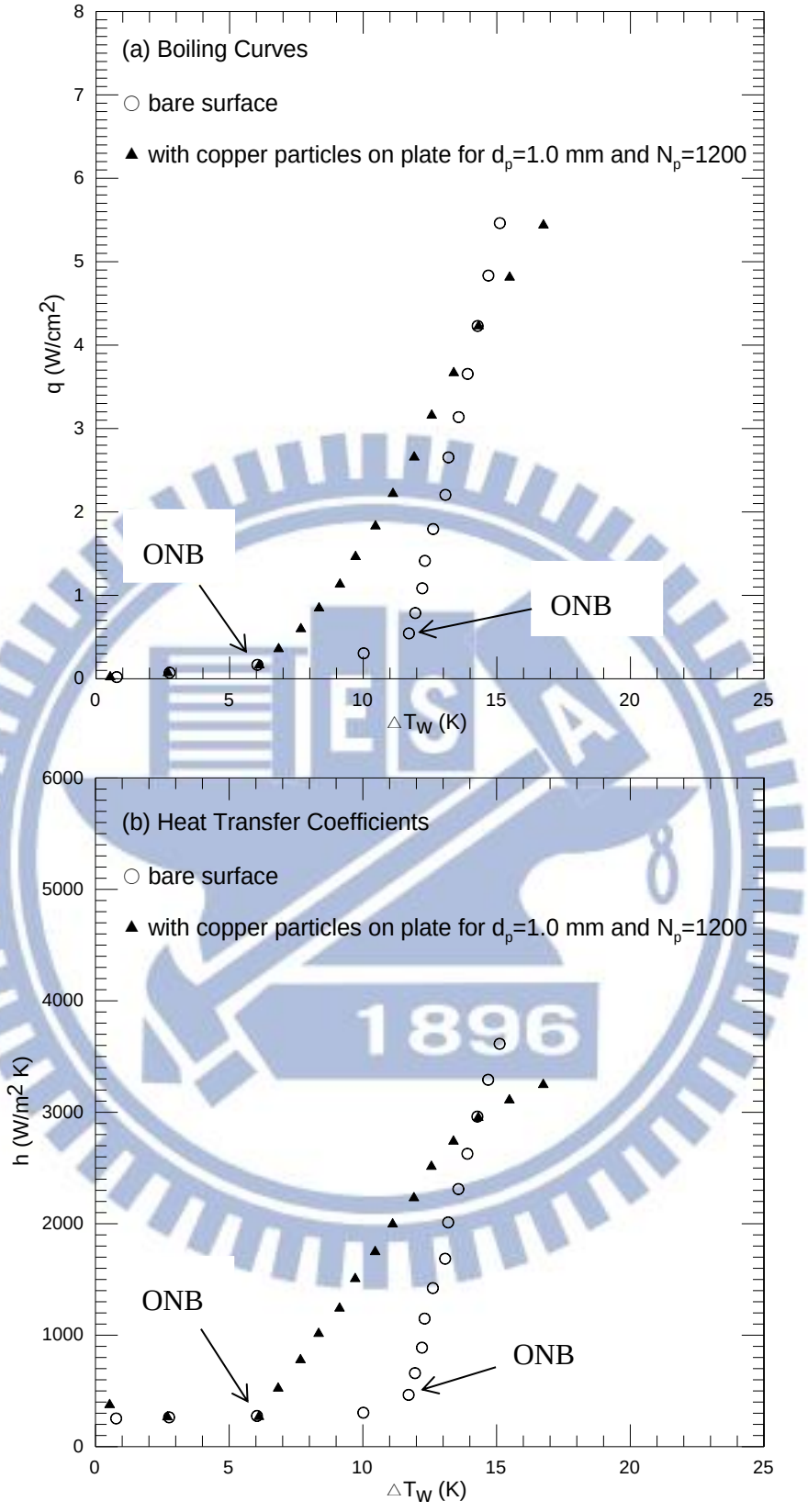


Fig. 4.15 Effects of copper particle diameter and number on saturated pool boiling curves (a) and boiling heat transfer coefficients (b) at $d_p$=1.0 mm and $N_p = 1200$ .

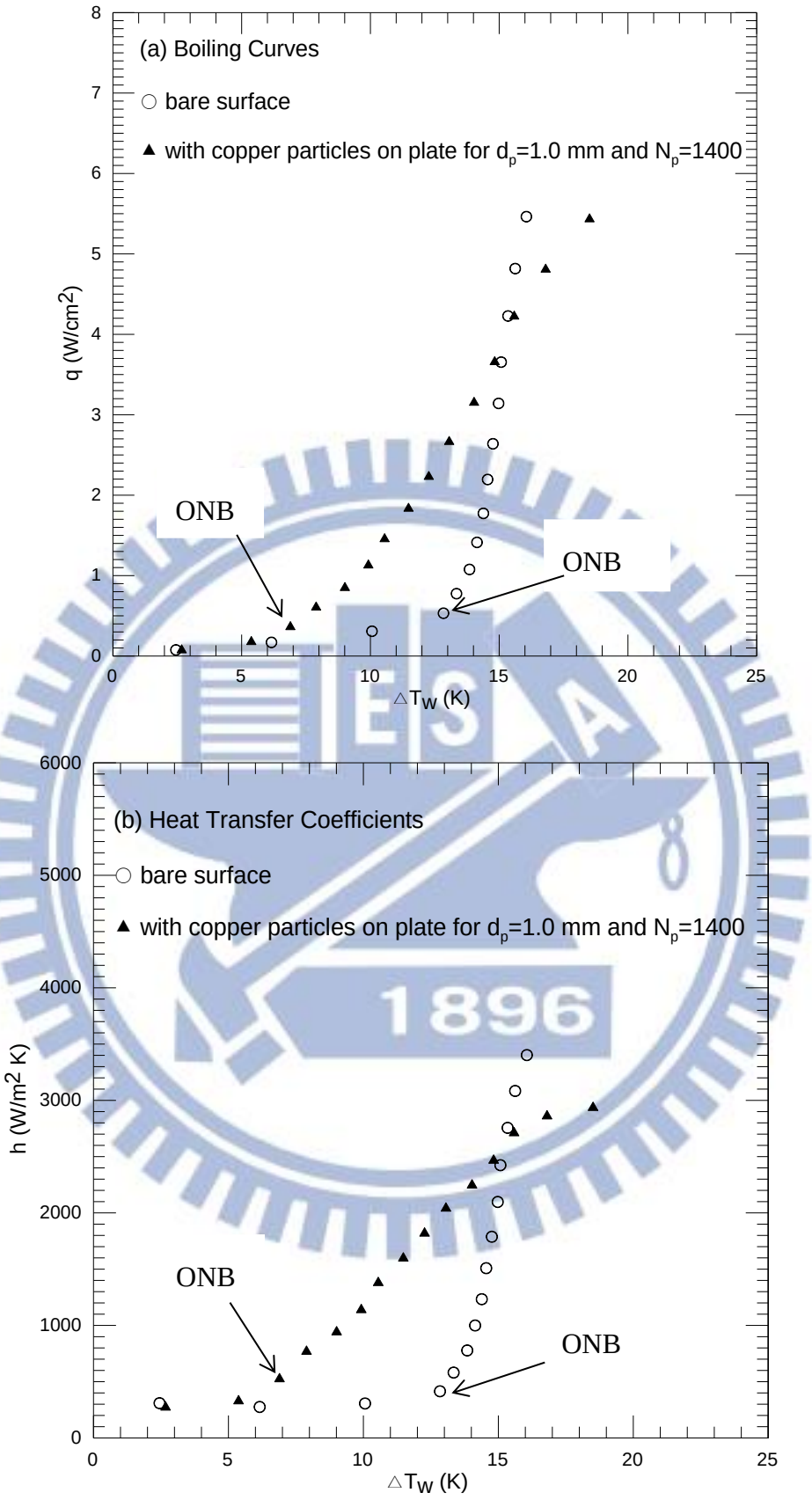


Fig. 4.16 Effects of copper particle diameter and number on saturated pool boiling curves (a) and boiling heat transfer coefficients (b) at $d_p$=1.0 mm and $N_p = 1400$ .

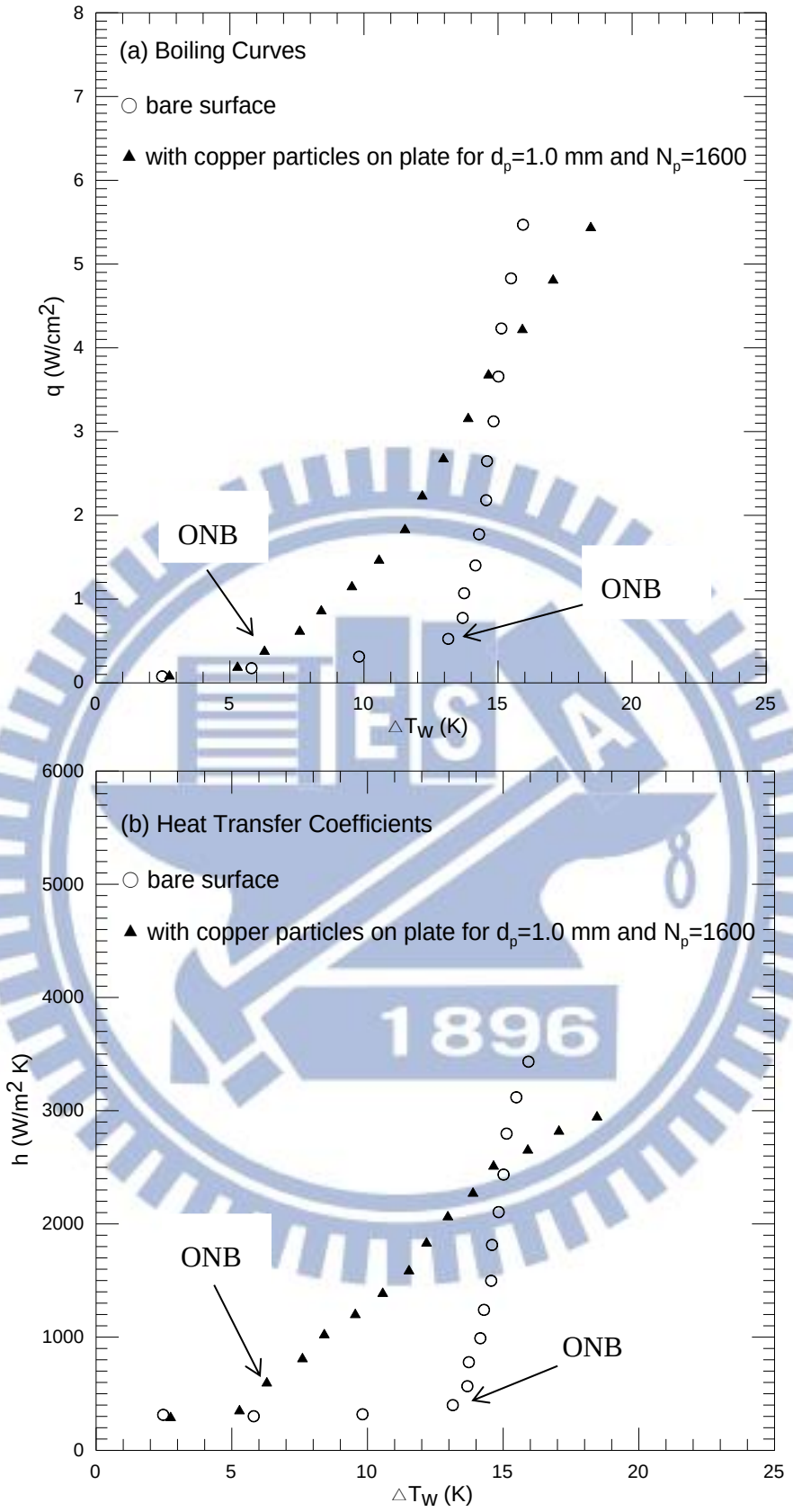


Fig. 4.17 Effects of copper particle diameter and number on saturated pool boiling curves (a) and boiling heat transfer coefficients (b) at $d_p$=1.0 mm and $N_p = 1600$ .

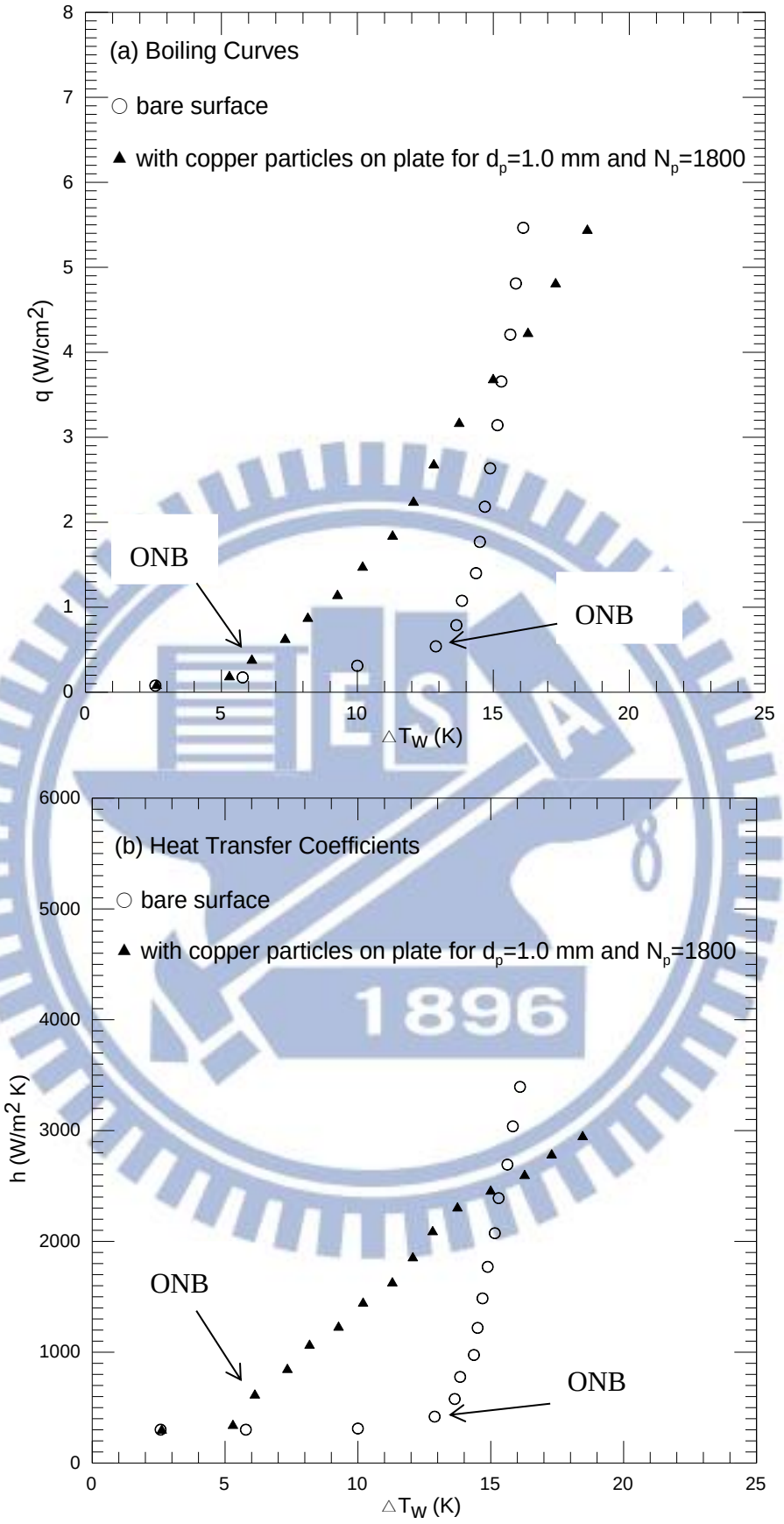


Fig. 4.18 Effects of copper particle diameter and number on saturated pool boiling curves (a) and boiling heat transfer coefficients (b) at $d_p$=1.0 mm and $N_p = 1800$ .

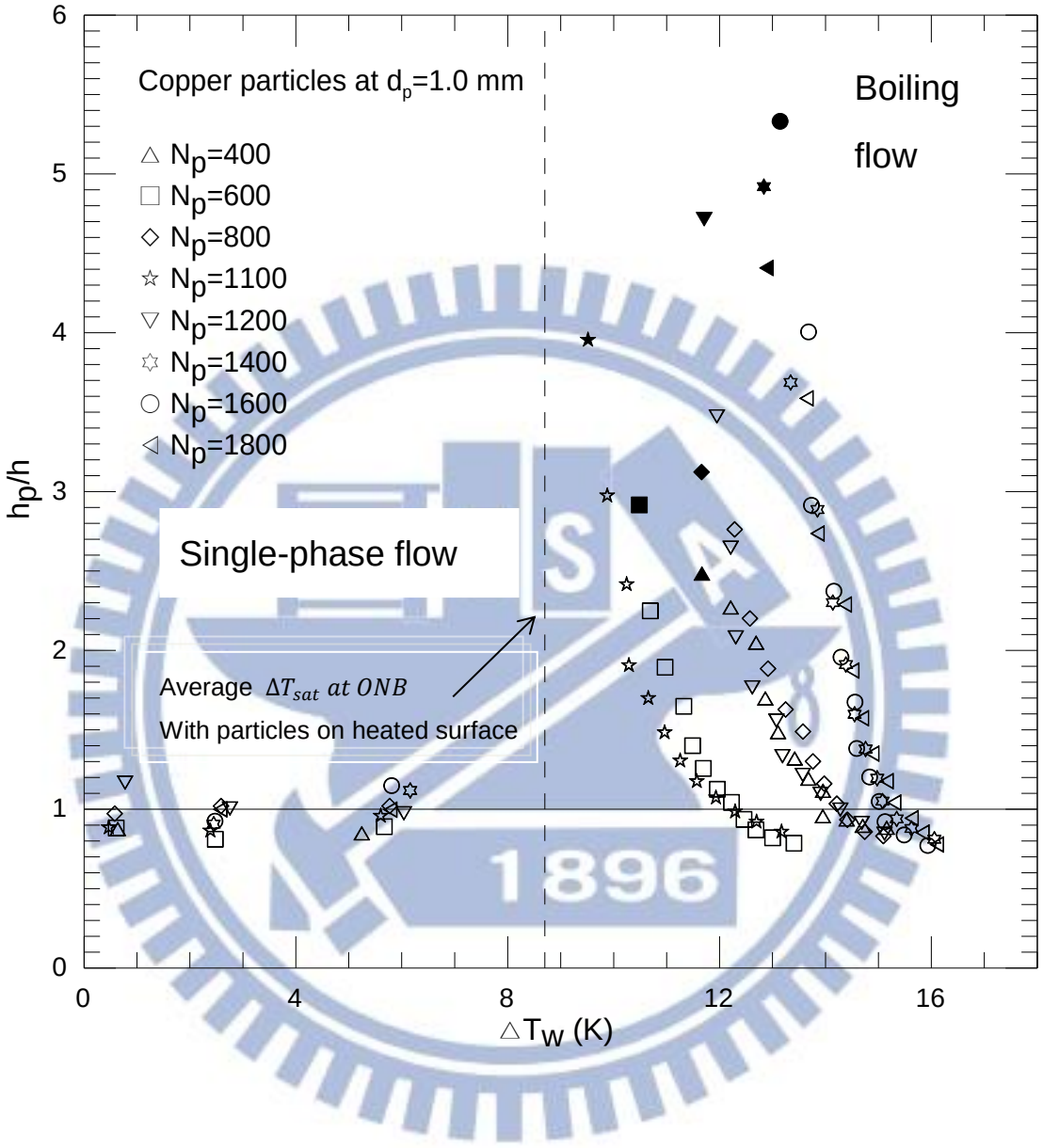


Fig. 4.19 Variations of $h_p/h$ with wall superheat for various copper particle numbers at $d_p$=1.0 mm (solid symbols denote best boiling heat transfer enhancement for various $N_p$)

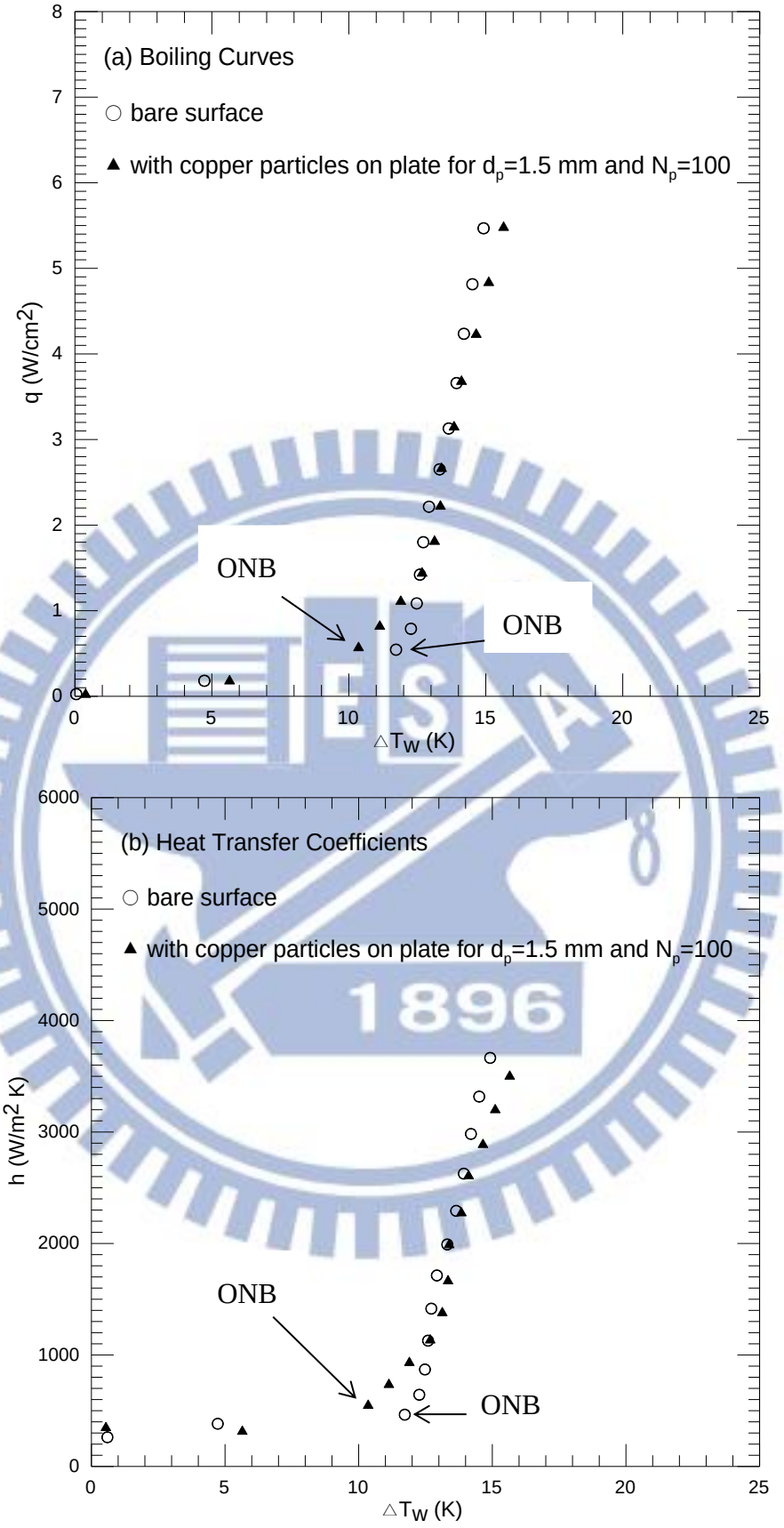


Fig. 4.20 Effects of copper particle diameter and number on saturated pool boiling curves (a) and boiling heat transfer coefficients (b) at $d_p$=1.5 mm and $N_p = 100$ .

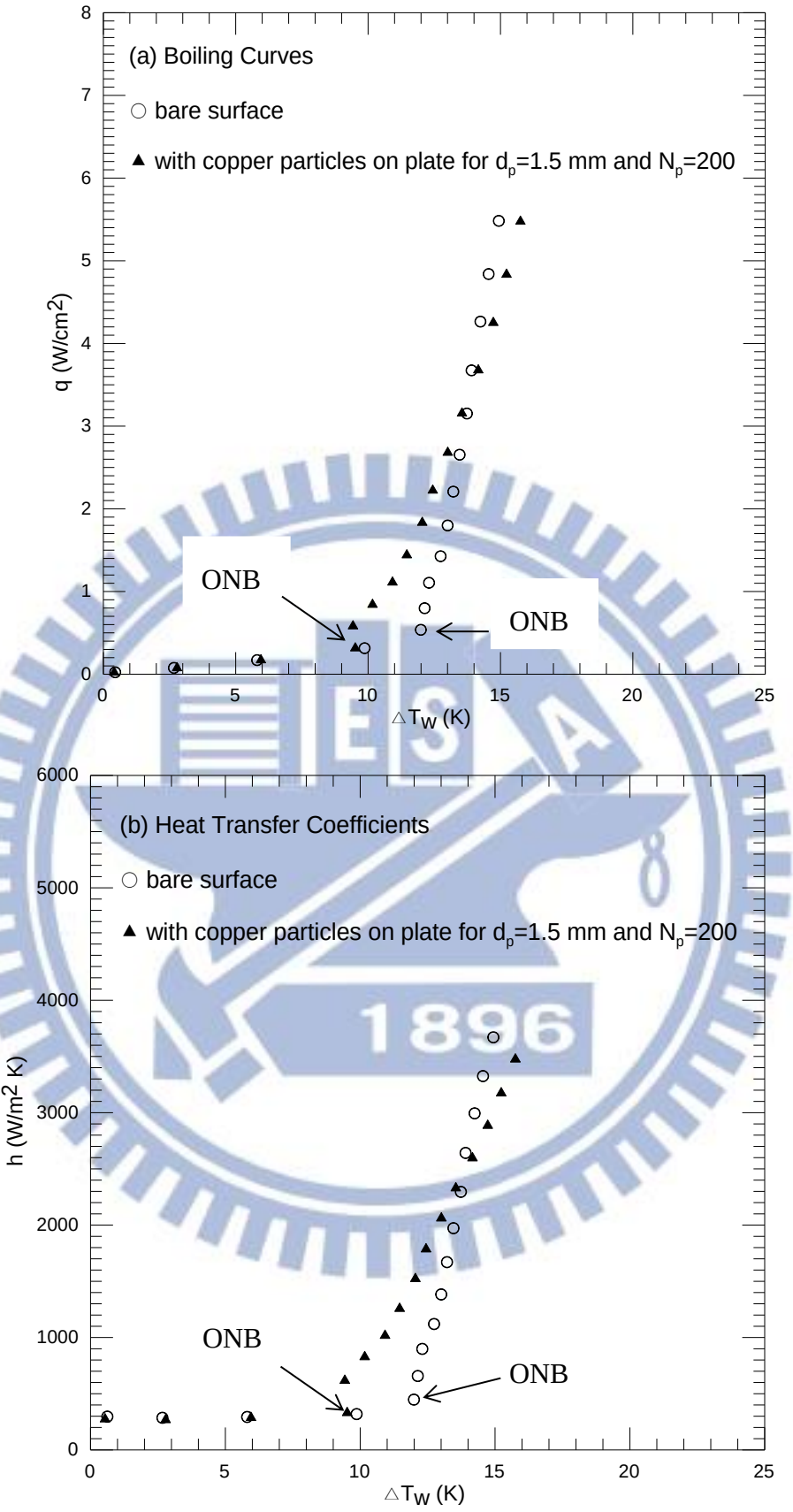


Fig. 4.21 Effects of copper particle diameter and number on saturated pool boiling curves (a) and boiling heat transfer coefficients (b) at $d_p$=1.5 mm and $N_p = 200$ .

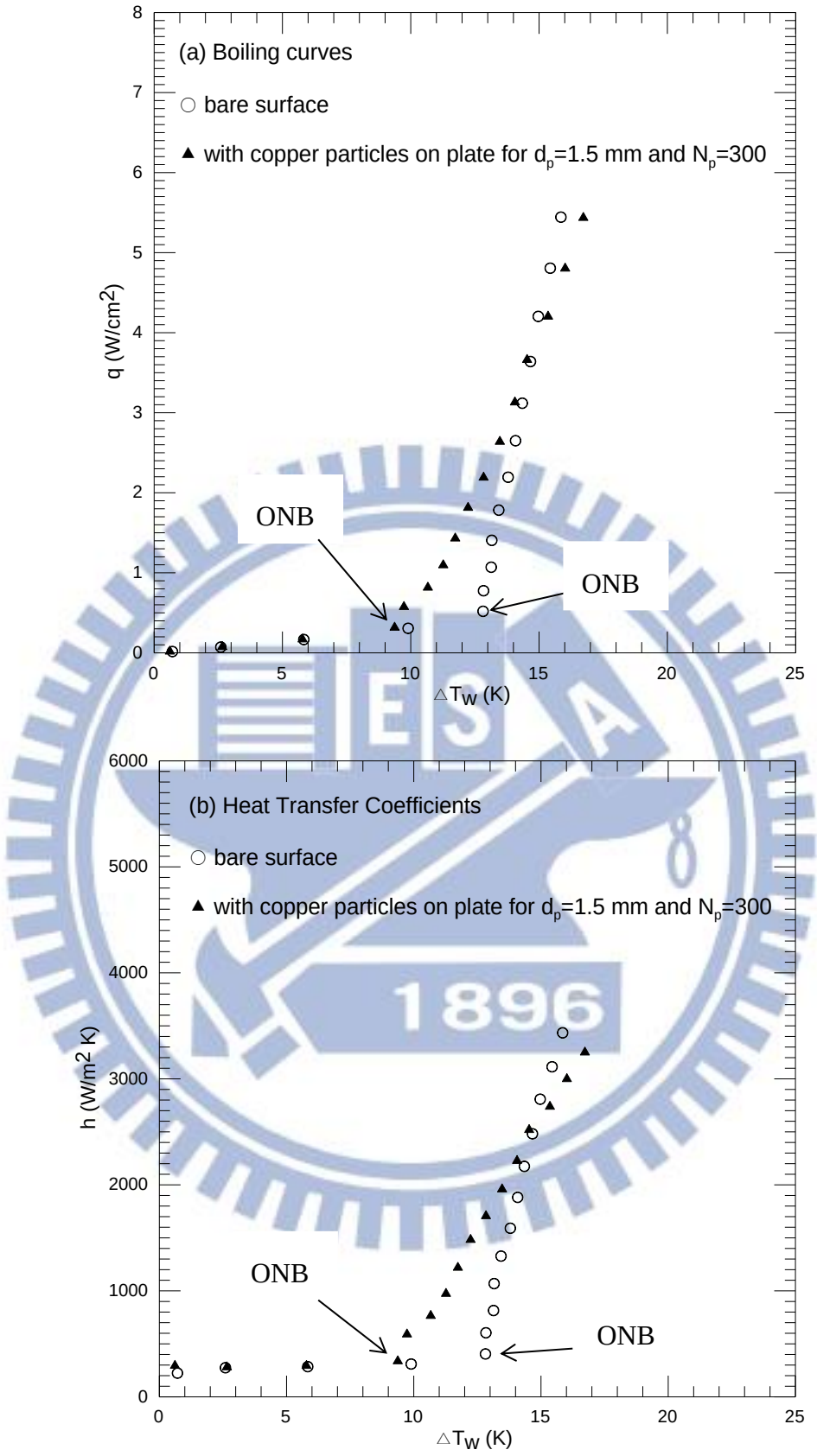


Fig. 4.22 Effects of copper particle diameter and number on saturated pool boiling curves (a) and boiling heat transfer coefficients (b) at $d_p$=1.5 mm and $N_p = 300$ .

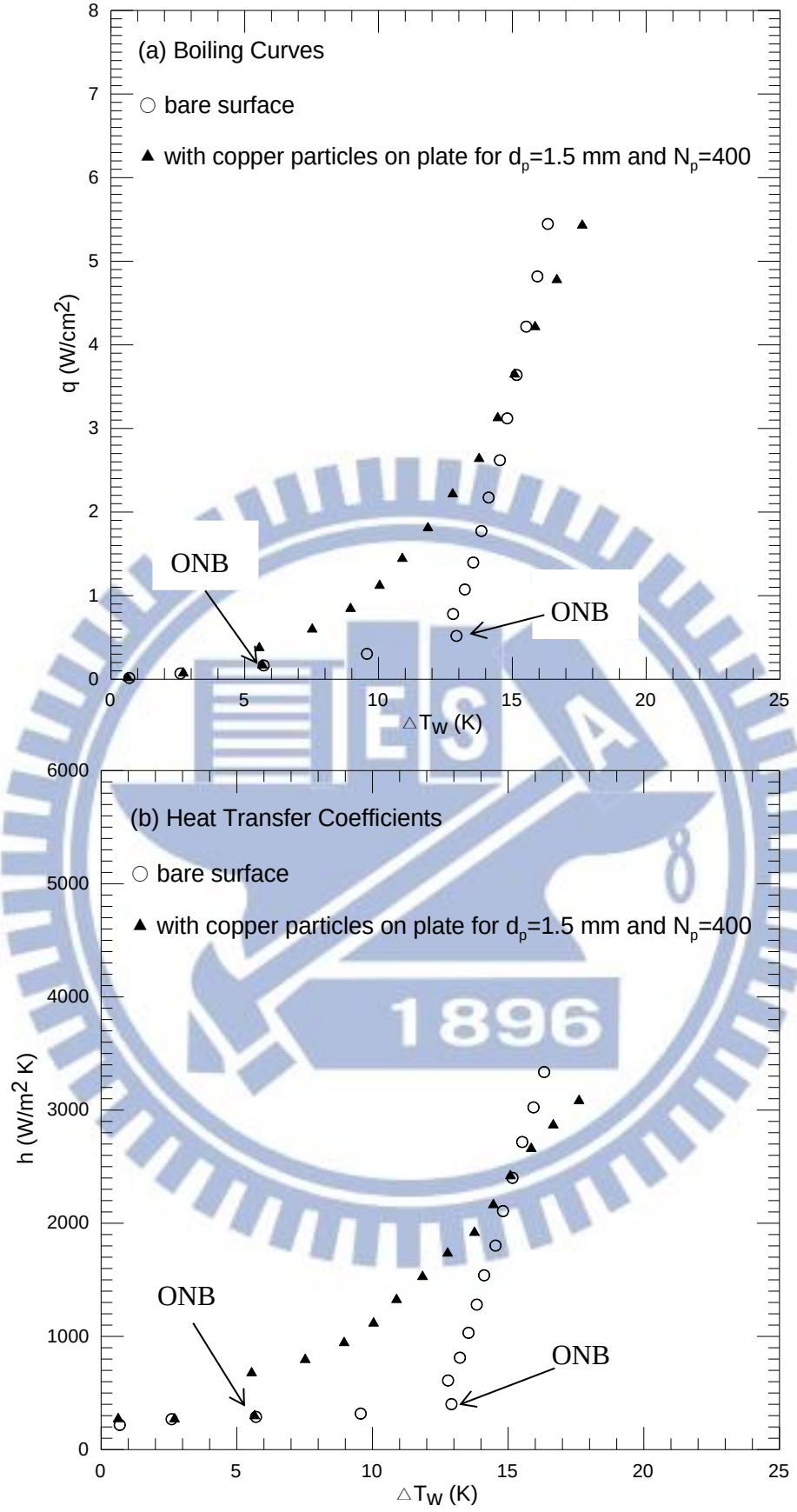


Fig. 4.23 Effects of copper particle diameter and number on saturated pool boiling curves (a) and boiling heat transfer coefficients (b) at $d_p$=1.5 mm and $N_p = 400$ .

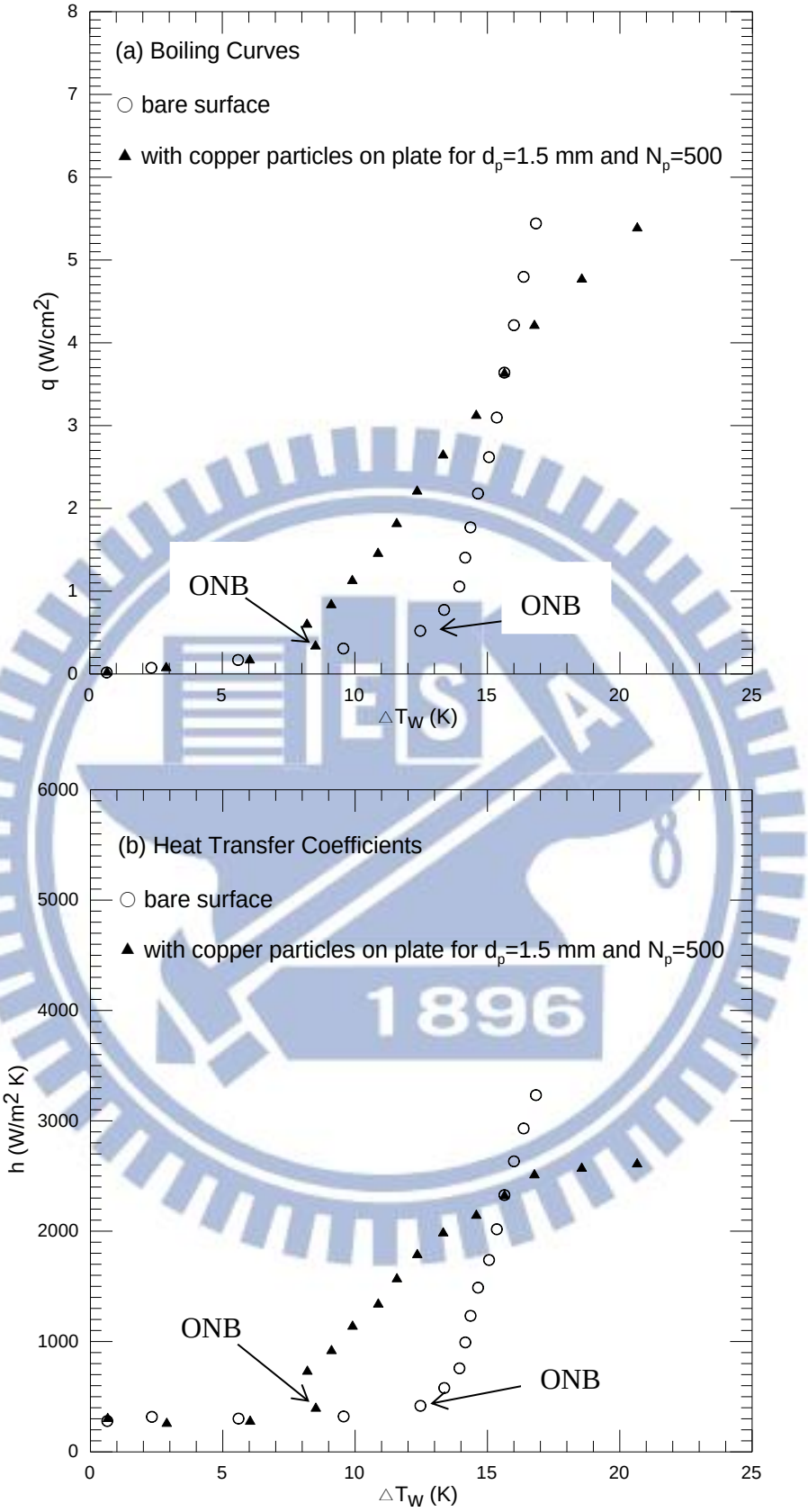


Fig. 4.24 Effects of copper particle diameter and number on saturated pool boiling curves (a) and boiling heat transfer coefficients (b) at $d_p$=1.5 mm and $N_p = 500$ .

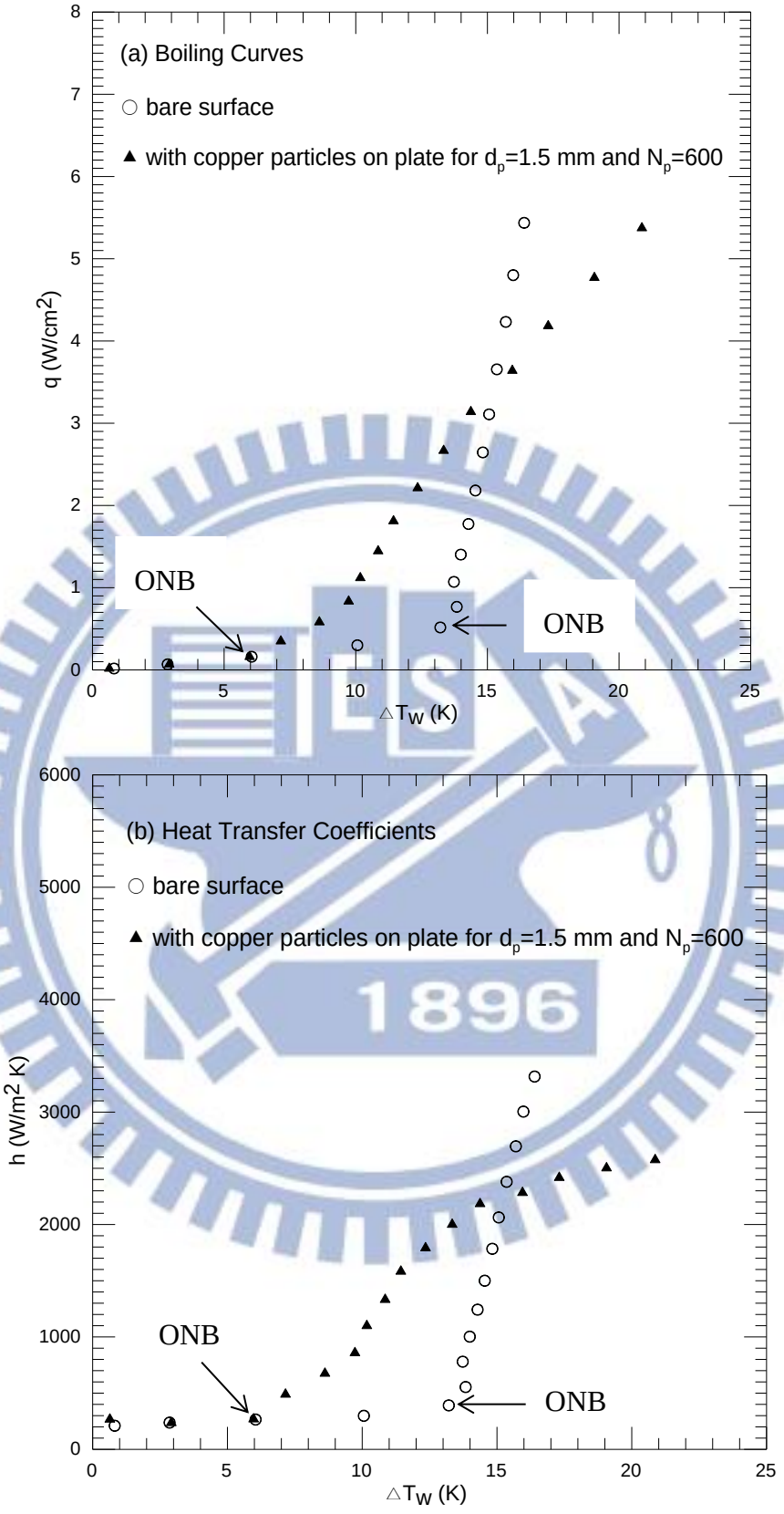


Fig. 4.25 Effects of copper particle diameter and number on saturated pool boiling curves (a) and boiling heat transfer coefficients (b) at $d_p$=1.5 mm and $N_p = 600$ .

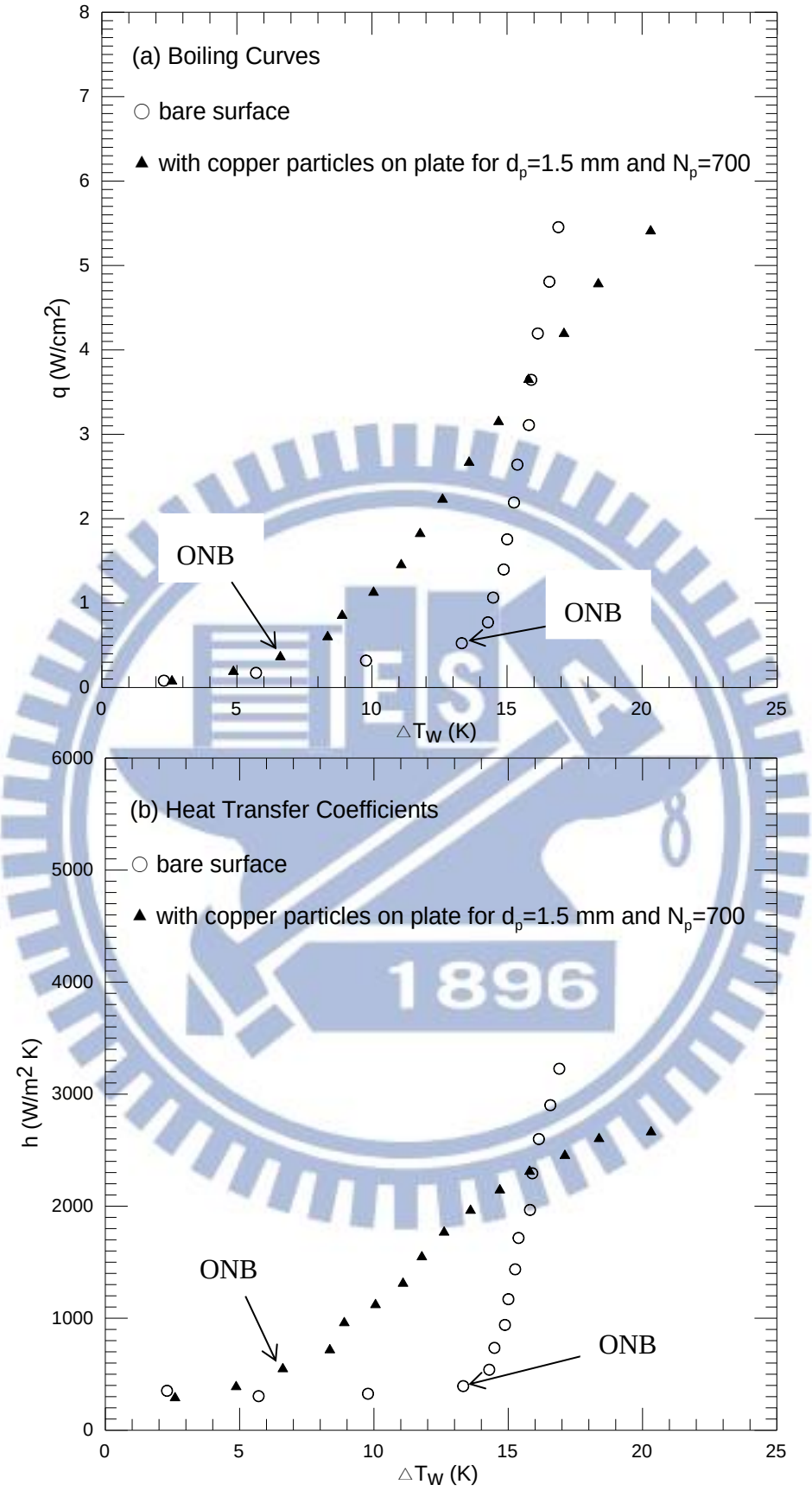


Fig. 4.26 Effects of copper particle diameter and number on saturated pool boiling curves (a) and boiling heat transfer coefficients (b) at $d_p$=1.5 mm and $N_p = 700$ .

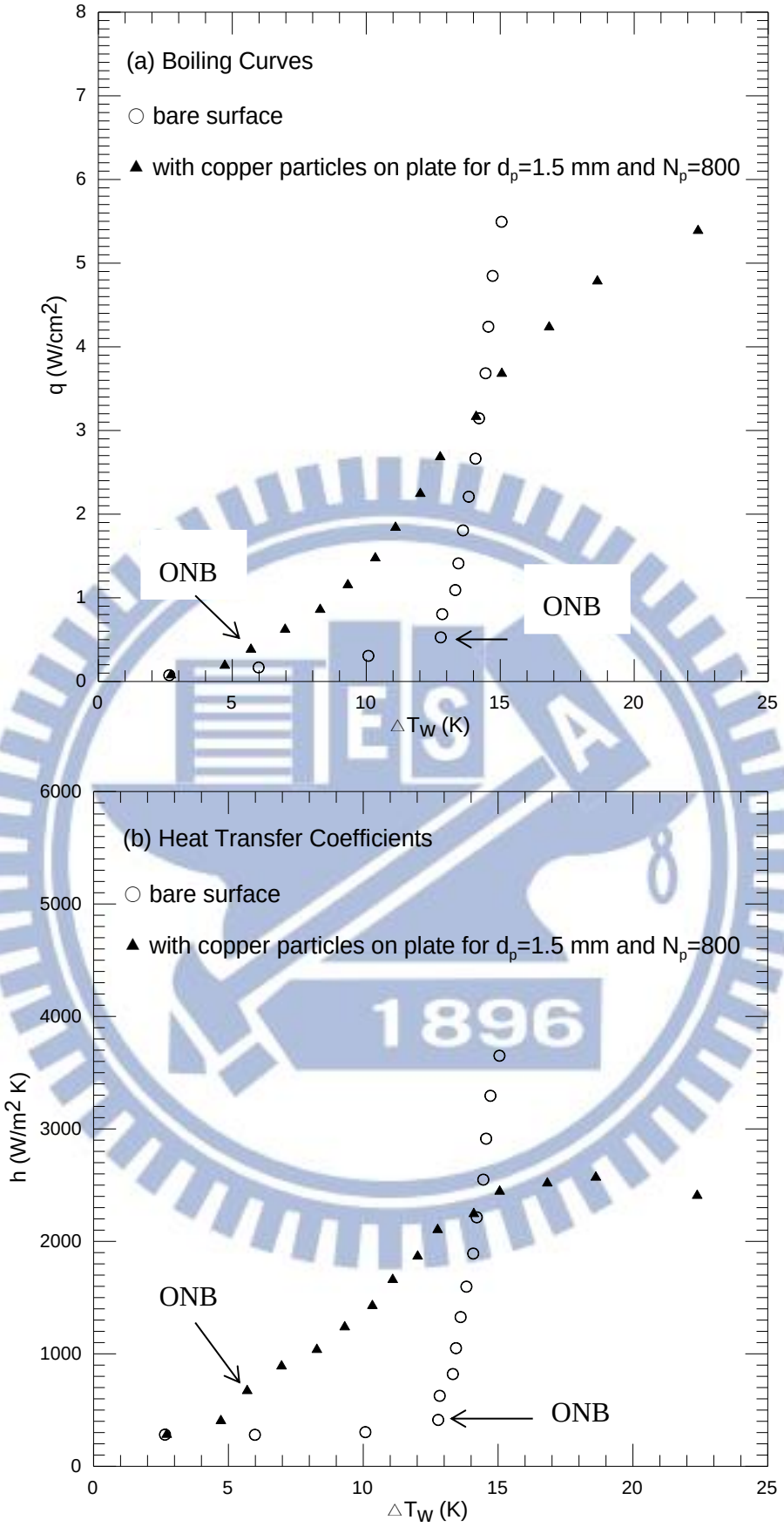


Fig. 4.27 Effects of copper particle diameter and number on saturated pool boiling curves (a) and boiling heat transfer coefficients (b) at $d_p$=1.5 mm and $N_p = 800$ .

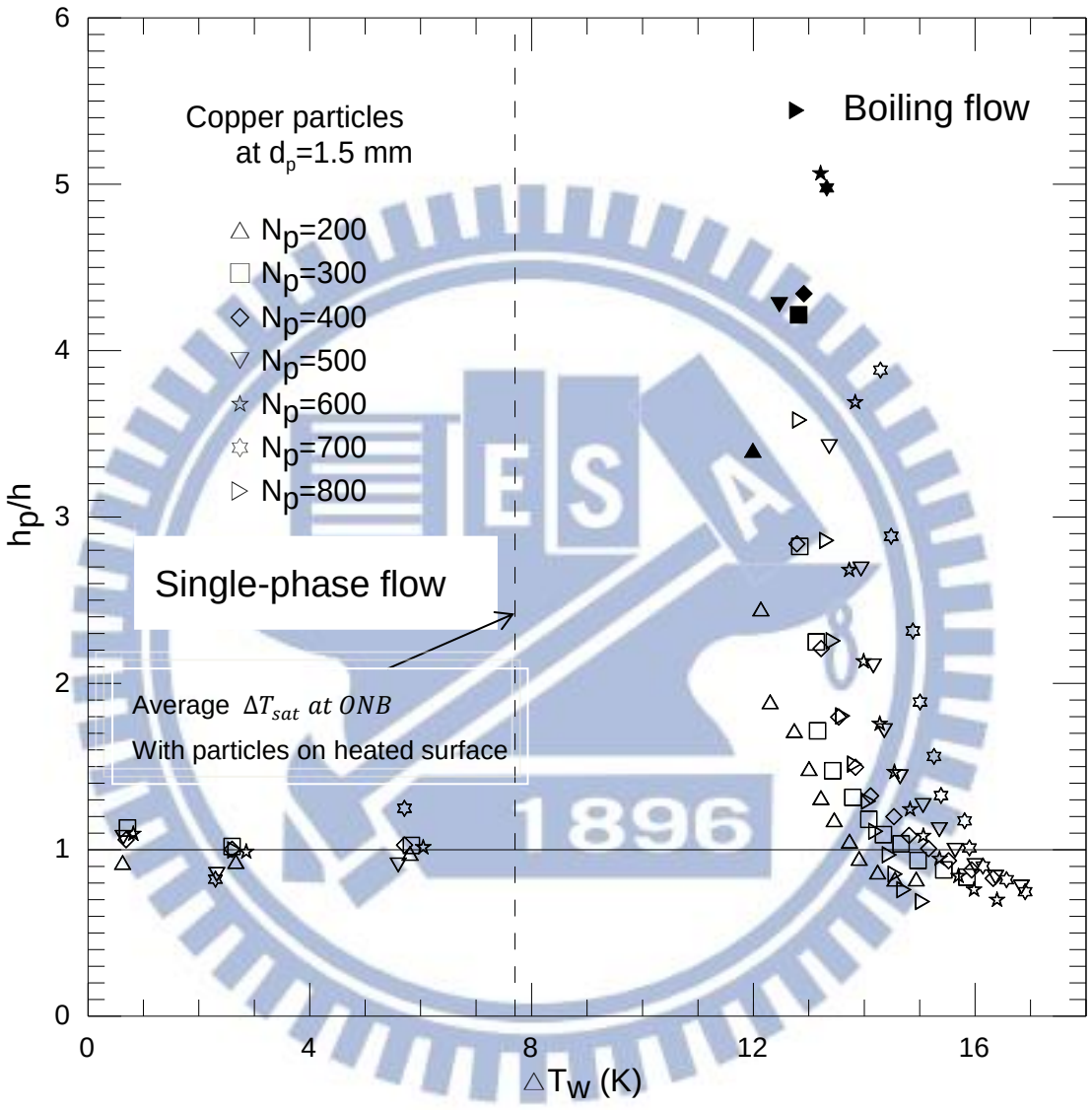


Fig. 4.28 Variations of $h_p/h$ with wall superheat for various copper particle numbers at $d_p$=1.5 mm (solid symbols denote best boiling heat transfer enhancement for various $N_p$)

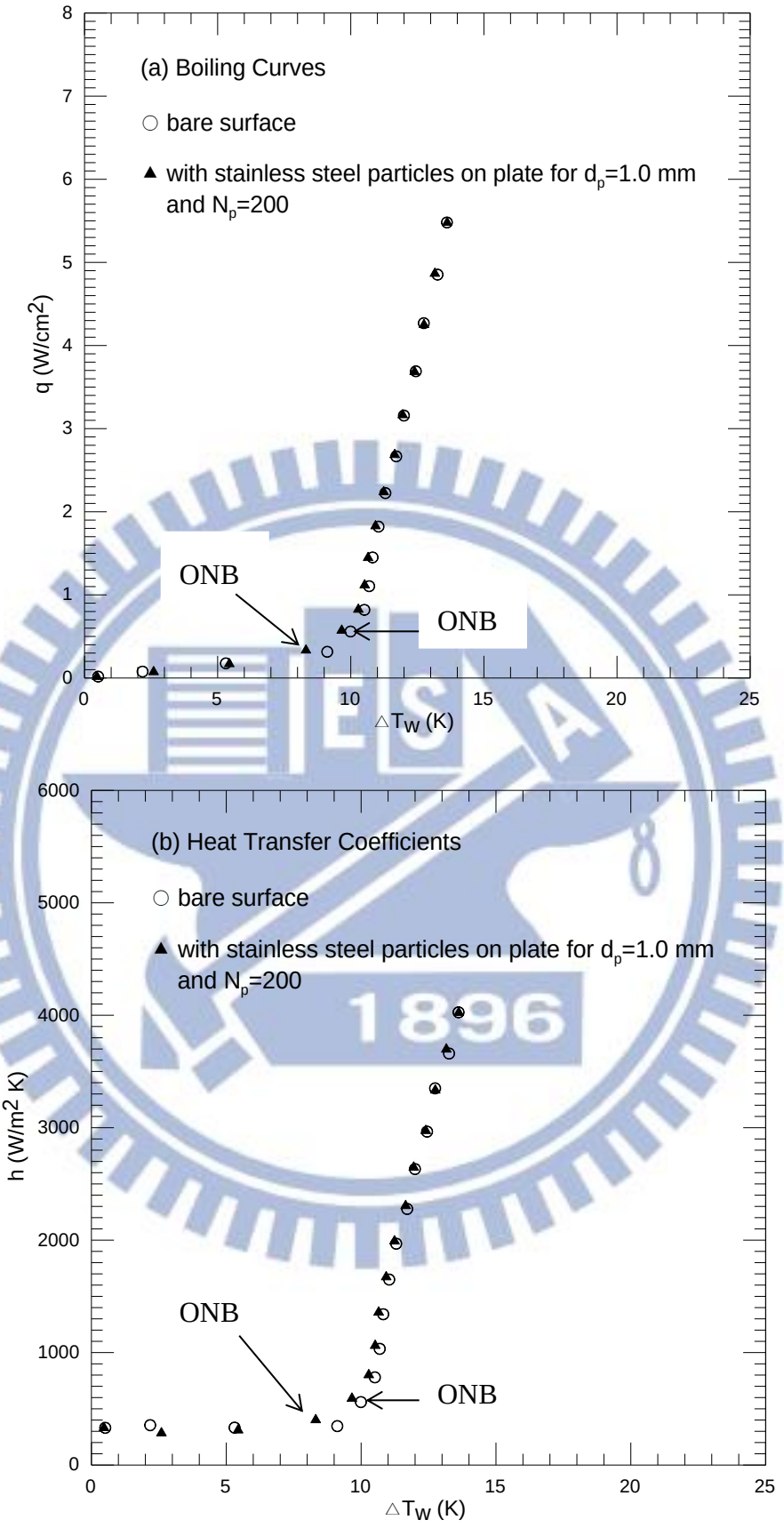


Fig. 4.29 Effects of stainless steel particle diameter and number on saturated pool boiling curves (a) and boiling heat transfer coefficients (b) at $d_p$=1.0 mm and $N_p = 200$.

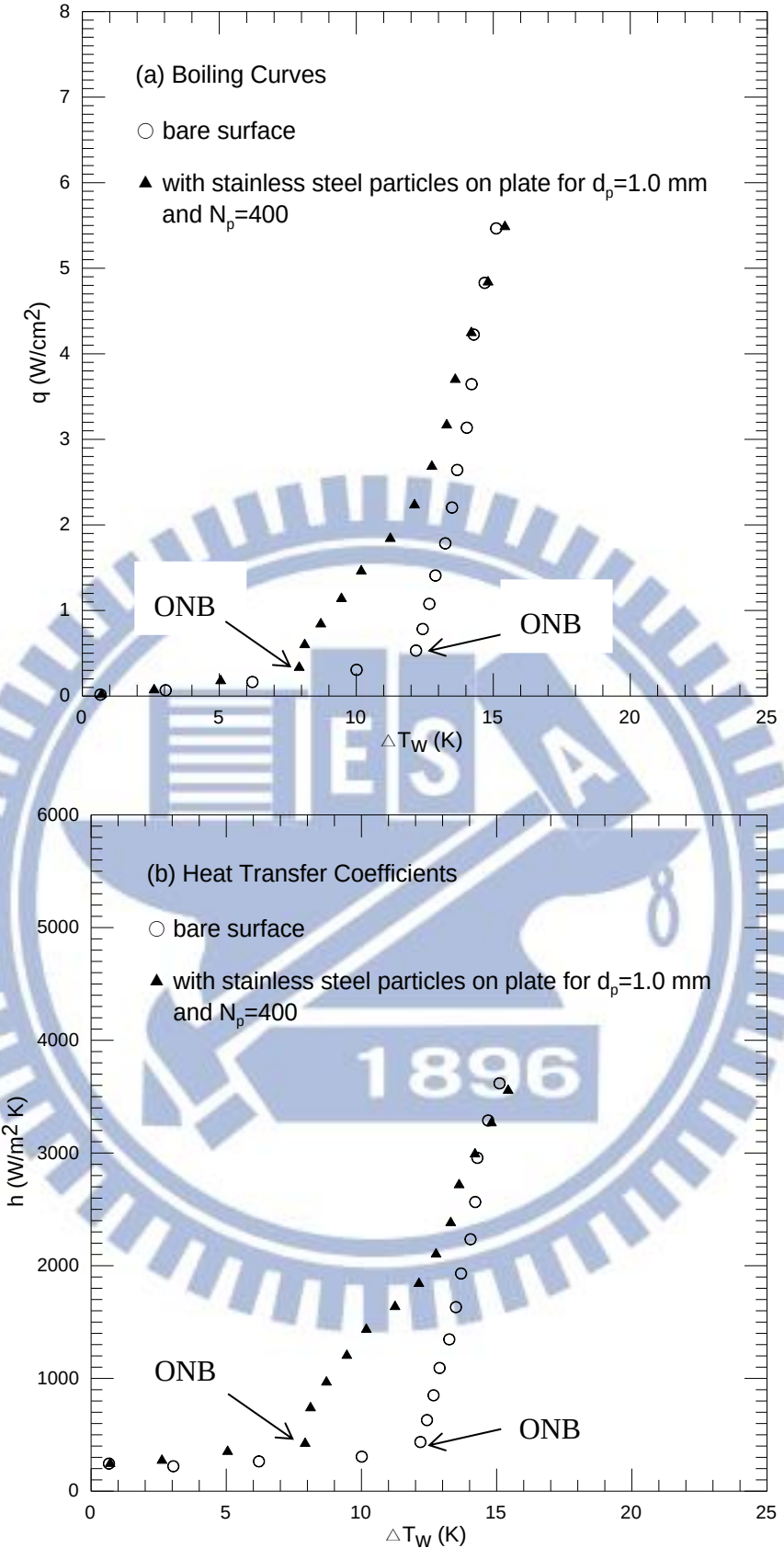


Fig. 4.30 Effects of stainless steel particle diameter and number on saturated pool boiling curves (a) and boiling heat transfer coefficients (b) at $d_p$=1.0 mm and $N_p = 400$ .

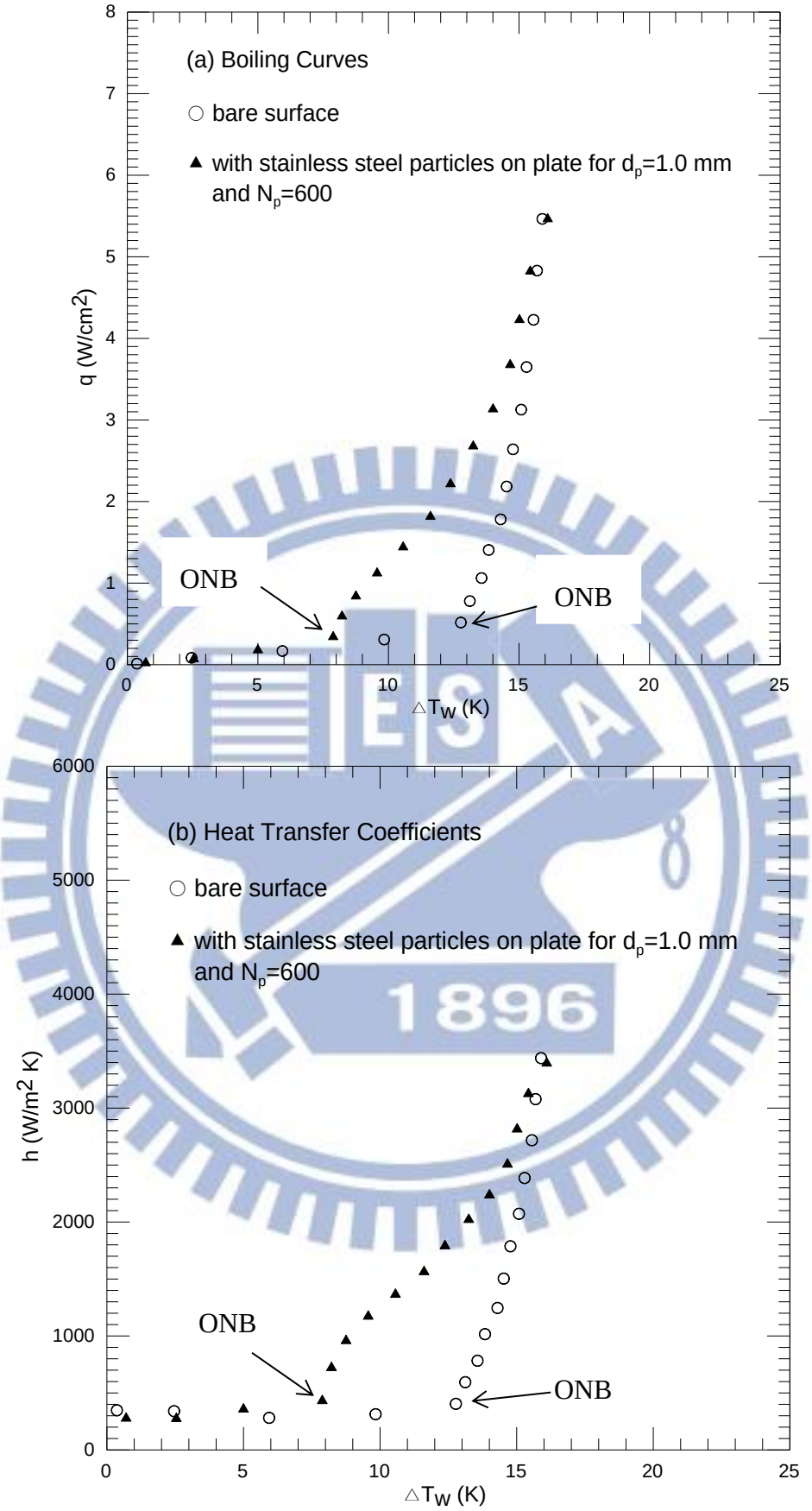


Fig. 4.31 Effects of stainless steel particle diameter and number on saturated pool boiling curves (a) and boiling heat transfer coefficients (b) at $d_p$=1.0 mm and $N_p = 600$.

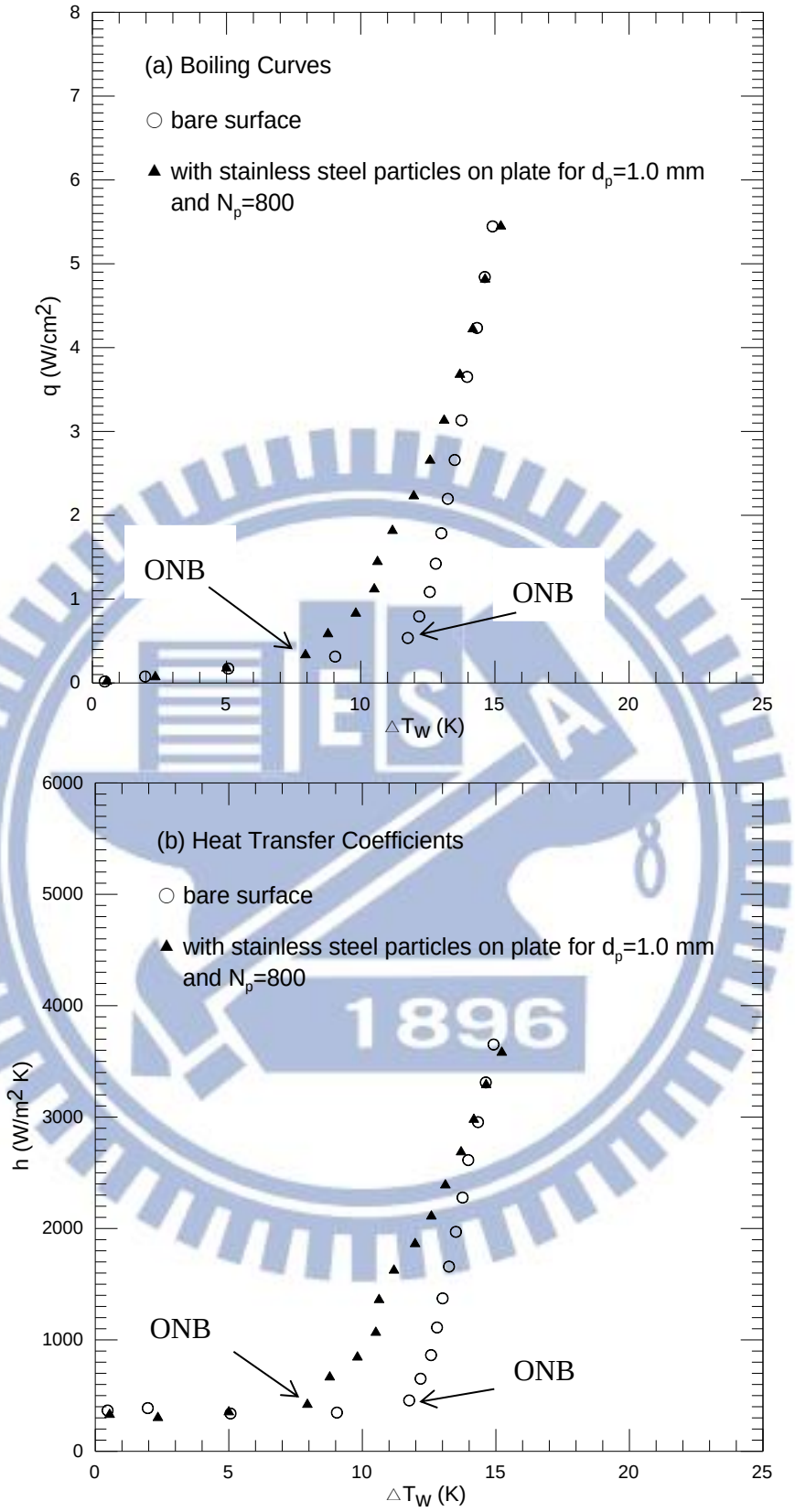


Fig. 4.32 Effects of stainless steel particle diameter and number on saturated pool boiling curves (a) and boiling heat transfer coefficients (b) at $d_p$=1.0 mm and $N_p = 800$ .

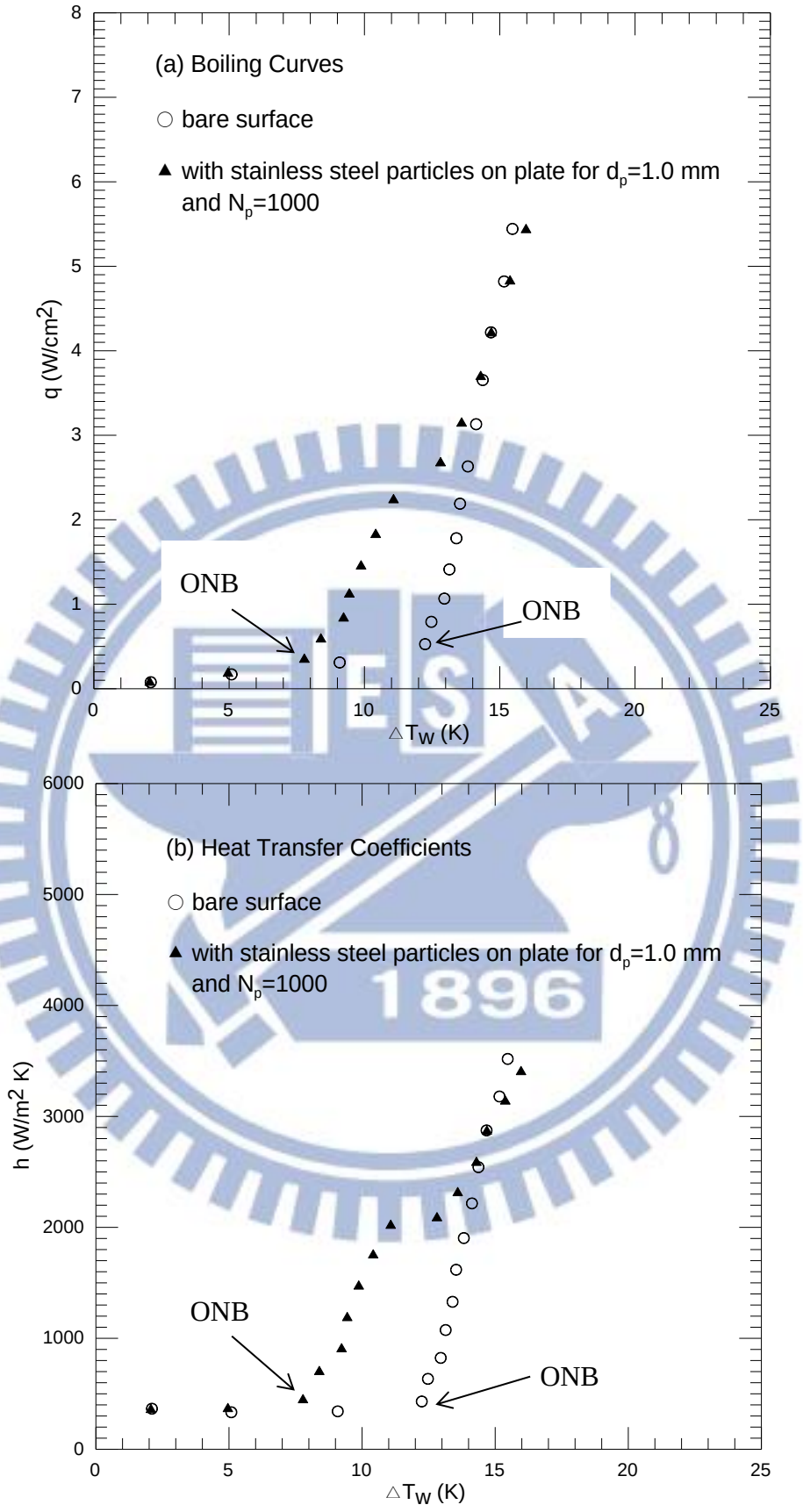


Fig. 4.33 Effects of stainless steel particle diameter and number on saturated pool boiling curves (a) and boiling heat transfer coefficients (b) at $d_p$=1.0 mm and $N_p = 1000$ .

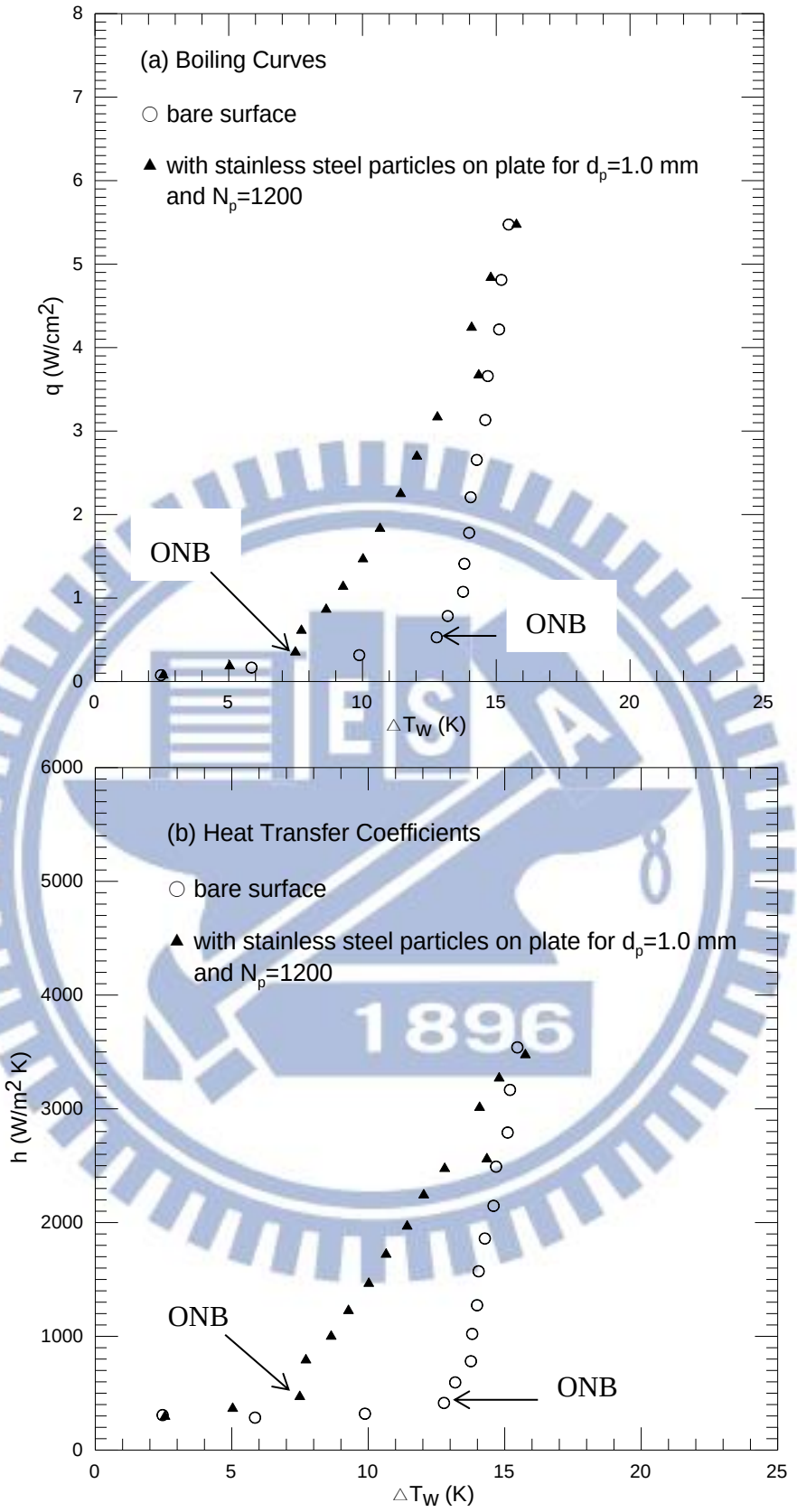


Fig. 4.34 Effects of stainless steel particle diameter and number on saturated pool boiling curves (a) and boiling heat transfer coefficients (b) at $d_p$=1.0 mm and $N_p = 1200$ .

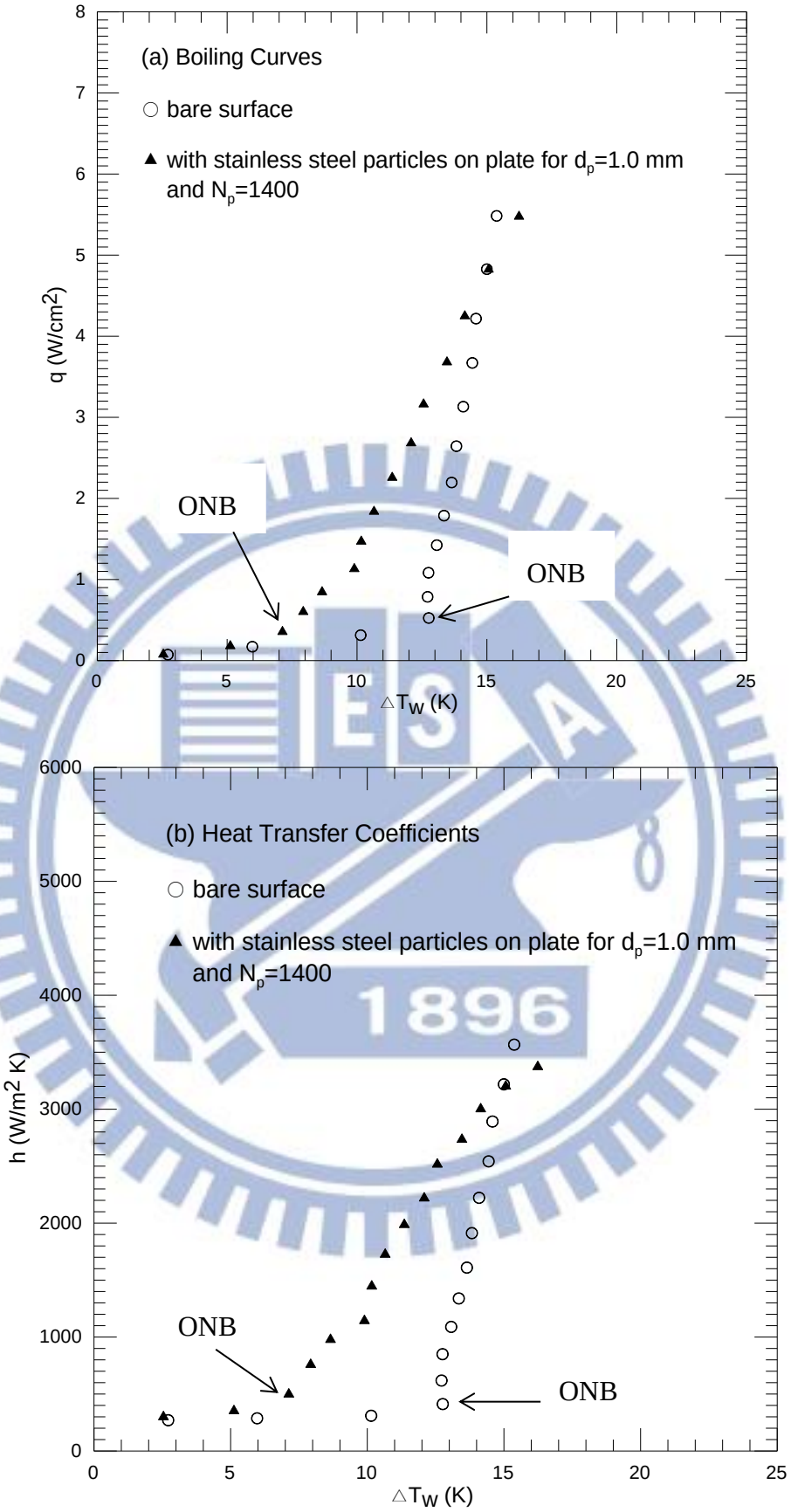


Fig. 4.35 Effects of stainless steel particle diameter and number on saturated pool boiling curves (a) and boiling heat transfer coefficients (b) at $d_p$=1.0 mm and $N_p = 1400$ .

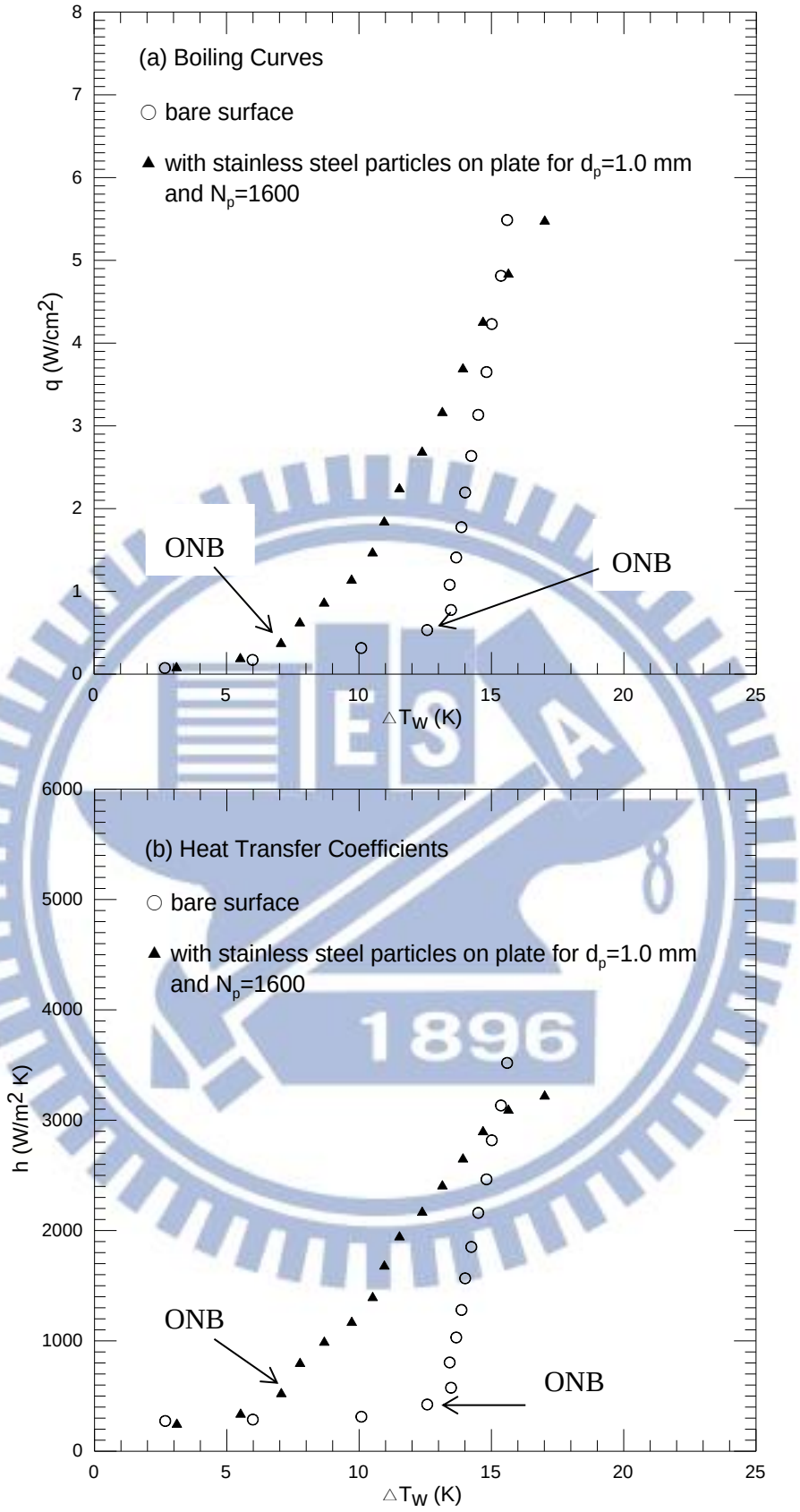


Fig. 4.36 Effects of stainless steel particle diameter and number on saturated pool boiling curves (a) and boiling heat transfer coefficients (b) at $d_p$=1.0 mm and $N_p = 1600$ .

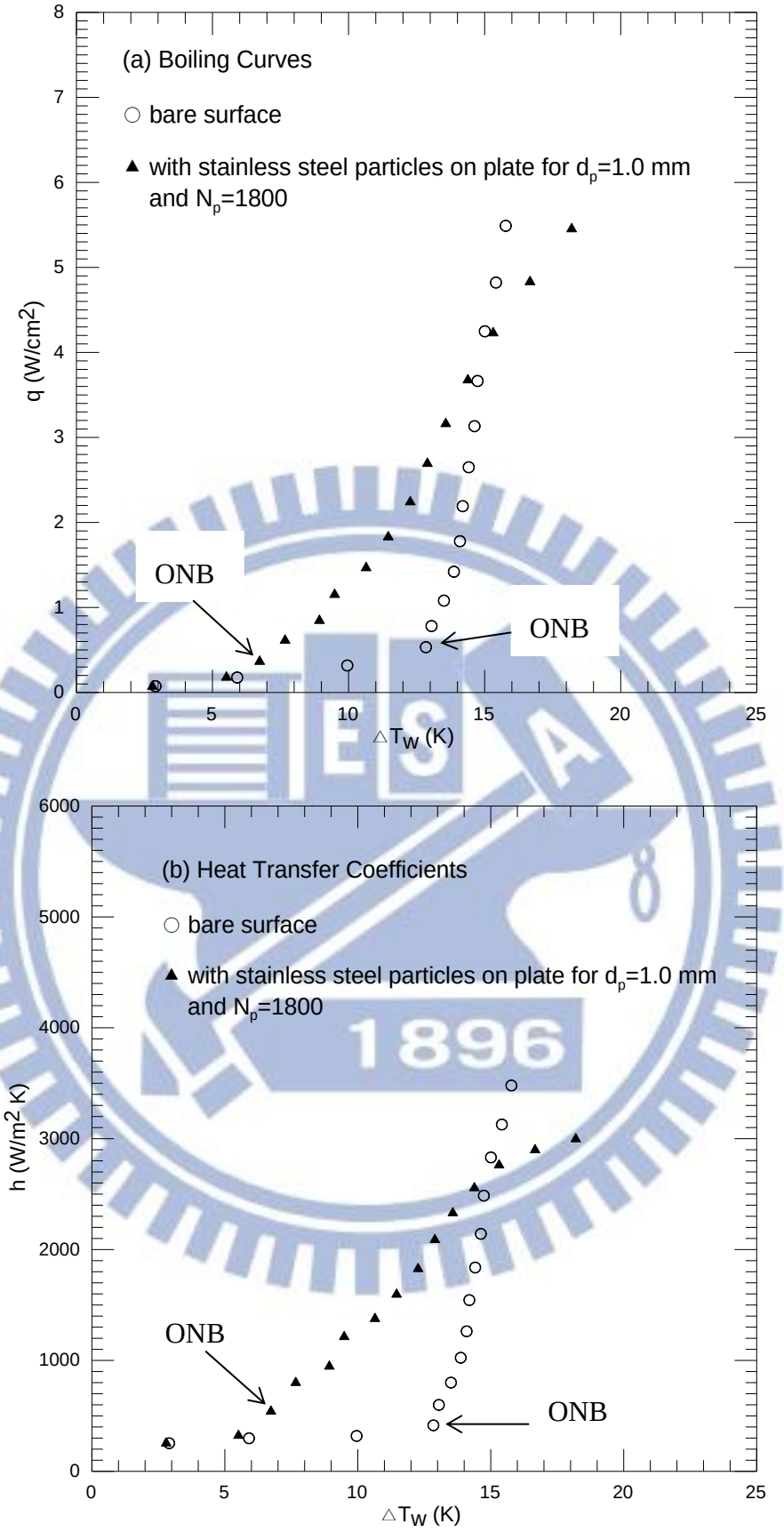


Fig. 4.37 Effects of stainless steel particle diameter and number on saturated pool boiling curves (a) and boiling heat transfer coefficients (b) at $d_p$=1.0 mm and $N_p = 1800$ .

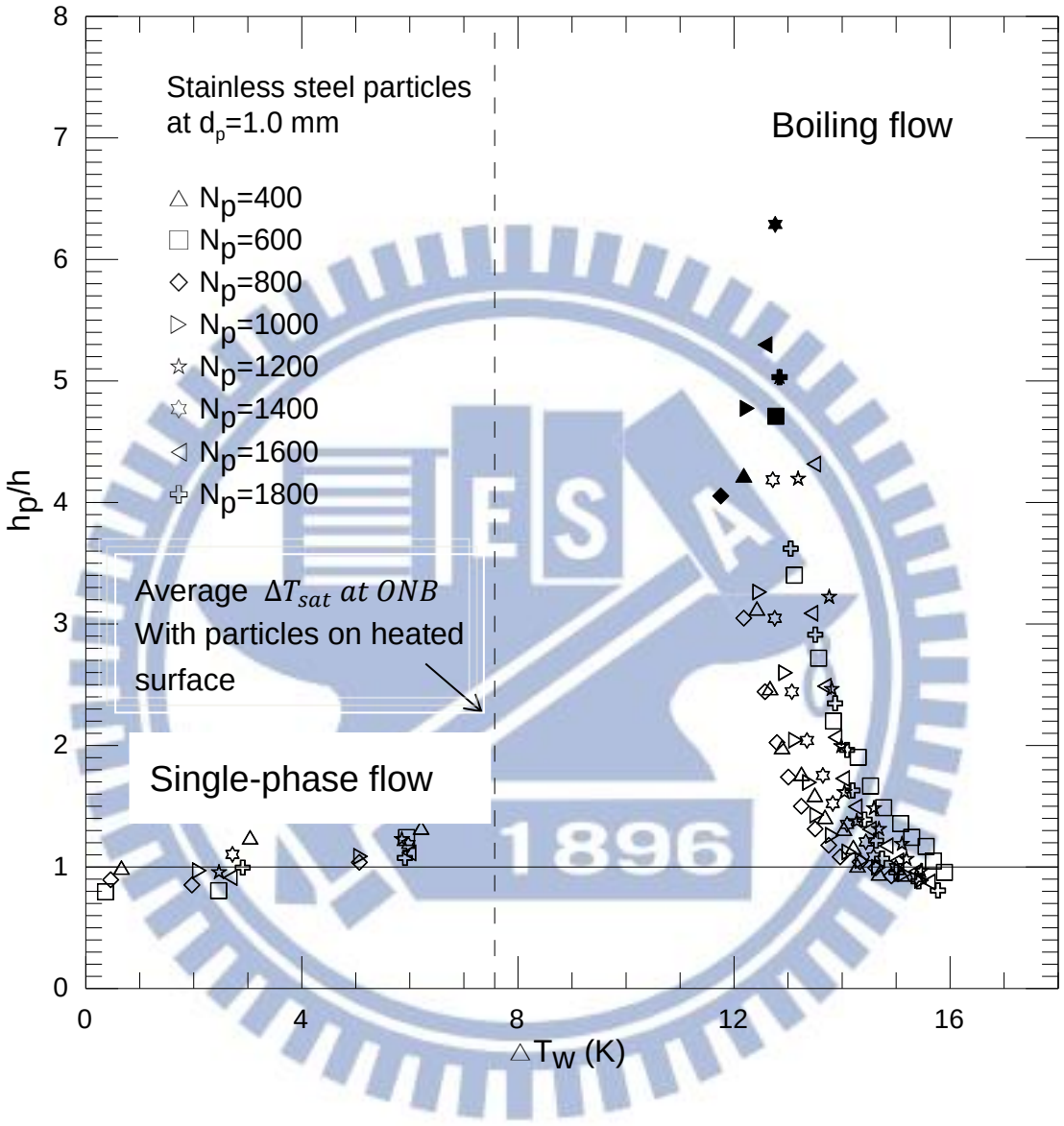


Fig. 4.38 Variations of $h_p/h$ with wall superheat for various stainless steel particle numbers at $d_p$=1.0 mm (solid symbols denote best boiling heat transfer enhancement for various $N_p$)

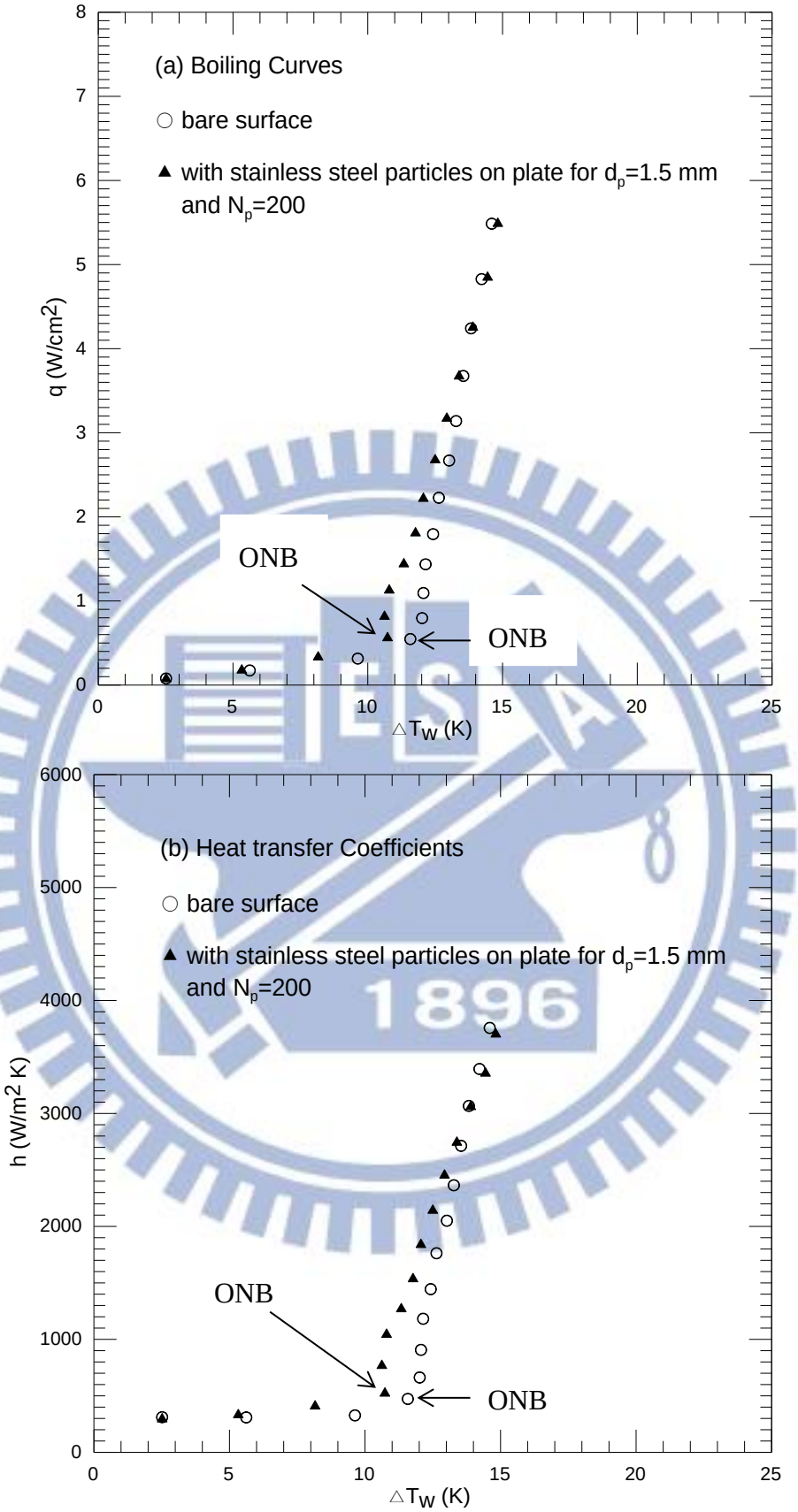


Fig. 4.39 Effects of stainless steel particle diameter and number on saturated pool boiling curves (a) and boiling heat transfer coefficients (b) at $d_p$=1.5 mm and $N_p = 200$ .

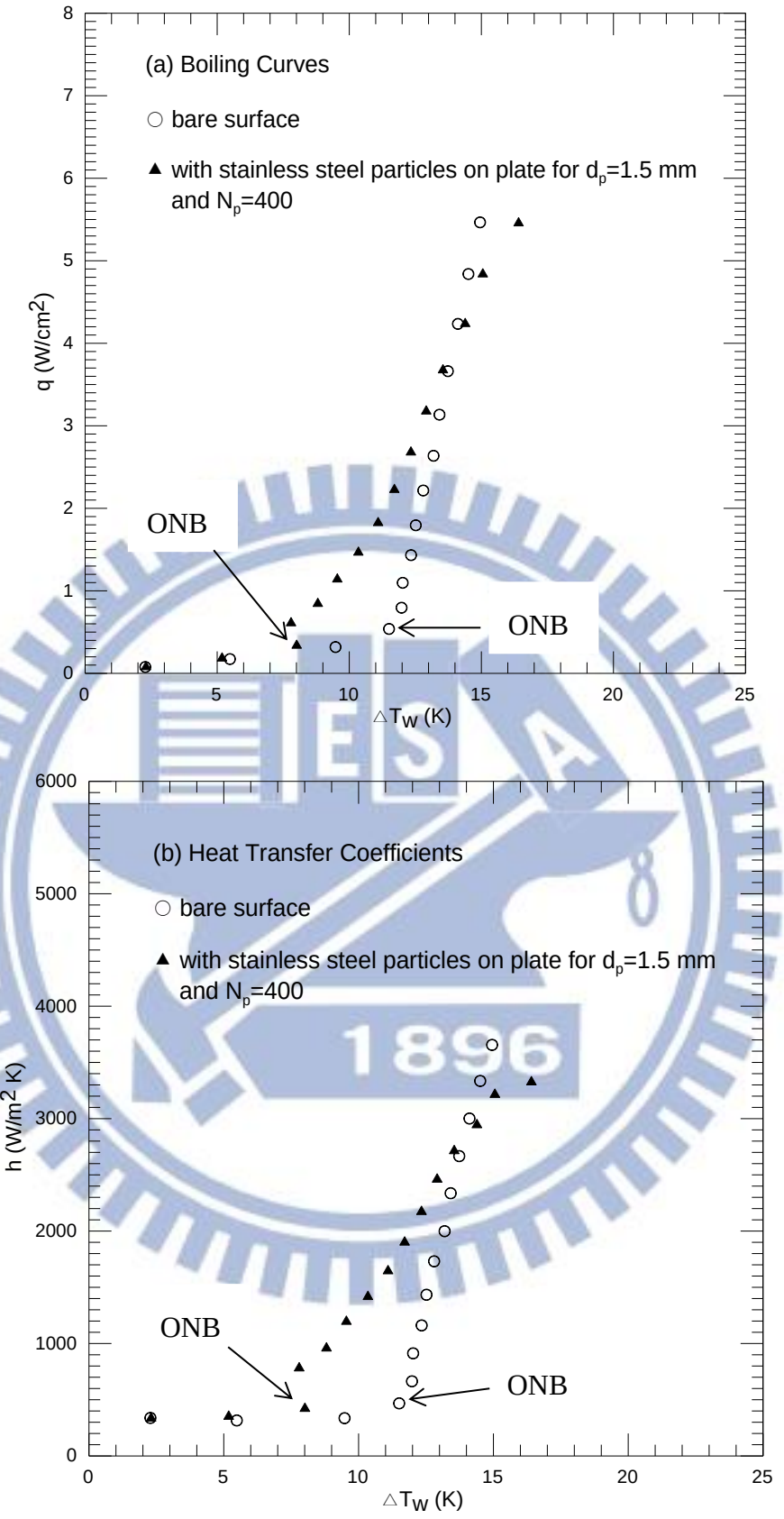


Fig. 4.40 Effects of stainless steel particle diameter and number on saturated pool boiling curves (a) and boiling heat transfer coefficients (b) at $d_p$=1.5 mm and $N_p = 400$ .

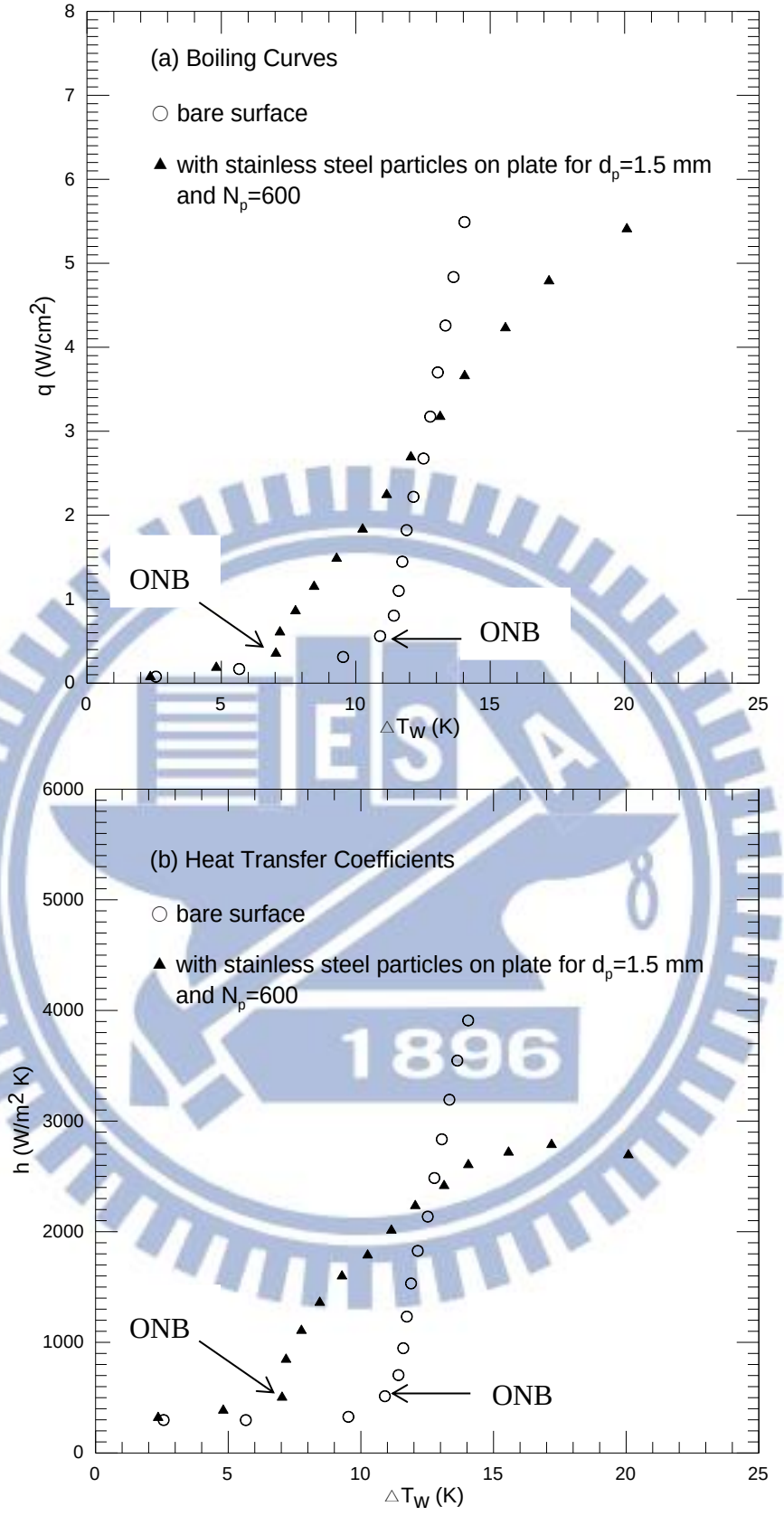


Fig. 4.41 Effects of stainless steel particle diameter and number on saturated pool boiling curves (a) and boiling heat transfer coefficients (b) at $d_p$=1.5 mm and $N_p = 600$ .

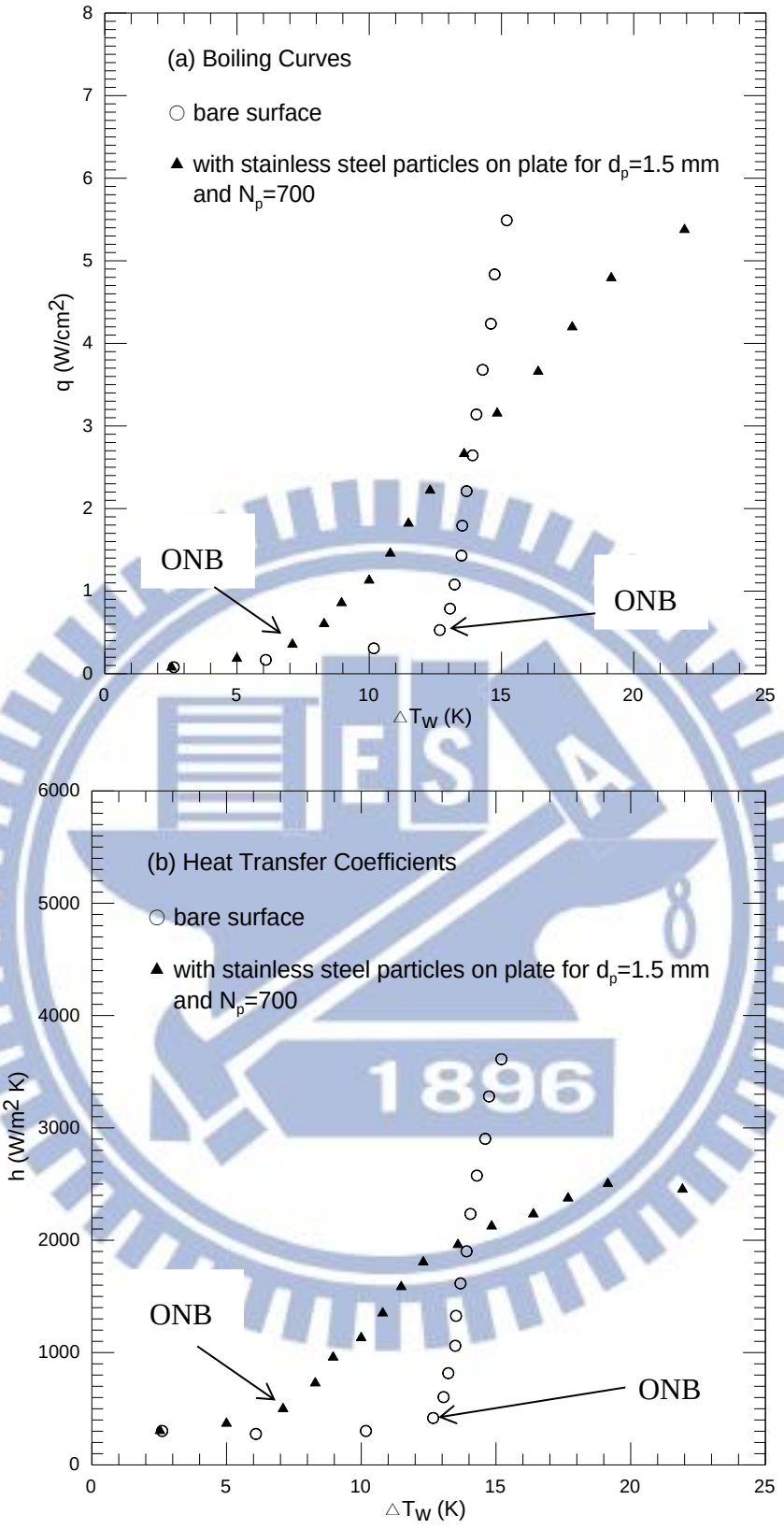


Fig. 4.42 Effects of stainless steel particle diameter and number on saturated pool boiling curves (a) and boiling heat transfer coefficients (b) at $d_p$=1.5 mm and $N_p = 700$.

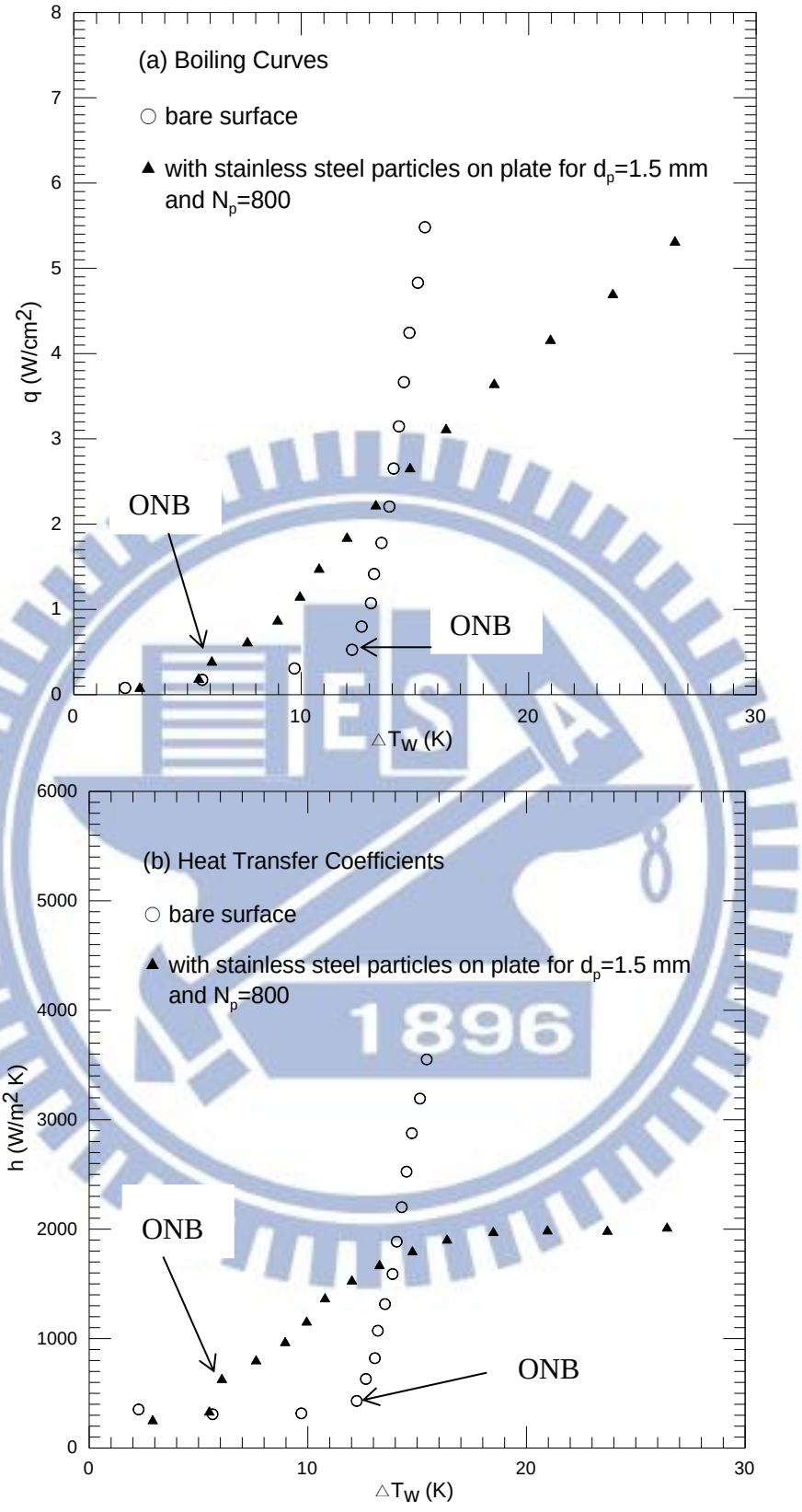


Fig. 4.43 Effects of stainless steel particle diameter and number on saturated pool boiling curves (a) and boiling heat transfer coefficients (b) at $d_p$=1.5 mm and $N_p = 800$ .

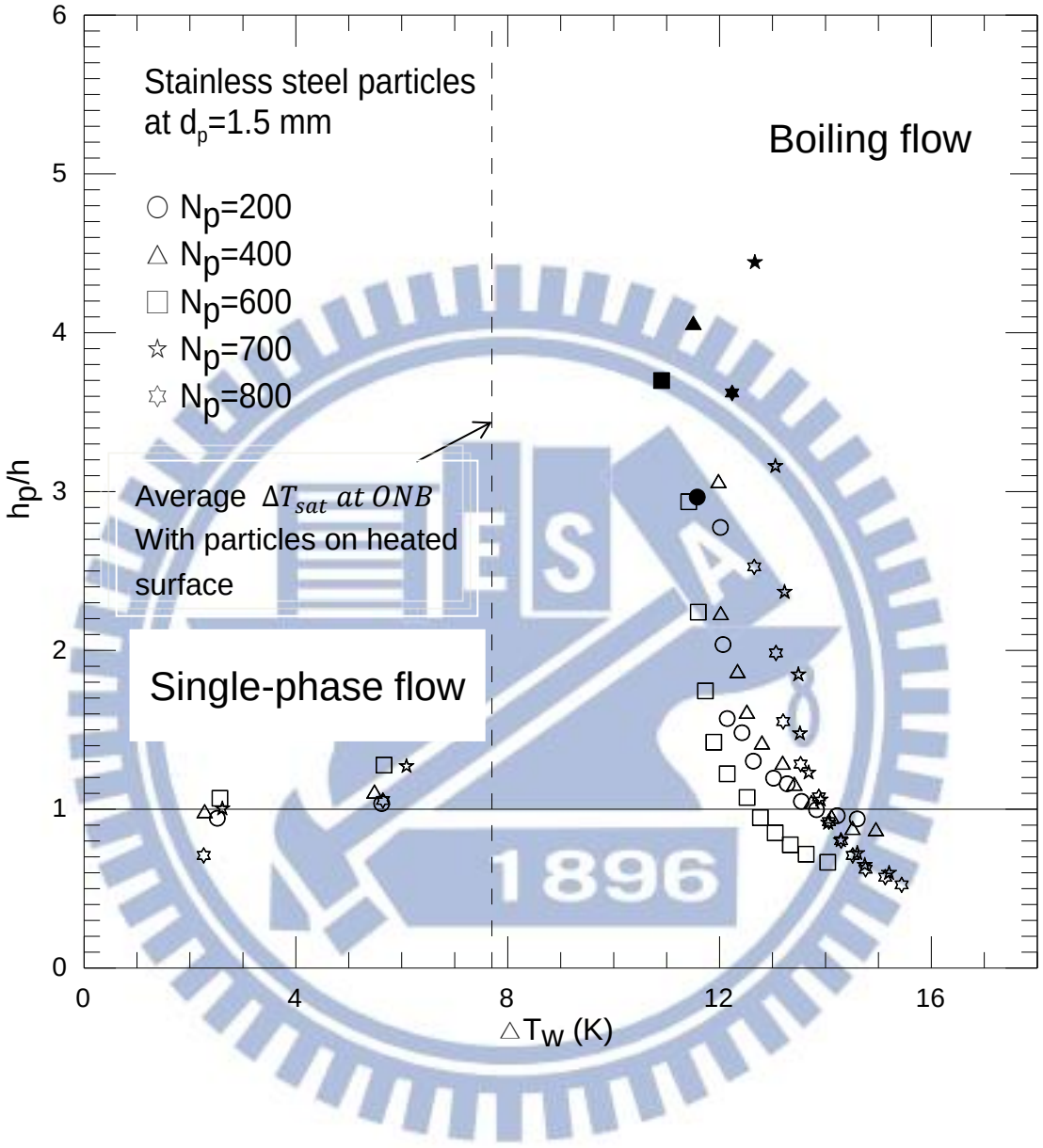


Fig. 4.44 Variations of $h_p/h$ with wall superheat for various stainless steel particle numbers at $d_p$=1.5 mm (solid symbols denote best boiling heat transfer enhancement for various $N_p$)

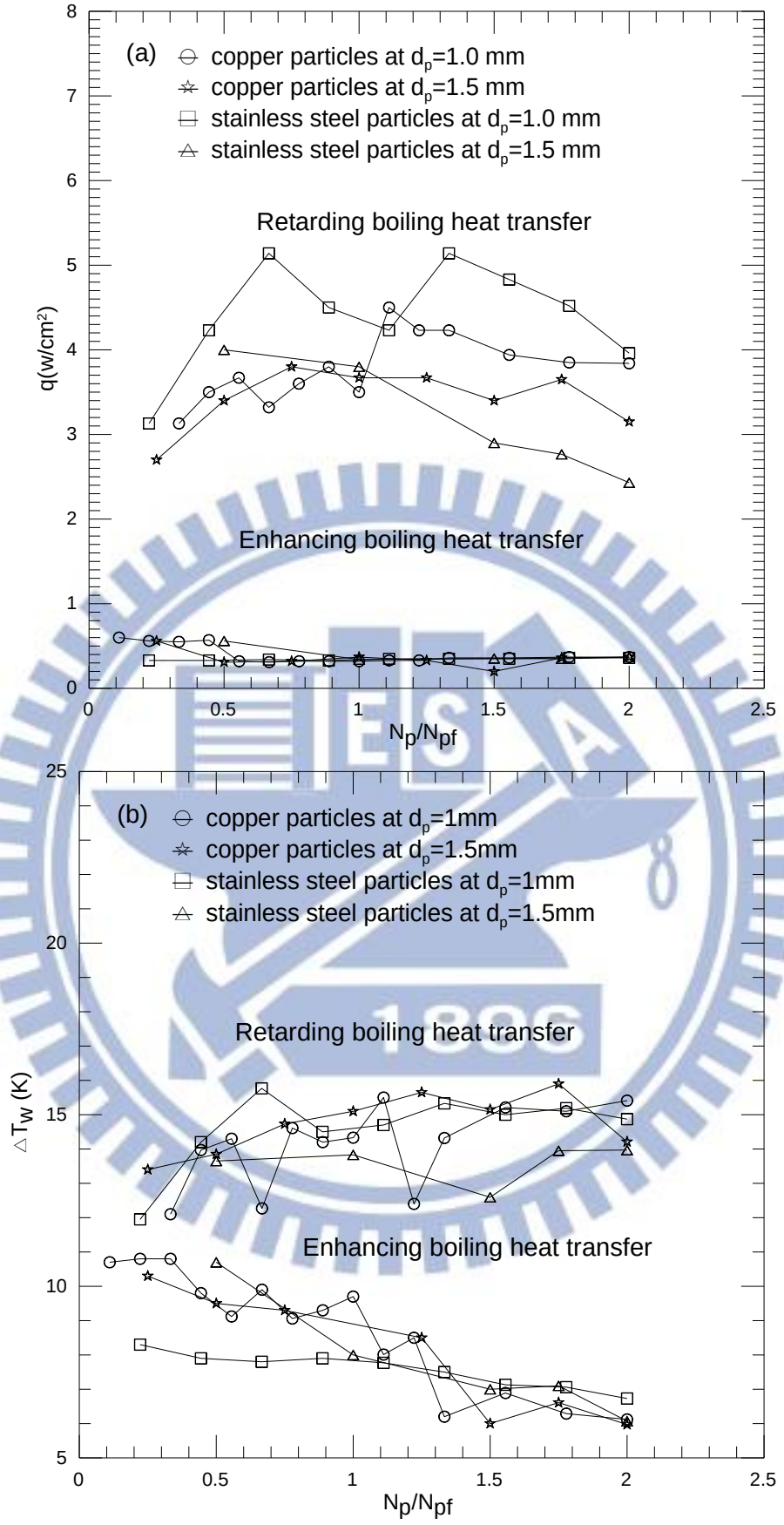


Fig. 4.45 Boundaries for boiling heat transfer augmentation and retardation for copper and stainless steel particles with different $d_p$ and $N_p$ based on (a) q vs. $N_p/N_{pf}$ and (b) $\Delta T_w$ vs. $N_p/N_{pf}$.

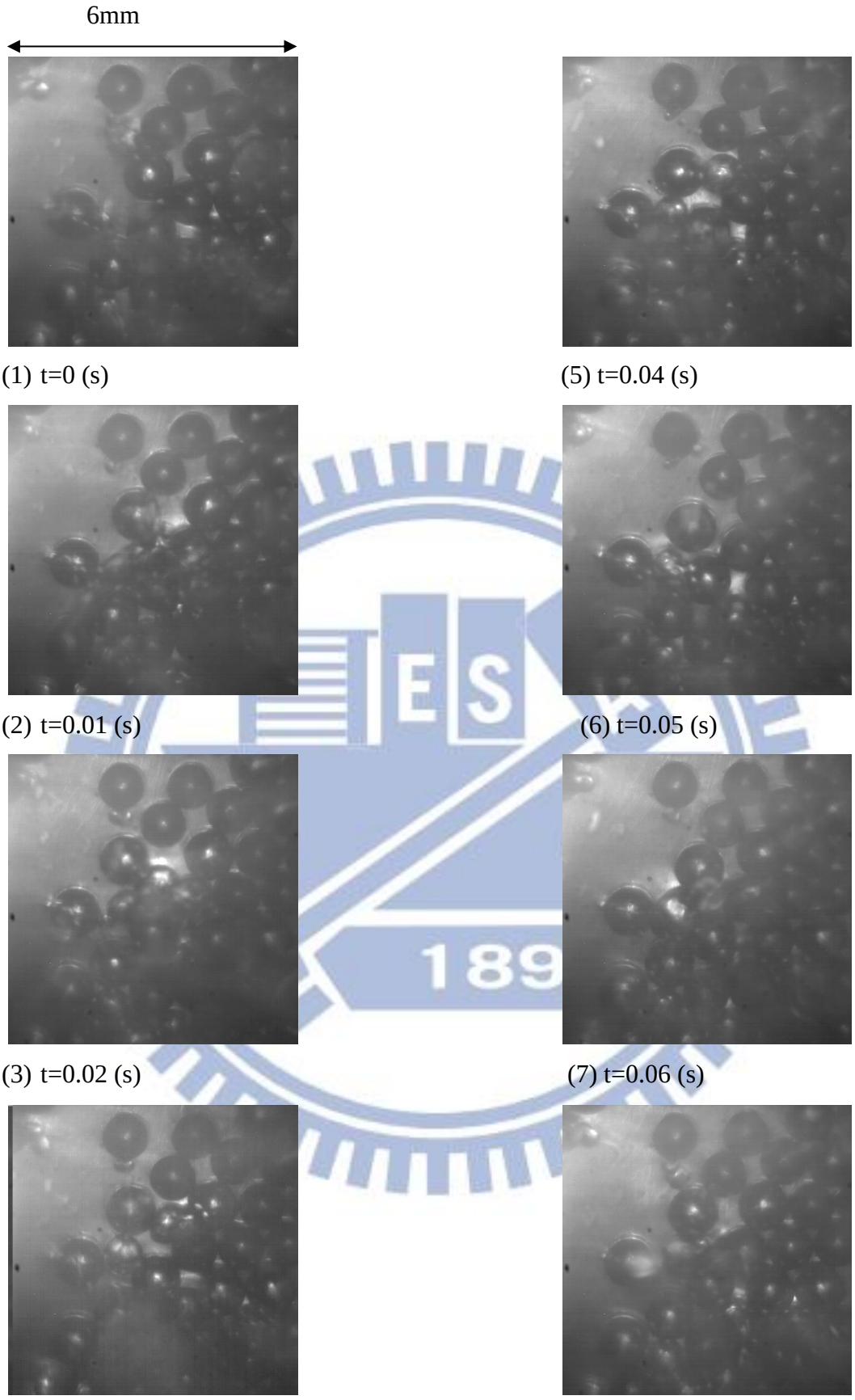


Fig. 4.46 Photos taken from top view of boiling flow at selected time instants for q= 0.85 W/ $cm^2$ with copper particles on heated surface at $d_p$=1.0 mm and $N_p = 600$

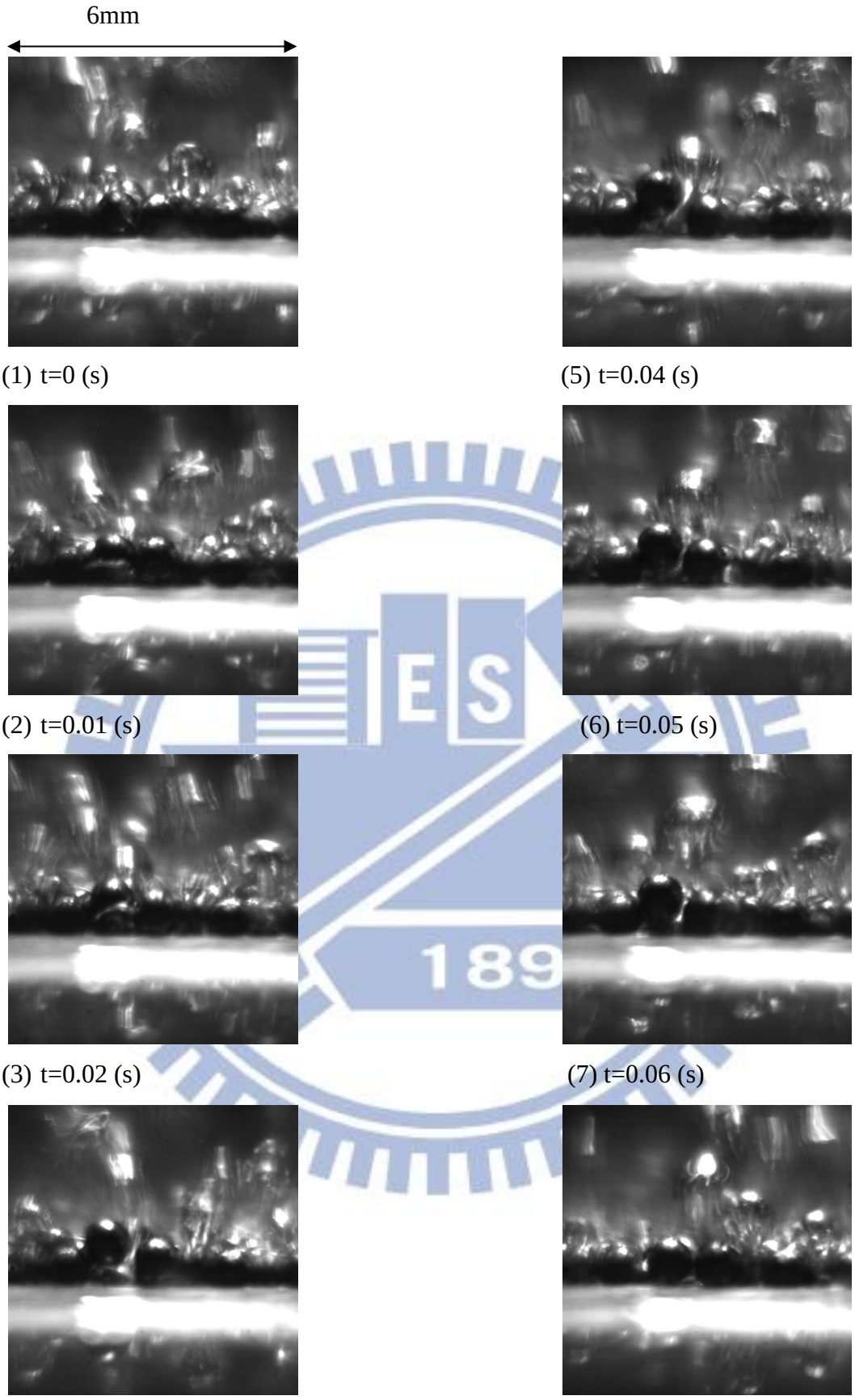


Fig. 4.47 Photos taken from side view of boiling flow at selected time instants for q= 0.85 W/ $cm^2$ with stainless steel particles on heated surface at $d_p$=1.0 mm and $N_p = 600$

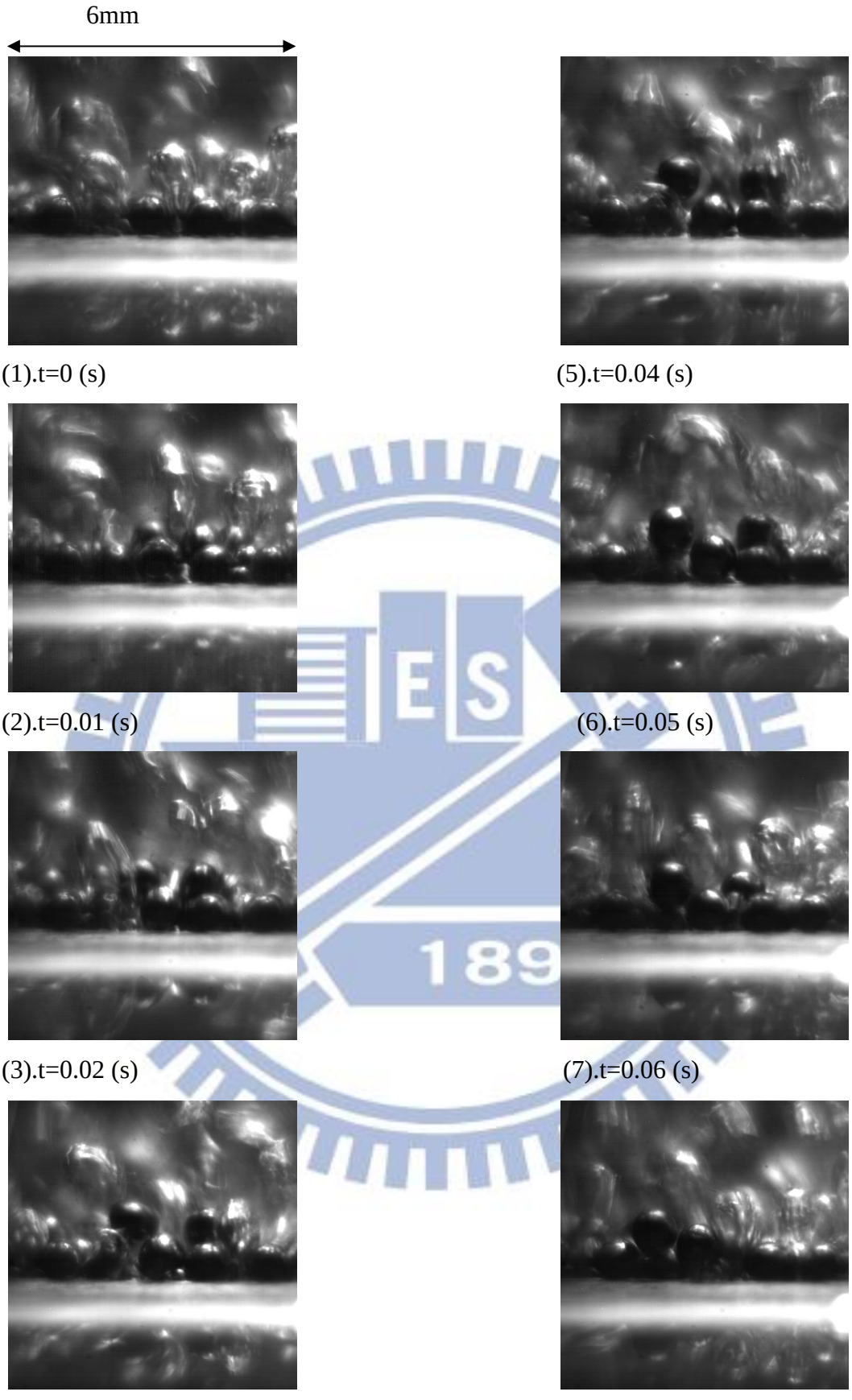


Fig. 4.48 Photos taken from side view of boiling flow at selected time instants for q= 1.45 W/ $cm^2$ with stainless steel particles on heated surface at $d_p$=1.0 mm and $N_p = 600$

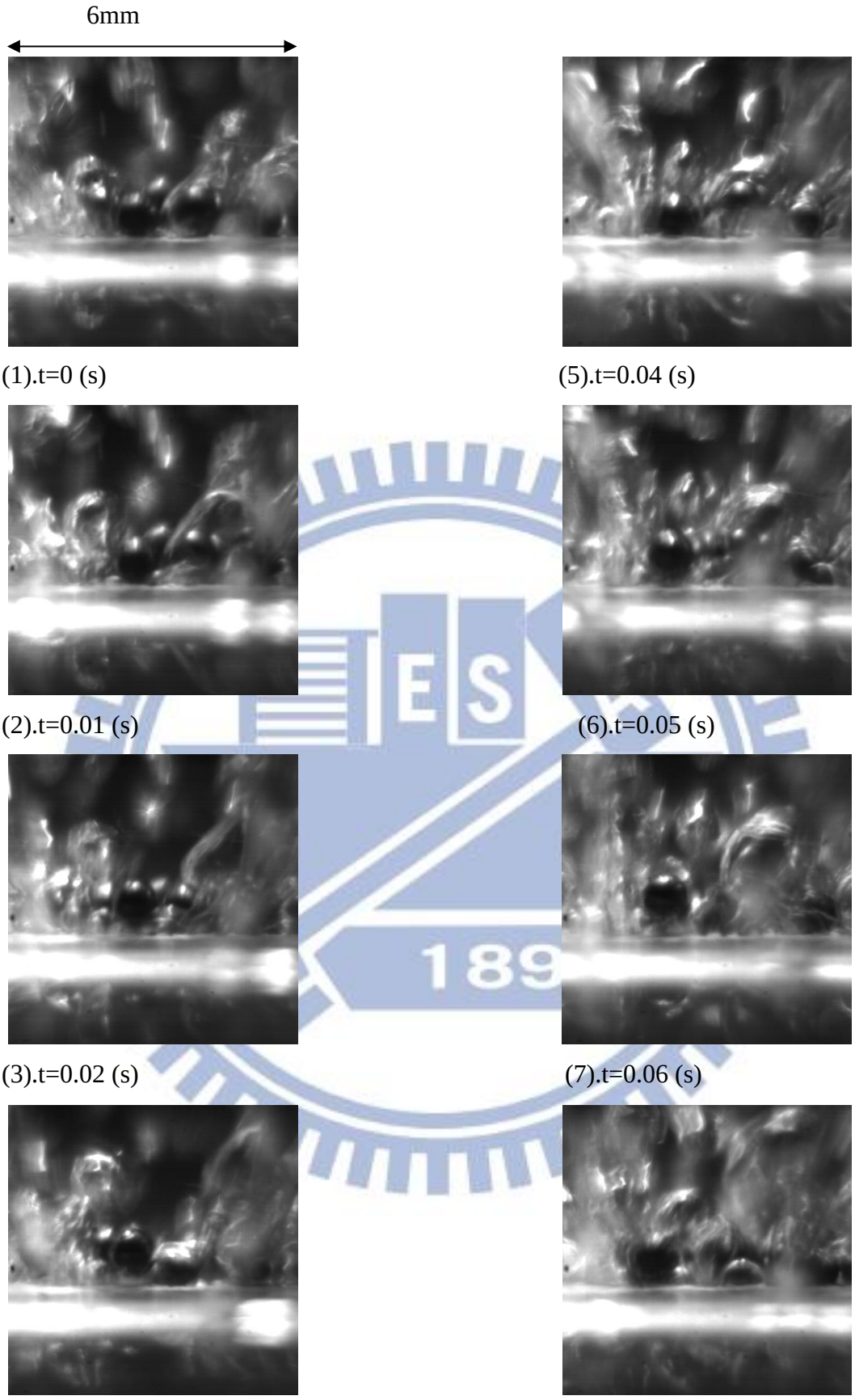


Fig. 4.49 Photos taken from side view of boiling flow at selected time instants for q= 2.25 W/ $cm^2$ with stainless steel particles on heated surface at $d_p$=1.0 mm and $N_p = 600$

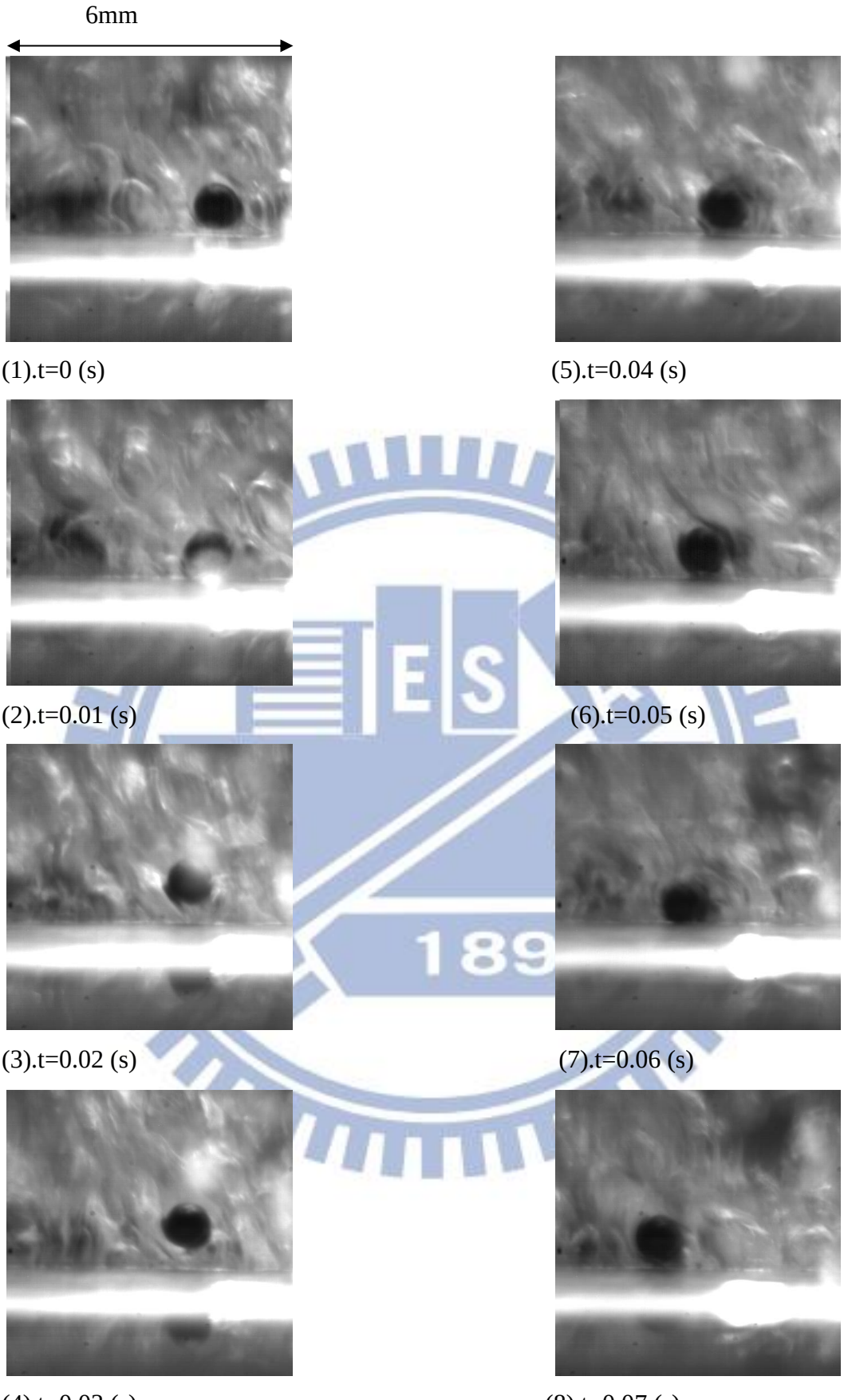


Fig. 4.50 Photos taken from side view of boiling flow at selected time instants for q= 3.69 W/ $cm^2$ with stainless steel particles on heated surface at $d_p$=1.0 mm and $N_p = 600$

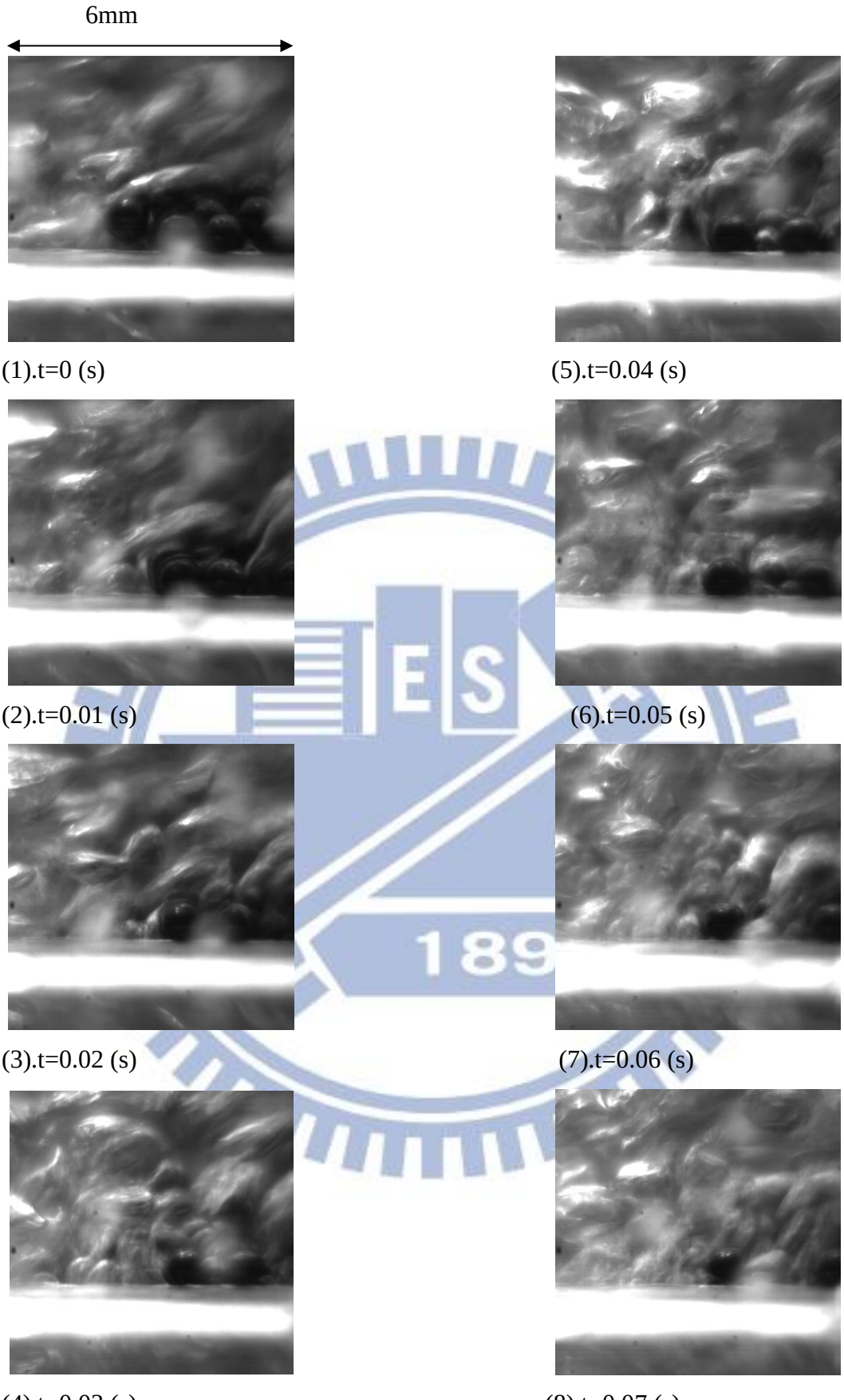


Fig. 4.51 Photos taken from side view of boiling flow at selected time instants for q= 5.48 W/ $cm^2$ with stainless steel particles on heated surface at $d_p$=1.0 mm and $N_p = 600$

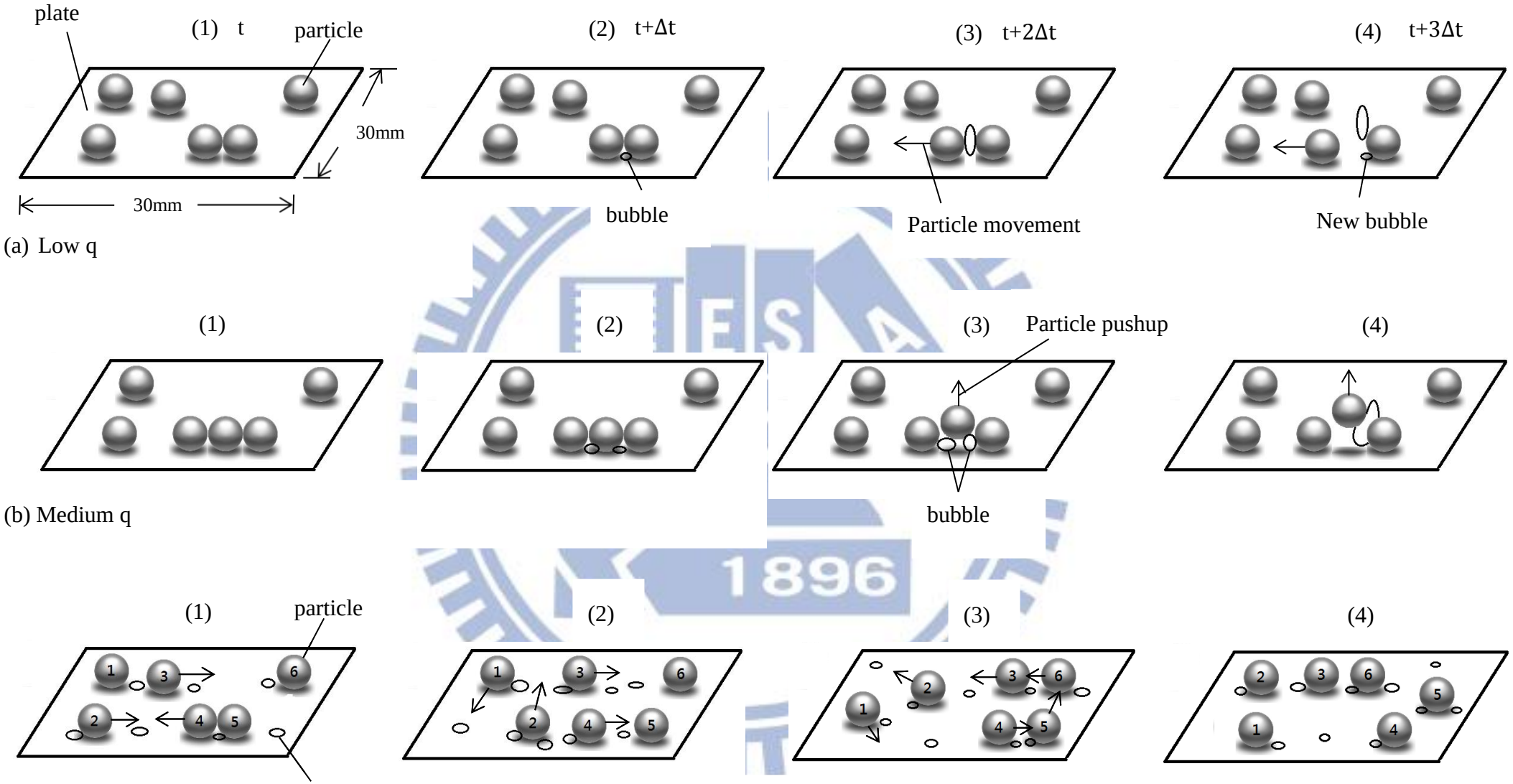


Fig. 4.52 Schematic illustration of particle-bubble interactions in boiling flow on heated surface at (a) low flux, (b) medium flux and (c) high flux($\Delta t \approx 0.01$ sec.)

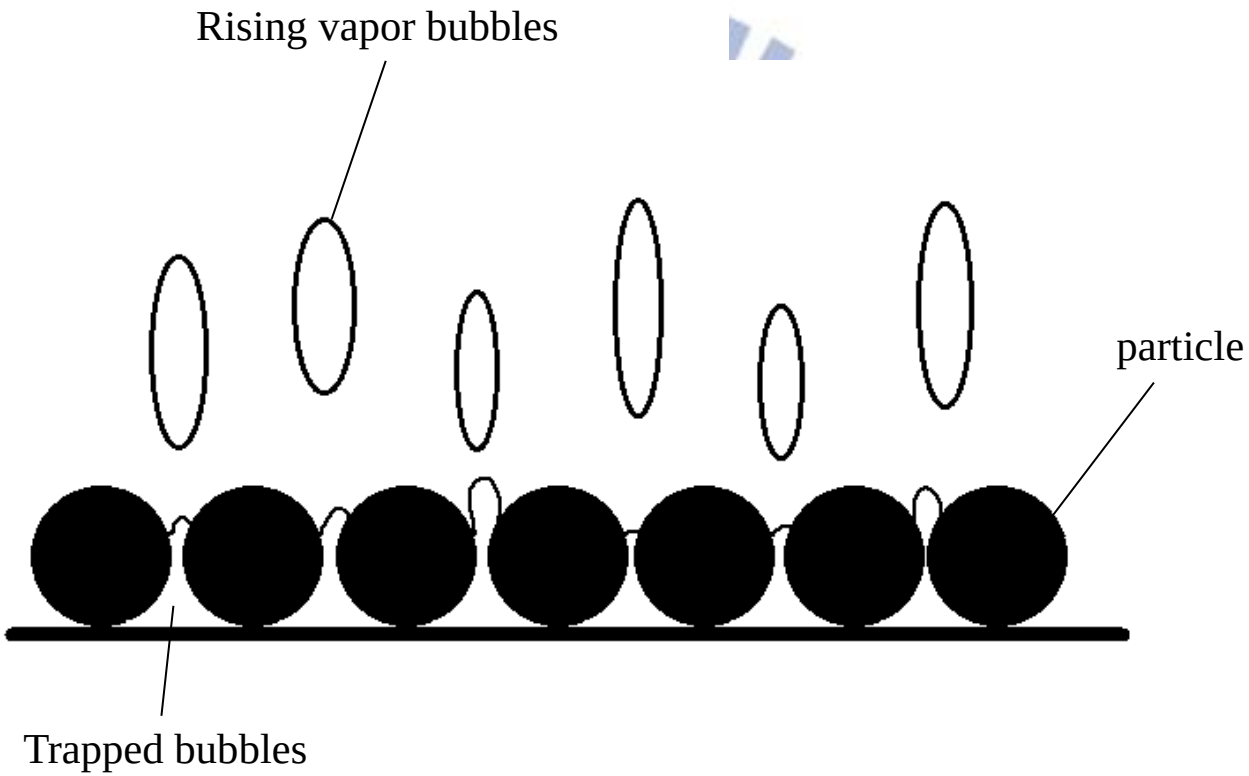


Fig. 4.53 Schematic illustration of retarding bubble growth and departure by particles at high heat flux.

# CHAPTER 5

## CONCLUDING REMARKS

In this study we conduct an experiment to investigate the possible pool boiling heat transfer enhancement of FC-72 by placing movable metallic particles on the boiling surface. The effects of the particle diameter, sort of particles (copper and stainless steel) and particle number on the boiling heat transfer enhancement have been examined in detail. The major results obtained from this investigation can be summarized as follows.

(1) The boiling heat transfer enhancement is closely related to the particle diameter, sort of particles (copper and stainless steel), particle number, and heat flux applied.

(2) The boiling heat transfer can be significantly enhanced by placing movable particles on the heated plate at lower and medium heat fluxes (wall superheats) when the total number of the particles in the flow exceeds 40% of the maximum number of particles forming a single closed packed particle layer. For the copper particles the boiling heat transfer can be enhanced up to 430% for a suitable choice of the experimental parameters. The best boiling heat transfer enhancement is even higher for the stainless steel particles at 530%. Even for the particle number in the flow well exceeding $N_{pf}$ the enhancement in the boiling heat transfer can be rather significant. Besides, the wall superheat for the boiling incipience can be substantially reduced by the moving metallic particles. This result is conjectured to be the consequence of that place particles on the plant enhances the roughness between copper plant and particles.

(3) At high heat flux (wall superheat) placing the particles in the flow can

substantially retard the boiling heat transfer especially for the large particles. The boiling heat transfer retardation can be up to 30% for the large copper particles and 50% for the large stainless steel particles.

(4) Interactions between the particles and bubbles are very strong at medium and high heat fluxes which result in two opposite effects of enhancing and retarding boiling heat transfer.

(5) Correlations for the boiling heat transfer augmentation and ranges of the experimental parameters for this augmentation by the moving metallic particles are proposed.

# References


1. G. Xu, B. Guenin, M. Vogel, “Extension of air cooling for high power processors”, Proceedings 9th Intersociety Conference on Thermal Phenomena 1 (2004) 186-193.

2. H.C Yang, “Enhancement of FC-72 Pool Boiling Heat Transfer and Associate Bubble Characteristics over a Small Horizontal Plate By Placing Copper Strings above the Plate” , M.S. Theses, Department of Mechanical Engineering, National Chuao Tung University, Hsinchu, Taiwan(2009)

3. S. Nukiyama, “The maximum and minimum values of the heat *Q* transmitted from metal to boiling water under atmospheric pressure”, Journal Japan Society of Mechanical Engineers 37 (1934) 367-374.
(Translated in Int. J. Heat Mass Transfer 9 (1966) 1419-1433).

4. A Bar-Cohen, “Thermal management of air-and liquid-cooled multichip modules”, IEEE Transactions on components, hybrids, and manufacturing technology 10 (2) (1987) 159-175.

5. W. J. Miller, B. Gebhart, N. T. Wright, “Effects of boiling history on a microconfigured surface in a dielectric liquid”, Int. Commun. Heat Mass Transfer 17 (4) (1990) 389-398.

6. J. Y. Chang, S. M. You, “Enhanced boiling heat transfer from micro-porous surfaces: effects of a coating composition and method”, Int. J. Heat Mass Transfer 40 (18) (1997) 4449-4460.

7. S. Vemuri, K. J. Kim, “Pool boiling of saturated FC-72 on nano-porous surface”, Int. Commun. Heat Mass Transfer 32 (2005) 27-31.

8. K. N. Rainey, S. M. You, “Pool boiling heat transfer from plain and microporous, square pin-finned surfaces in saturated FC-72”, Trans. ASME J. Heat Transfer 122 (3) (2000) 509-516.

9. K. N. Rainey, S. M. You, “Effect of pressure, subcooling, and dissolved gas on pool boiling heat transfer from microporous, square pin-finned surfaces in FC-72”, Int. J. Heat Mass Transfer 46 (1) (2003) 23-35.

10. H. Honda, H. Takamatsu, J. J. Wei, “Enhanced boiling of FC-72 on silicon chips with micro-pin-fins and submicron-scale roughness”, Trans. ASME J. Heat Transfer 124 (2) (2002) 383-390.

11. J. J. Wei, L. J. Guo, H. Honda “Experimental study of boiling phenomena and heat transfer performances of FC-72 over micro-pin-finned silicon chips”, Heat and Mass Transfer 41 (8) (2005) 744-755.

12. L. Zhang, M. Shoji “Nucleation site interaction in pool boiling on the artificial surface”, Int. J. Heat Mass Transfer 46 (2003)513-522

13. C. K. Yu. , D. C. Lu. and T. C. Cheng “Pool boiling heat transfer on artificial micro-cavity surface in dielectric fluid FC-72 ”, J. Micromech. Microeng. 16 (1989)752-759

14. Chen Li, G. P. Peterson and Y. Wang “Evaporation/Boiling in Thin Capillary Wick (I) –Wick Thickness Effects” Transaction of the ASME 128 (2006) 1312-1319

15. Chen Li, G. P. Peterson “Evaporation/Boiling in Thin Capillary Wick (II) –Effects of Volumetric Porosity and Mesh Size” Transaction of the ASME 128 (2006) 1320-1328

16. T. M. Anderson, I. Mudawar, “Microelectronic cooling by enhanced pool boiling of a dielectric fluorocarbon liquid”, Trans. ASME J. Heat Transfer 111 (3) (1989) 752-759.

17. J. P. O’Connor, S. M. You, “A painting technique to enhance pool boiling heat transfer in saturated FC-72”, Trans. ASME J. Heat Transfer 117 (2) (1995) 387-393.

18. J. P. O’Connor, S. M. You, D. C. Price, “A dielectric surface coating technique to enhance boiling heat transfer from high power microelectronics”, IEEE Transactions on components, packaging and manufacturing technology Part A 18 (3) (1995) 656-663.

19. J. Y. Chang, S. M. You, “Boiling heat transfer phenomena from micro-porous and porous surfaces in saturated FC-72”, Int. J. Heat Mass Transfer 40 (18) (1997) 4437-4447.

20. J. Y. Jung, H. Y. Kwak, “Effect of surface condition on boiling heat transfer from silicon chip with submicron-scale roughness”, Int. J. Heat Mass Transfer 49 (23-24) (2006) 4543-4551.

21. H. Honda, J. J. Wei, “Enhanced boiling heat transfer from electronic components by use of surface microstructures”, Experimental Thermal and Fluid Science 28 (2-3) (2004) 159-169.

22. K. N. Rainey, S. M. You, “Effects of heater size and orientation on pool boiling heat transfer from microporous coated surfaces”, Int. J. Heat Mass Transfer 44 (14) (2001) 2589-2599.

23. K. N. Rainey, S. M. You, S. Lee, “Effect of pressure, subcooling, and dissolved gas on pool boiling heat transfer from microporous surfaces in FC-72” Trans. ASME J. Heat Transfer 125 (1) (2003) 75-83.

24. H. M. Chou, R. F. Horng, Y. S. Liu, J. L. Wong, “The effect of grooved pattern on enhanced boiling heat transfer in a cylindrical tank base with a constant surface area”, Int. Comm. Heat Mass Transfer 29 (7) (2002) 951-960.

25. S. Hasegawa, R. Echigo, S. Irie, “Boiling characteristics and burnout phenomena on heating surface covered with woven screens”, Journal of Nuclear Science and Technology 12 (11) (1975) 722-724.

26. J. Y. Tsay, Y. Y. Yan, T. F. Lin, “Enhancement of pool boiling heat transfer in a horizontal water layer through surface roughness and screen coverage”, Heat and Mass Transfer 32 (1-2) (1996) 17-26.

27. J. W. Liu, D. J. Lee, A. Su, “Boiling of methanol and HFE-7100 on heated surface covered with a layer of mesh”, Int. J. Heat Mass Transfer 44 (1) (2001) 241-246.

28. A. Franco, E. M. Latrofa, V. V. Yagov, “Heat transfer enhancement in pool boiling of a refrigerant fluid with wire nets structures”, Experimental Thermal and Fluid Science 30 (3) (2006) 263-275.

29. H. M. Kurihara, J. E. Myers, “The effects of superheat and surface roughness on boiling coefficients”, A.I.Ch.E. Journal 6 (1) (1960) 83-91.

30. M. Shi, Y. Zhao, Z. Liu, “Study on boiling heat transfer in liquid saturated particle bed and fluidized bed”, International Journal of Heat and Mass Transfer 46(2003) 4695-4702.

31. M. MATIJEVIC, M. DJURIC, Z. ZAVARGO, M. NOVAKOVIC, “Improving Heat Transfer with Pool Boiling by Covering of Heating Surface with Metallic Spheres”, HEAT TRANSFER ENGINEERING 13(3)(1992) 49-57.

32. D. Wen, Y. Ding, “Experimental investigation into the pool boiling heat transfer of aqueous based $\gamma$ -alumina nanofluids”, J. Nanoparticle Res.7 (2) (2005) 265-274.

33. I. C. Bang, S. H. Chang, “boiling heat transfer performance and phenomena of Al2O3-water nano-fluids from a plain surface in a pool”, Int. J. Heat Mass Transfer 48 (12) (2005) 2420-2428.

34. S. J. Kline, F. A. McClintock, “Describing uncertainties in single sample experiments”, Mechanical Engineering 75 (1953) 3-8.

35. R. J. Moffat, “Contributions to the theory of single-sample uncertainty analysis”, Journal of Fluids Engineering 104 (2) (1982) 250-260.

36. J. H. Jeong, Y. C. Kwon, “Effects of ultrasonic vibration on subcooled pool boiling critical heat flux”, Heat Mass Transfer (2006) 42 : 1155-1161.

37. M. Cipriani, P. Di Marco, W. Grassi, “Effect of an externally applied electric field on pool film boiling of FC-72”, HEAT TRANSFER ENGINEERING 26 (2010) : 3-13.

38. Y. V. Navruzov, P. V. Mamontov, A. V. Stoychev, “Subcooled liquid Pool Boiling Heat Transfer on a Vibration Heating Surface”, Heat Transfer Research 24 (6) (1992) 771-776.

39. E. Radziemska, W. M. Lewandowski, “The effect of plate size on the natural convective heat transfer intensity of horizontal surfaces”, Heat Transfer Engineering 26 (2) (2005) 50-53.